PHYSICAL CHARACTERIZATION OF SMECTIC LIQUID CRYSTALS FORMED BY BENT-SHAPED MOLECULES

DISSERTATION

zur Erlangung des akademischen Grades doctor
rerum naturalium (Dr. rer. nat)

vorgelegt der

Mathematisch-Naturwissenschaftlich-Technischen
Fakultät

(mathematisch-naturwissenschaftlicher Bereich) der Martin-Luther-Universität Halle-
Wittenberg

von Herrn Dipl.- Phys. Alexey B. Eremin
geboren am 14.02.1976 in Moskau

Gutachter   1. Prof. Gerhard Pelzl

                2. Prof. Horst Kresse

                3. Prof. Boris Isakovich Ostrovskii

Halle (Saale), den 10 Februar 2003

This thesis is based on the following publications:

A. Eremin, S. Diele, G. Pelzl, H. Nádasi, W. Weissflog, J. Salfetnikova, H. Kresse, *Experimental evidences for an achiral orthogonal biaxial smectic phase without in-plane order exhibiting antiferroelectric switching,* Phys. Rev. E, **64**, 51707 (2001)

A. Eremin, I. Wirth, S. Diele, G. Pelzl, H. Schmalfuss, H. Kresse, H. Nádasi, K. Fodor-Csorba, E. Gacs-Baitz, W. Weissflog, *Structural characterization of the new polymorphic mesophases formed by bent-core molecules,* Liq. Cryst, **29,** 775 (2002**)**

I. Wirth, S. Diele, A. Eremin, G. Pelzl, S. Grande, L. Kovalenko, N. Panchenko, W. Weissflog, *New variants of polymorphism in banana-shaped mesogens with cyano-substituted central core,* J. Mater. Chem., **11**, 1642 (2001)

H. Nádasi, W. Weissflog, A. Eremin, G. Pelzl, S. Diele, B. Das, S. Grande, *Ferroelectric and antiferroelectric „banana phases" of new fluorinated five-ring bent-core mesogens,* J. Mater. Chem., **12**, 1316 (2002)

W. Weissflog, H. Nádasi, U. Dunemann, G. Pelzl, S. Diele, A. Eremin, H. Kresse, *Influence of lateral substituents on the mesophase behaviour of banana-shaped mesogens,* J. Mater. Chem., **11**, 2748 (2001)

G. Pelzl, A. Eremin, S. Diele, H. Kresse, W. Weissflog, *Spontaneous chiral ordering in the nematic phase of an achiral banana-shaped compound,* J. Mater. Chem.*,* **12**, 2591 (2002)

G. Dantlgraber, A. Eremin, S. Diele, A. Hauser, H. Kresse, G. Pelzl, C. Tschierske, *Chirality and macroscopic polar order in a ferroelectric smectic liquid-crystalline phase formed by achiral polyphilic bent-core molecules*, Angew. Chem., **41**, 2408 (2002)

A. Eremin, S. Diele, G. Pelzl, W. Weissflog, *Switching between opposite chiral states in a tilted smectic phase formed by an achiral banana-shaped mesogens*, Phys. Rev. E, submitted

A. Eremin, S. Diele, G. Pelzl, H. Nádasi, W. Weissflog, *Experimental evidence for Sm-CG → Sm-CP polymorphism in fluorinated bent-shaped mesogens*, Phys. Rev. E, submitted

Publications not included in this thesis:

A. Eremin, S. Diele, G. Pelzl, L. Kovalenko, K. Pelz, W. Weissflog, *Polymorphic smectic A phases in perfluoroalkylated mesogenic dimers*, **28**, 1451 (2001)

Contents

Chapter 1

Introduction

1.1 Ordering and diversity of "banana" phases

In the class of thermotropic liquid crystals [1, 2], liquid crystalline materials formed by bent-shaped molecules [3] open the door to a rich array of new mesophases not found among the compounds formed by rod-like molecules [4]. Orientation of a bent molecule can be defined by two directors: one **n** along the long molecular axis and another in direction of the bow **p**. Because of packing constrains, bent-core molecules tend to segregate into planes, with their polar axis defined by **p** aligned along a common direction. Since the layer normal **k** defines a direction independently of **n** and **p** a large variety of mesophases with different symmetries may result [5].

To have a better understanding of the grounds lying behind such richness of mesophases encountered among bent-shaped molecules, some recent theoretical progress on molecular theories should be mentioned [6].

Notwithstanding that the theoretical approach in describing of such complex systems is in its infancy a minimal theory capable for exhibiting isotropic and nematic phases has been proposed by L. Radzihovsky *et al* [7]. In this work, for instance, in the frame of the mean-field theory they have proposed a model of the isotropic→tetrahedratic phase transition.

A choice of order parameters, which should comprise the features of such asymmetrical molecules, is more sophisticated even in the simplest case of the nematic phase. Single nematic order parameter Q_{ij} is not enough to describe the polar ordering of bent molecules. The approach highlighted in ref. [6, 7] consists in constructing the order parameter from mass-moment tensors. Since the first mass moment tensor relative to the center of mass is zero, bent molecules do not have mass-moment vector order parameter. Two first moments are given below. The first moment specifies the center of mass of the molecule

$$B^i = \sum_\alpha m_\alpha r^i \tag{1.1}$$

where m_α is the mass of particle α and its position is defined by the vector r^i. It can always be taken as the origin of coordinates and is unimportant, however, the higher moments contain more information about the symmetry of the molecules and can even be used for obtaining the parameters that describe chirality [6, 8]

$$C^{ij} = \sum m_\alpha (r^i r^j - \frac{1}{3} r_\alpha^2 \delta^{ij}) \tag{1.2}$$

$$D^{klm} = \sum m_\alpha \left[r_\alpha^k r_\alpha^k r_\alpha^l - \frac{1}{5} (r_\alpha^2)(r_\alpha^k \delta^{lm} + r_\alpha^l \delta^{km} + r_\alpha^m \delta^{kl}) \right]$$

These tensors are symmetric and traceless, and are invariant under the mirror operation that interchanges any two axes. Non-zero third rank mass-moment tensor contains the information about the polar shape of the molecules. This tensor can be decomposed into a symmetric-traceless part T^{ijk}, which transforms under the $l = 3$ representation of the group SO(3), and a part transforming like a vector ($l = 1$) p^i. Even in the mean field approximation a rich polymorphism of phases of different symmetries depending on values of Q, T and **p** have been predicted [7].
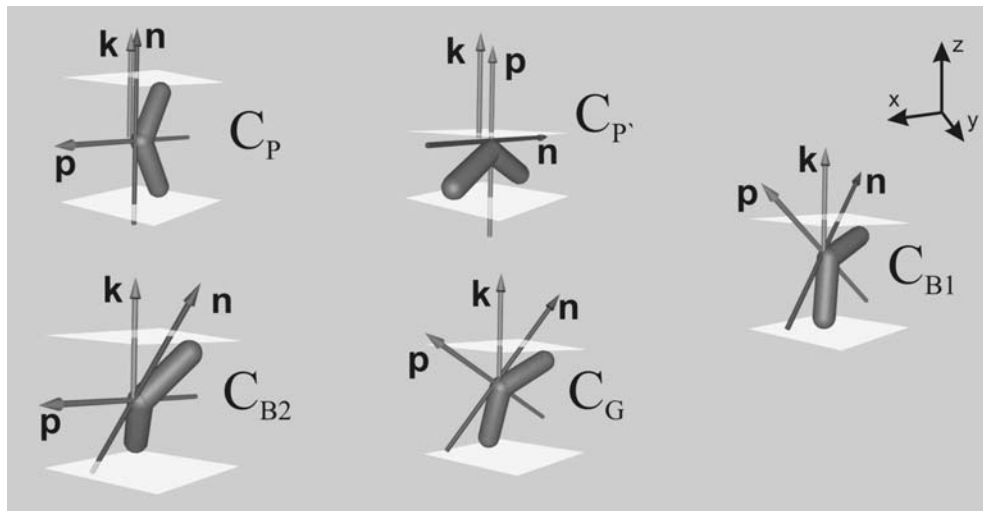
Fig. 1.1: Possible arrangements of the molecules in the smectic layers

Another approach is based on the Monte Carlo simulations performed by R. Memmer [10] In his work achiral bent-shaped molecules spontaneously formed helical superstructure in the nematic phase. This possibility, as a consequence of the coupling between bent and twist deformations, has also been suggested by I. Dozov [11].

It is important to notice that we will consider mostly compounds with achiral molecules. One of the striking features of the mesophases formed by achiral bent-shaped molecules is that they show spontaneous breaking of achiral symmetry. In case of conventional smectic liquid crystals formed by bent-shaped molecules possible arrangements have been proposed by Brand *et al* [12]. So-called "minimal banana smectics" have one polarization vector and corresponding arrangements and symmetries are sketched in Fig. 1.1 and Table 1.1. Among these polar structures two phases with C_2 and C_1 symmetries are chiral. The experimental realizations of such mesophases are considered in the following section.

Table 1.1

Class	Symmetry	Electro-optics	Helix
C_P	C_{2v}	Ferri- or ferroelectric $P = (P_x, 0, 0)$	no
$C_{P'}$	C_{2v}	Ferri- or ferroelectric $P = (0, 0, P_z)$	no
C_{B2}	C_2	Ferri- or ferroelectric $P = (P_x, 0, 0)$	yes
C_{B1}	C_{1h}	Ferri- or ferroelectric $P = (P_x, 0, P_z)$	no
C_G	C_1	Ferri- or ferroelectric $P = (P_x, P_y, P_z)$	yes

1.2 Experimental advances in bent-shaped liquid crystals

Theoretical models predict tremendously rich variety of smectic and nematic mesophases of various symmetries, yet only few unusual smectic phases have been observed experimentally. Among them there are two phases with a simple layer structure of C_2 and C_{2v} symmetry and no order within the layers as well as there are some higher ordered phases (two- or three dimensional). Recently some evidence has been found for the phase with the C_1 symmetry (Chapter 11).

A phase with C_{2v} symmetry is called C_P or SmAP. The bent molecules are arranged orthogonally in the liquid-like smectic layers. The molecules are packed in the direction of the bow within each layer, which results in spontaneous macroscopic polarization. Therefore the SmAP phase is different from the SmA phase where there is no preferred direction perpendicular to the layer normal. A similar phase (SmAP) was found in side-chain polymers [13] quite a while ago, however, in low-molecular bent-shaped compounds it was observed and described in Chapter 5 of this thesis for the first time [14].

Up to date the most common phase is the one with C_2 symmetry. There is no all-accepted nomenclature so far and this phase is designated by different authors as C_{B2} or B_2 or SmCP. The structure of the phase consists of smectic liquid-like layers with tilted molecules and the polar order in the direction perpendicular to the layer normal. It is a unique mesophase since despite liquid disorder within the layers it shows a breaking of achiral symmetry, natural for solids but has never been found in liquids. The molecules are achiral and the chirality appears as consequence of the mesophase structure. Indeed the structure is defined by three vectors **p**, **n** and **k**. These vectors are coplanar unless the value of $[\mathbf{n} \times \mathbf{k}] \cdot \mathbf{p} = q \neq 0$ which, actually, defines the chirality since the vector product is a pseudo-vector. The states with $q < 0$ and $q > 0$ are of opposite handedness: have no mirror symmetry (Fig. 1.2). Whereas, the state with $q = 0$ is achiral. In our system the latter case corresponds to the SmAP phase. An excellent review of the topic
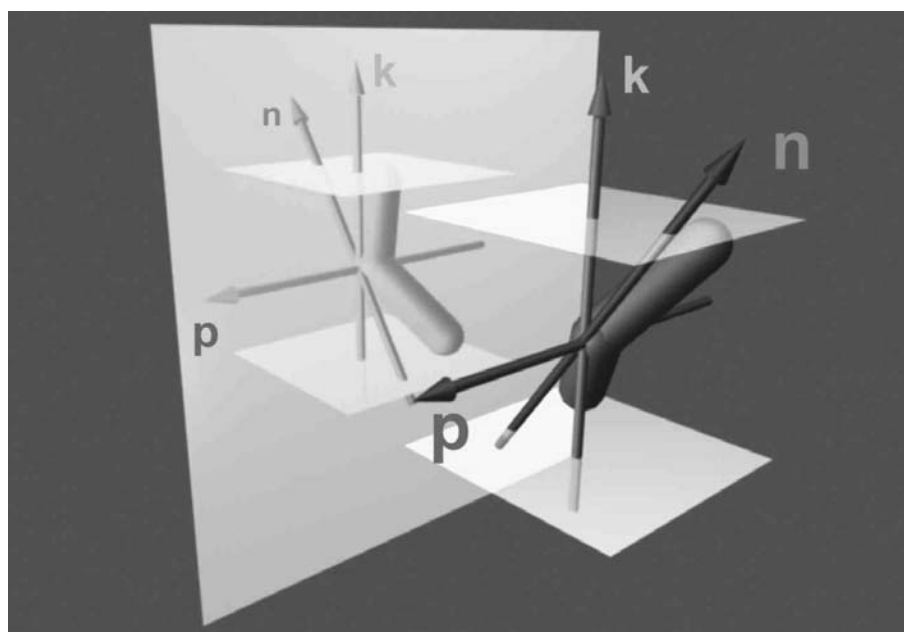

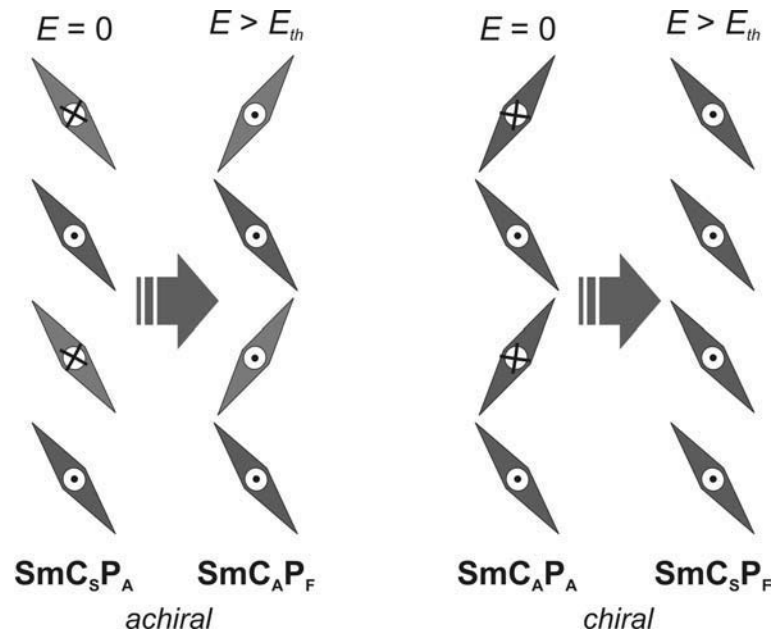Fig. 1.2: Structural chirality of the SmCP phase

Fig. 1.3: Various arrangements of the smectic layers in the SmCP phase and the effect of the switching on the structure of the layers

of chirality and its measure can be found in ref. [8, 9].

An extensive research made on thin SmCP films [15] showed that besides the polar packing of the molecules within the smectic layers the arrangement of the layers with respect to each other plays an important role. In particular, there are two possible interface arrangements: *synclinic* and *anticlinic* as well as two possible orientations of the polarization vectors in the adjacent layers: *ferroelectric* (FE) and *antiferroelectric* (AFE). In most cases the ground state is antiferroelectric and applying an electric field along the layers one can switch to the ferroelectric state. As it has already been mentioned above each layer is chiral. However, among these four different structures the two are *macroscopically chiral* (SmC_AP_A and SmC_SP_F) and the other two are *achiral* (or racemic as designated in ref. [15]) (SmC_SP_A and SmC_AP_F). Application of an electric field leads to an electro-optical switching from the ground AFE state into the FE state. The chirality of the layers usually remains conserved (the exceptions are discussed in further chapters). A more explicit discussion is given in Chapter 2.

Among other mesophases the B_5 phase is similar to the SmCP phase: it consists of smectic layers with tilted molecules and shows electro-optical switching. In contrast to the SmCP phase the B_5 phase possesses an in-plane density modulation which can be described by a rectangular two-dimensional network [16, 17]. So far it is not fully characterized and probably is a candidate to an analogue to hexatic phases of calamitics.

An intercalated version of the SmCP phase is called B_6. It is a rare phase and in contrast to the SmCP phase it does not show the electro-optical switching [16].

A long search for simple smectic phases with triclinic (C_1) symmetry seems to have good chances to be of success in the field of bent-shaped liquid crystals. Recently some candidates for the general SmC_G phase have been found, which have made up a separate chapter in this thesis. In connection with this topic it is important to mention a family of the B_7 phases which are under intense discussions nowadays [18]. Unusual bright and artistic textures attracted many liquid-crystal researchers and endeavored

them to unravel the structure of this enigmatic phase. However, inability to form free-standing films and absence of oriented samples is a main obstacle since the X-ray shows a complex two- or three- dimensional structure of the mesophase. Currently, columnar models with triclinic symmetry [19] as well as modulated lamellar structures with C_2 symmetries are under consideration [20].

Additionally, except of conventional smectic phases described above, the bent-shaped mesogens form some exotic columnar phases designated as B_1 (it is rather a group of phases of different symmetries) [16, 21]; a crystalline B_3 phase [16], distorted soft-crystalline B_4 phase [22]. These more exotic cases are out of the scope of this thesis.

1.3 This thesis

This thesis is based on the material of a two year experimental research on structure and ordering in smectic phases formed by bent-shaped molecules. The research employed a variety of experimental techniques as disparate as X-ray diffraction, polarizing microscopy, NMR spectroscopy, differential calorimetry, dielectric spectroscopy. A review of these methods can be found in Chapter 2.

In the frame of this thesis some theoretical calculations have been performed to simulate the effect of the tilt and bent of the molecules on the wide-angle scattering of the X-rays. To do that some software have been developed using Digital Fortran (Compaq) programming language. We also employed commercial Accerlys Cerius2 (Version 4.6) molecular modeling software which has been employed to simulate the X-ray scattering by crystals. The discussion of the algorithms and the results constitutes Chapter 3.

The rest of the chapters is dedicated to the experimental characterization of different mesophases and is arranged in the order of lowering symmetry: starting from the nematic phase and finishing with the SmC_G phase.

Chapter 4 is a short review of some recent research being currently made on the nematic phases of bent-shaped molecules. We discuss a first observation of the chiral twist in the nematic phase formed by achiral bent-shaped molecules. Besides, a new isotropic "banana" mesophase has been reported for the first time.

In Chapter 5 the experimental results on switchable orthogonal SmAP phase are presented. The symmetry of the phase is C_{2v}. This is the first observation of the low-molecular mesogens exhibiting such mesophase.

The next chapter introduces the phase with lower C_2 symmetry. It is a conventional antiferroelectric SmCP phase. The chapter summarizes some already known aspects of the SmCP phase obtained from the isotropic or nematic phase by means of a first-order transition.

Another Chapter 7 describes the SmCP phase appearing on cooling of the SmC phase. The SmC→SmCP transition is not quite a new phenomena [23, 24], however, the new fluorinated bent-shaped compounds show weakly first order paraelectric→ferroelectric transition, which has not been observed before. The bending angle of the molecule is changing continuously and its role in the formation of the "banana" phases is discussed.

Chapter 8 about polymorphic SmCP phases sheds some more light upon complicity of the topic even in case of such simple phase as SmCP. Here we report some new phases which give the same X-ray pattern standing for the tilted smectic phase without in-plane order.

A slightly more complex case is the B_5 phase. The properties of this phase are quite similar to the properties of the SmCP phase. In Chapter 9 a first ferroelectric B_5 phase is reported. Moreover, similarly to the SmCP phase we found some polymorphic B_5 phases between the AFE and FE versions of the B_5 phase.

Since most of the SmCP phases are antiferroelectric it became an endeavor for the researchers to find compounds with the ferroelectric SmCP phase. In Chapter 10 for the first time we describe the mesophase behavior of such compound synthesized by G. Dantlgraber (Martin-Luther University, group of C. Tschierske). It is an asymmetric bent-shaped mesogens with an oligosiloxane terminal chain and it shows ferroelectric bistable switching.

Chapter 11 is devoted for possible candidates for the phase without symmetry (C_1) – a general SmC$_G$ phase. This is a very topical subject nowadays and despite we do not have indisputable experimental evidence, our measurements give some more arguments in favor of the existence of such phase.

The last chapter is a preliminary report of the newest finding of a "banana" mesophase showing electro-optical switching between the chiral states of opposite handedness.

Chapter 2

Experimental techniques

2.1 Polarizing microscopy

Characterization of the optical textures of mesophase is essential in primary phase assignment. It was done using polarizing microscope Leitz (Laborlux 12 Pol S, Germany). Preparations of the liquid crystal films sandwiched between two glass plates were put in a temperature controlled oven (Linkam TMS 92, England). Two glass windows on the top and the bottom of the oven provided light transmission through the sample. With a help of a CCD-color camera (Hitachi, Model KP-C 551, Japan) the images could be saved on the video tape. Photo prints of the textures were possible using a camera Leica (Model Wild MPS 52, Germany).

2.2 Calorimetric studies

2.2.1 Theoretical description

Measurement of the temperature dependence of the heat capacity C_p and/or the enthalpy ΔH determines the thermal behavior of the liquid crystal phases and helps to characterize the phase transitions which occur.

By far the most common thermal technique used to study liquid crystals has been differential scanning calorimetry (DSC). This method has the advantages of high sensitivity for detecting enthalpy changes, very small sample size, rapid and convenient operation. However, DSC is not well suited to making detailed quantitative measurements near liquid crystal phase transitions.

The disadvantage of DSC measurements is the difficulty to distinguish first- and second-order transitions. In operation, a constant heating (or cooling) rate dH_{ref}/dt is imposed on the reference sample, which results in a constant and rapid linear temperature ramp. Scan rates dT/dt of 5-l0 K/min are commonly used. Although slower rates can be used, DSC machines work best for fairly rapid scans ($dT/dt \geq 1$ K/min) and require minimum scan rates of 0.1 K/min. A servosystem forces the sample temperature to follow that of the reference by varying the power input dH_{sample}/dt. The differential power $dH/dt = dH_{sample}/dt - dH_{ref}/dt$ is measured, and the integral $\int (dH/dt)dt$ for a DSC peak approximates the enthalpy associated with the corresponding transition.

A quantitative distinction between first and second order transitions could be found by making a series of measurements at different scan rates with further extrapolating of the transition enthalpy to rate zero. Strongly first order transition does not exhibit dependence of the latent heat on the cooling/heating rate. Whereas, the enthalpy H shows almost linear dependence in case of the second or weakly first order transitions.

2.2.2 Experimental setup

In the experiments the thermal behavior was investigated using a Perkin-Elmer Pyris 1 differential scanning calorimeter.

2.3 Electro-optical measurements

Electro-optical switching is of primary importance in technological applications of liquid crystals. Therefore, studying of the underlying processes of switching and phenomena of ferroelectricity in the new liquid crystals became an essential part of the research.

2.3.1 Historical introduction

The phenomenon which was later called ferroelectricity was discovered in 1920 by J. Valsek at University of Minnesota [25]. He recognized the electric hysteresis in a material called Rochelle salt, whose piezoelectric coefficients had been found to be much higher than those of quartz.

After some time, it was found that ferroelectric materials were not only extremely interesting, but also had the most powerful piezoelectric and pyroelectric properties. Unfortunately only 20 years later just in 1937 H.R. Jaffe [26] mentioned a possibility for phase transitions in Curie points of Rochelle salt. Important projects were started in Leningrad headed by I.V. Kurchatov (Курчатов). Further on a phenomenological theory of ferroelectricity was developed [27]. War time research efforts during the World War II led to the discovery in 1945 of the very important perovskite class starting with barium titanate ($BaTiO_2$) by B.M. Wul (Б.М. Вул) and I.M. Goldman (И.М. Гольдман) at the Lebedev Institute in Moscow (ФИАН).

In 1937 L.D. Landau presented a general framework based on symmetry changes in phase transitions. If one can choose a small parameter which is defined by the symmetry of, let us say, the low-temperature phase and is zero in the high-temperature phase, the free energy can be expanded in powers of this parameter in the vicinity of the phase transition. The first attempt to apply Landau's theory to $BaTiO_2$ was made by V.L. Ginzburg (В.Л. Гинзбург) [28]. Today, a unified microscopic theory is still not available for these different ferroelectrics.

2.3.2 Theoretical overview

The various crystalline modifications of a given substance may include some which are pyroelectric and some which are not. If the change from one into the other takes place by means of a second-order phase transition, then near the transition point the substance has a number of unusual properties which distinguish it from ordinary pyroelectrics; these are called *ferroelectric* substances [29, 30].

In an ordinary pyroelectric crystal, a change in the direction of the spontaneous polarization involves a considerable reconstruction of the crystal lattice. Even if the final result of this reconstruction is energetically favorable, its realization may still be impossible because it would require the surmounting of very high energy barriers.

In a ferroelectric body, however, the situation is quite different because, near a second-order phase transition point, the arrangement of the atoms in the crystal lattice of the pyroelectric phase is only slightly different from the arrangement in the non-pyroelectric lattice (and so the spontaneous polarization is also small). For this reason the change in the direction of the spontaneous polarization in this case requires only a slight reconstruction of the lattice and can occur quite easily.

There are also, however, ferroelectric transitions in which the order parameter is transformed by an irreducible representation of the symmetrical phase which does not correspond to the components of a vector. In such cases, the order parameter is not the

polarization but a physically different quantity; the spontaneous polarization arises as a secondary effect (it is assumed, of course, that the symmetry of the unsymmetrical phase allows pyroelectricity). These substances are called *improper ferroelectrics;* they differ considerably from ordinary ferroelectrics as regards the nature of the dielectric anomalies.

In case of calamitic liquid crystals the most common ferroelectric phase is SmC* [31, 32]. There spontaneous polarization of smectic layers results from chiral symmetry breaking. According to the Neumann principle the absence of mirror symmetry in the SmC* phase allows in-plane macroscopic polarization. These compounds are improper ferroelectrics: the primary order parameter is the tilt which results in the macroscopic polarization (secondary order parameter). In the SmC* phase the symmetry properties of the chiral phase would allow the spontaneous polarization directed perpendicular to the tilt plane which was first recognized by R.B. Meyer in 1974 [33]. In collaboration with French chemists he studied the first such materials [34]. In case of the achiral SmC materials chirality can be brought by admixing chiral dopants. As it was first demonstrated by W. Kuczynski and H. Stegemeyer [35] such mixtures exhibit a linear dependence of **P** on concentration (for low values) as well as the linear relation between **P** and the tilt angle ψ. A review of molecular models for the ferroelectric smectic SmC* phase can be found in ref. [36].

Recently, liquid crystalline compounds have been designed which, in contrast to the well known ferroelectric calamitics, are composed of achiral bent molecules and show high values of the electric polarization. These compounds can form orthogonal (SmAP) as well as tilted (SmCP) switchable phases.

As it has already been mentioned above (Chapter 1) the molecules in the SmCP phase can adjust four kinds of structures: AFE anticlinic and synclinic (SmC$_A$P$_A$, SmC$_S$P$_A$), FE anticlinic and synclinic (SmC$_A$P$_F$, SmC$_S$P$_F$) [15, 37]. The two states AFE and FE are separated by a small energy barrier. In most instances the energy of the AFE state is somewhat lower than one of the FE state resulting in the AFE ground state either synclinic or anticlinic. Application of an electric field leads to the transition from the AFE state into FE. The chirality of the layers is mainly conserved (observed transitions are SmC$_A$P$_F\rightarrow$ SmC$_S$P$_F$ and SmC$_S$P$_A \rightarrow$ SmC$_A$P$_F$). Recent Fourier transform infrared spectroscopic measurements also indicated a motion of the long molecular axis on the cone as in the SmC* phase [38]. The first indication of the switching between the states of different chirality have been found in bent-shaped liquid crystals [39], although, the mesophase was different from the SmCP.

A detailed investigation of the switching in the SmCP phase is reported in the ref. [40]. They observed that the appearance of the synclinic or anticlinic ground state can also be influenced by the shape of the oscillating external field. However, the SmC$_S$P$_A$ ground state has lower energy. Dielectric spectroscopy measurements separately performed on racemic and homochiral samples showed quite different properties of the domains. In the racemic state the switching is about twice as fast as in chiral state. The dielectric strength $\Delta\varepsilon$, however, is about twice as high in the chiral state. Further analysis of the effects of the chiral and racemic domains in the SmCP phase has been reported by L.M. Blinov *et al* [41] on the base of the analysis of the fine structure of the current response peaks.

There is not much information about switching dynamics in the SmCP phase. In reference [42, 43], for example, a helix free model of antiferroelectric liquid crystal has

been considered. Defining the tilt angle ψ and the azimuth angle of the molecules by Φ the density of the bulk free energy in the simplest case can be taken in the form:

$$F = \frac{1}{2} K \left[\left(\frac{\partial \Phi_i}{\partial x} \right)^2 + \left(\frac{\partial \Phi_i}{\partial z} \right)^2 \right] + W \cos(\Phi_{i+1} - \Phi_i) - P_0 E \cos \Phi_i \qquad (2.1)$$

Here K is the elastic constant and P_0 is the polarization of one layer. The first term describes the nematic-like elastic energy in one constant approximation and the third term stands for the interaction with the external field. The middle term corresponds to the inter-layer interaction (first harmonic approximation) with the energy W. If one assumes that the director in the odd layers is not affected by the external field then the torque balance equation reduces to

$$\gamma_\varphi \frac{\partial \Phi}{\partial t} = K \frac{\partial^2 \Phi}{\partial x^2} + (2W - P_0 F) \sin \Phi \qquad (2.2)$$

Disregarding the elastic term we would conclude that the distortion has a threshold character with the threshold field:

$$E_{th} = \frac{2W}{P_0} \qquad (2.3)$$

The inversed switching times for AF→FE and FE→AFE transitions give

$$\tau_{AF}^{-1} = \frac{1}{\gamma_\varphi} (P_0 E - 2W)$$

$$\tau_{FA}^{-1} = \frac{2W}{\gamma_\varphi} \qquad (2.4)$$

The experimental results reported by L.M. Blinov *et al* [41] show quite different switching kinetics for a low frequency triangular-wave external field and for the rectangular impulses of opposite sign. In the first case the switching between the AFE and FE states has been observed. The behavior is different when a wave of the rectangular impulses of opposite sign is applied: a straight switching occurs between two FE states without any indication of going through the AFE state. Measuring the switching times of these modes one can find the associated rotational viscosity coefficients γ_φ(AFE-FE), γ_φ(FE-FE) and viscosity γ_φ(FE-AFE) calculated from the time of free Φ-relaxation from FE to AFE state. All the three coefficients have the same temperature dependence but their magnitude differs by factor 3 [41]. The latter is related to oversimplified approximations used for the calculations. The electro-optical response was also observed below the AFE-FE threshold. In this regime, the optical transmission depends on electric field squared. This effect was attributed to the antiferroelectric soft mode distortion of the amplitude of the molecular tilt angle in the vicinity of the transition from the SmCP phase to the isotropic phase.

2.3.3 Experimental setup
The electro-optical measurements were carried out using commercial ITO cells (EHC). The following devices were used in the setup:

Table 2.1

Device	Model
Polarizing microscope	LEIC DMRXP
Heating stage	METTLER-TOLEDO, FP900, Switzerland
Video camera	JVC, TK-1280E, Japan
Functional generator	KEITHLEY, 3910, USA
Amplifier	KROHN-HITE, 7500, USA
Oscilloscope	HEWLETT PACKARD, HP54601A, USA
Resistors	TIME ELECTRONICS, Model 800, UK

The spontaneous polarization was measured using the following methods:
- The Sawyer-Tower circuit
- Polarization current measurements

The Sawyer-Tower circuit is shown in Fig. 2.1. The oscilloscope displays the hysteresis loop of polarization versus applied field. This circuit was used only for qualitative observation of the transition from AFE into FE phase described in Chapter 9.

The switching polarization was measured by integration of the repolarization current. The scheme is shown in Fig. 2.2. Besides different shapes of the applied field waves mainly triangular-wave voltage was employed in polarization measurements. The current density through the cell is given by

$$\mathbf{j}(t) = \sigma \mathbf{E}(t) + \frac{\partial \mathbf{D}(t)}{\partial t} \tag{2.5}$$

where $\mathbf{D}(t)$ and σ are the electric displacement and conductivity along the electric field direction, respectively. In case of polar liquid crystal $\mathbf{D}(t)$ can be given by

$$\mathbf{D}(t) = \varepsilon_0 \mathbf{E}(t) + \mathbf{P}(t) = \varepsilon_0 \varepsilon \mathbf{E}(t) + \mathbf{P}_{sw}(t) \tag{2.6}$$
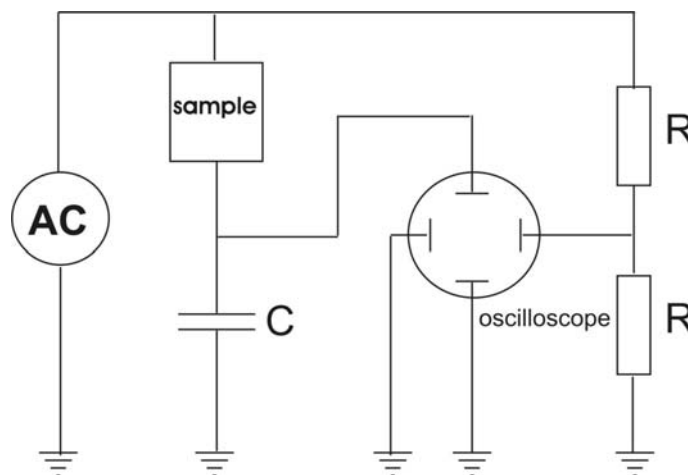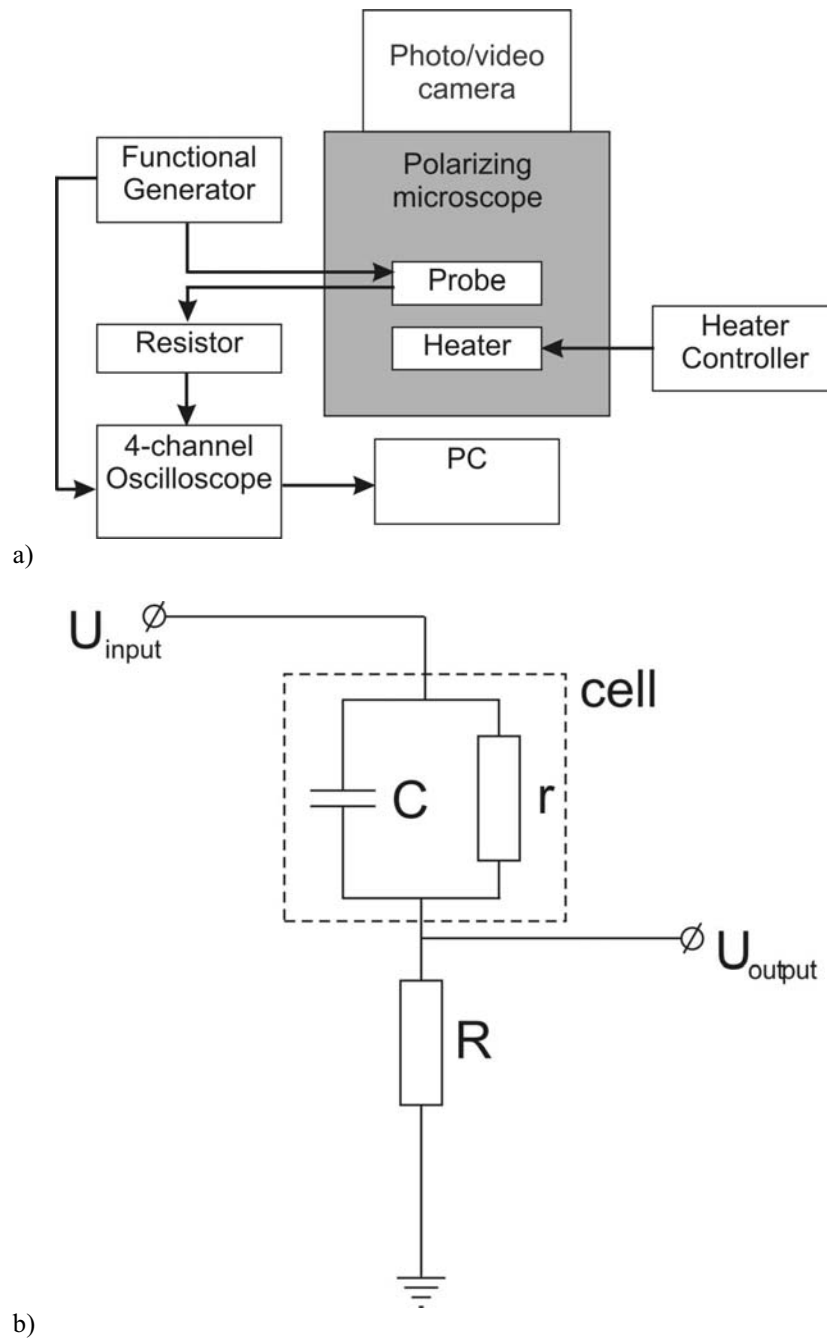

Fig. 2.1: Sawyer-Tower circuit

Fig. 2.2: a) Block scheme of the electro-optic setup and b) the electrical scheme: C and r are the internal capacitance and resistance of the LC cell, R is the external resistor

where $\mathbf{P}(t)$ is the total electric polarization, $\varepsilon(t)$ is an anisotropic relative "background" permittivity without the contribution of the switching polarization, $\mathbf{P_{sw}}(t)$ is the field dependent switched component of the spontaneous polarization. Then the total current through the surface defined by the area element $\mathbf{A}$ gives:

$$i(t) = \mathbf{A}\left[\sigma\mathbf{E}(t) + \varepsilon_0\varepsilon(t)\frac{d\mathbf{E}(t)}{dt} + \varepsilon_0\frac{d\varepsilon(t)}{dt}\mathbf{E}(t) + \frac{d\mathbf{P}_{sw}(t)}{dt}\right]$$

$$i(t) = \mathbf{A}\left[\sigma\mathbf{E}(t) + \left[\varepsilon_0\varepsilon(t) + \varepsilon_0\frac{d\varepsilon(t)}{d\mathbf{E}}\mathbf{E}(t) + \frac{d\mathbf{P}_{sw}(t)}{d\mathbf{E}}\right]\frac{d\mathbf{E}(t)}{dt}\right] \qquad (2.7)$$

When the external field takes triangular shape the term $\dfrac{d\mathbf{E}(t)}{dt}$ is constant in one-half period giving $\pm 4\mathbf{E}_m f$ where $\mathbf{E_m}$ is the amplitude and f is the frequency of the signal. Finally, the expression for the current is

$$i(t) = \mathbf{A}\left[\sigma\mathbf{E}(t) \pm 4\mathbf{E_m}f\left[\varepsilon_0\varepsilon(t) + \varepsilon_0\frac{d\varepsilon(t)}{d\mathbf{E}}\mathbf{E}(t) + \frac{d\mathbf{P}_{sw}(t)}{d\mathbf{E}}\right]\right] \qquad (2.8)$$

This current consists of the resistive current due to ion flow through the cell and two currents caused by dipole realignment. The sum of the 2nd and 3rd term is determined by "background" permittivity of the liquid crystal and the 4th term is due to the spontaneous polarization $\mathbf{P_{sw}}$. Usual parameters for bent-shaped compounds are $\varepsilon \sim 4$, $P_{sw} \sim 200 - 1000$ nCcm[-2]. The oscillograms obtained for AFE switching contain two peaks per half period corresponding to AFE→FE and FE→AFE transitions. The spontaneous polarization can be calculated by integrating of the area under the peaks when the other contributions (described above) are subtracted.

2.3.4 Dielectric spectroscopy

Dielectric measurements were done by Prof. H. Kresse (Institute for Physical Chemistry, Halle). For the experiments the samples were put into two-plate condensator with area $S = 2$ cm[2] and distance $d = 0.02$ cm apart. The signals were recorded using Hewlett Packard (HP 4192A) impedance analyzer.

2.4 NMR technique

Nuclear magnetic resonance (NMR) is well established in structural characterizations of liquids or compounds in solution [44]. Recent development of this powerful technique is also employed in research of solid polymers [45]. NMR offers numerous ways to study dynamic aspects over a large range of characteristic motional rates. The main advantage of NMR is its unprecedented selectivity. Since the discovery of NMR technique it has been intensively used in liquid crystal research [46, 47]. The most important aspect of NMR for study of liquid crystals is that the splitting of the proton and deuteron NMR lines is directly related to the orientational order parameter S and to the orientation of the nematic director $\mathbf{n}$. NMR has a variety of applications in liquid crystals: study of structure and conformation of mesogens [48], study of orientational order [46,49], determination of elastic constants [50] etc.

2.4.1 Theoretical overview

To describe a splitting observed in the NMR spectrum in the liquid crystalline state the following effects should be considered. A group giving the signal has a certain orientation with respect to the molecular core, which is defined by time-averaged molecular conformation. Then the molecular cores are somehow oriented with respect

to the magnetic field. This orientation is defined by the surface interaction (anchoring) and/or the structure of the phase. The molecules fluctuate and their orientational order is described by the orientational order parameter. Thus we have a series of co-ordinate frames and the transformations of the initial components of interaction tensor to the laboratory frame with a respective averaging will give the observed splitting.

Considering a certain physical quantity as a second-rank tensor $\hat{Q}$ which is related to a fragment of the molecule [51] it is useful to introduce a co-ordinate frame where this tensor is diagonal. Such frame we will call principle axis frame (PAF). For a quantitative description of the relation between molecular and microscopic properties it is necessary to define two more frames of reference. One is molecular-fixed frame (MF) with the axes (ζ, η, ξ) and the laboratory frame (LF) with the axis (x, y, z). The tensor which describes the ordering of the axis of the MF with respect to the axis of the LF is the so-called Saupe ordering tensor

$$S_{lm}^{\alpha\beta} = \frac{3}{4}\overline{\left(e_\alpha e_l \otimes e_\beta e_m + e_\alpha e_m \otimes e_\beta e_l\right)} - \frac{1}{2} \qquad (2.9)$$

where e designates the unit vectors of the LF ($\alpha, \beta = \zeta, \eta, \xi$) and MF ($l, m = x, y, z$). Then the averaged anisotropic part of the tensor $\hat{Q}$ in the LF can be expressed in terms of its components in the MF

$$\overline{Q}_{lm} = \frac{4}{9}Q_{ii}\overline{K_{\alpha\beta}^{ii}S_{lm}^{\alpha\beta}} \qquad (2.10)$$

here the tensor $\hat{K}$ is a so-called "conformation tensor" [52] which informs about the orientation of the PF with respect to the MF. Designating an interaction of interest by W, we can write the observed splitting in the form

$$\delta\nu^{(k)} = W_{zz} = S_{zz}^{\zeta\zeta}W_{\zeta\zeta} + \frac{1}{3}\left(S_{zz}^{\xi\xi} - S_{zz}^{\eta\eta}\right)\left(W_{\xi\xi} - W_{\eta\eta}\right) + \frac{4}{3}\left(S_{\xi\xi}W_{\xi\xi} + S_{\xi\xi}W_{\xi\eta} + S_{\zeta\eta}W_{\zeta\eta}\right) \quad (2.11)$$

where the z-axis is along the magnetic field **B** and indices (ζ, η, ξ) correspond to the molecular frame and $S = S_{zz}^{\zeta\zeta}$, $D = S_{zz}^{\xi\xi} - S_{zz}^{\eta\eta}$ are longitudal and transversal order parameters, respectively. This formula suits all three types of interactions which is designated by the symbol k: dipolar, quadrupolar and chemical shift. In the principle axis frame of W, the observed splitting will take the form:

$$W_{zz} = SW_{\zeta\zeta} + \frac{D}{3}\left(W_{\xi\xi} - W_{\eta\eta}\right) \qquad (2.12)$$

The most important element with respect to practical applications is $S_{zz}^{\zeta\zeta}$ which is a measure of the average projection of the ζ-axis of the MF onto the z-axis LF (director). The transversal order parameter D shows the difference in the projections of the both molecular axes ξ and η onto the LF z-axis. Thus it represents a measure of the preferred fluctuations onto the LF z-axis. Biaxiality of the phase is expressed by a non-zero parameter $S_{xx}^{\zeta\zeta} - S_{yy}^{\zeta\zeta} = \frac{3}{2}\overline{\sin^2\theta\sin 2\varphi}$ where θ and φ are the Eulerian angles of the orientation of the long molecular axis with respect to the LF (a choice of the MF so that the elements $S_{zz}^{\xi\eta}$, $S_{zz}^{\xi\xi}$, $S_{zz}^{\eta\zeta}$ are vanishing define the molecular long axis). It indicates

the difference in the average projections of the long molecular axes onto the transverse axes (x, y) of the LF , and, therefore, the existence of a further preferred direction (besides the director along z). The determination of this parameter requires to record angular dependences of the NMR spectra what means that biaxiality cannot be deduced from the spectra taken at $\varphi = 0$. Mainly the expressions 2.10 and 2.12 will be used in the analysis of the experimental data regarding to three main interactions which will be reviewed in the following section.

2.4.1.1 Types of interactions

Constructing the Hamiltonian of the nuclear spins in magnetic field, we should consider the following types of interactions taking place: Zeeman, dipole-dipole and quadrupole. All these interactions have been used in this work for characterizing conformation and dynamics of mesogens [53].

2.4.1.1.1 Zeeman interaction

Zeeman interaction (or diamagnetic shielding) between the magnetic moment and the static magnetic field $\mathbf{B_0}$ is linear in the spin operators:

$$H_Z = -\gamma\hbar\mathbf{I} \cdot \mathbf{B_0} \tag{2.13}$$

In presence of chemical surrounding the effective field in the nuclear site is reduced and the expression for the Hamiltonian gives

$$H_Z = -\gamma\hbar\mathbf{I} \cdot (\hat{1} - \hat{\sigma}) \cdot \mathbf{B_0} \tag{2.14}$$

where $\hat{\sigma}$ is a second-rank tensor. The interaction is proportional to the applied field and therefore is more important at higher fields. ^{1}H has one of the smallest (isotropic) average chemical shift ranges (10 ppm) compared with others (e.g., ^{13}C, 250 ppm). Diagonalization of the chemical shift tensor gives three components and if the field is directed along one of the principle axis (OZ) then in approximation of weak shielding the Zeeman interaction can be written in the form

$$H_Z = \hbar\omega_0 I_z \tag{2.15}$$

with the Larmor frequency

$$\omega_0 = -\gamma[1 - \sigma_{zz}]B_0 \tag{2.16}$$

and the component of chemical shift σ_{zz} along the external field. The transformation from the principle coordinate frame into the laboratory frame can be written in the following form

$$\sigma_{\alpha\beta} = \sigma_{ab} \cos\theta_{a,\alpha} \cos\theta_{b,\beta} \tag{2.17}$$

where $\theta_{i,j}$ is the angle between the principle i axis and the laboratory j axis.

In the isotropic phase the averaging over all orientation gives the chemical shift

$$\sigma_{iso} = \frac{1}{3} Tr\hat{\sigma} \tag{2.18}$$

At the same time, in the mesophase the difference between the component of the shift anisotropy component σ_{aniso} and σ_{iso} in the direction of the external field is given by

$$\sigma_{aniso} - \sigma_{iso} = \frac{2}{3}\left[\sigma_{zz} - \frac{1}{2}(\sigma_{xx} + \sigma_{yy})\right]S_{zz} + \frac{1}{3}(\sigma_{xx} - \sigma_{yy})(S_{xx} - S_{yy}) \qquad (2.19)$$

where coordinates (x, y, z) are given in the principle frame of the orientational order tensor. For aromatic carbons, $\sigma_{xx} - \sigma_{yy}$ is of the order of 100 ppm. In the liquid crystalline phase, fast conformational changes, such as π-flip of benzene rings around the para-axis, which is to a first approximation along the principal z-axis (in calamitics), effectively average out this difference so that $\sigma_{xx} \approx \sigma_{yy}$.

2.4.1.1.2 Dipole-Dipole interaction

The dipolar Hamiltonian H_D arises from direct dipole-dipole interactions between the nuclear magnetic moments and has the form

$$H_D = \frac{\gamma_i \gamma_j \hbar^2}{r_{i,j}^3} \mathbf{I_i} \cdot \hat{D}_{ij} \cdot \mathbf{I_j} \qquad (2.20)$$

where r_{ij} is the internuclear distance and $\hat{D}_{ij}$ the dipolar coupling tensor, may be defined by $(\delta_{ij} - 3e_i e_j)$ with e_i being x, y, and z components of a unit vector pointing from one spin to the other. H_D can be treated as a first-order perturbation for the Zeeman Hamiltonian and the truncated expression for H_D commuting with I_z has a form

$$H_D = -\frac{\gamma_i \gamma_j \hbar^2}{r_{i,j}^3} P_2(\cos\theta_{ij})[3I_{iz}I_{jz} - \mathbf{I_i} \cdot \mathbf{I_j}] \qquad (2.21)$$

Time averaged dipolar splitting caused by two interacting protons can be written in terms of Euler angles $\Omega = (\alpha, \beta, \gamma)$ by which the laboratory system is brought into coincidence with the principle axis system

$$\delta\nu_D = 3\left(\frac{\gamma}{2\pi}\right)^2 \frac{h}{r_{ij}^3}\left[S_{zz}(\frac{3}{2}\cos^2\beta_{ij} - \frac{1}{2}) + \frac{1}{2}(S_{xx} - S_{yy})\sin^2\beta_{ij}\cos 2\alpha_{ij}\right] \qquad (2.22)$$

2.4.1.1.3 Electric quadrupole interaction

The quadrupolar interactions occur when $I > \frac{1}{2}$ and arise from the interactions of the nuclear quadrupole moment eQ with the non-spherically symmetric electric field gradient at the site of the nucleus due to the electronic charge distribution of the atom or molecule

$$H_Q = \frac{eQ}{2I(2I-1)}\mathbf{I} \cdot V \cdot \mathbf{I} \qquad (2.23)$$

where the quadrupolar coupling tensor has been written in terms of the electric field gradient tensor $\hat{V}$ at the nuclear site. Thus, the Hamiltonian H_Q can be written in its principle axis (x, y, z) system

$$H_Q = \hbar\omega_Q \{[I_z^2 - \frac{1}{3}I(I+1)] + \frac{\eta}{3}(I_x^2 - I_y^2)\} \tag{2.24}$$

where the quadrupolar frequency ω_Q is

$$\omega_Q = \frac{3e^2qQ}{4I(2I-1)\hbar} \tag{2.25}$$

and $\eta = \dfrac{V_{xx} - V_{yy}}{V_{zz}}$ is the asymmetry parameter. In the uniaxial liquid crystalline phase the time-averaged dipolar splitting can be written in the form

$$H_Q = \frac{eQV_{zz}}{4I(2I-1)}[3I_z^2 - I(I+1)]\frac{3\cos^2\alpha_0 - 1}{2} \tag{2.26}$$

where V_{zz} is the component of the electric gradient tensor averaged by conformational and overall molecular motions.

2.4.2 Applications for bent-shaped molecules

If we consider, for example, an aromatic ring in a bent-shaped molecule, the dynamic and the orientation of the group with respect to the molecular frame should be taken into account. In Fig. 2.5 the direction of the principle axis frame of chemical-shift tensor is schemed. In presence of a π-flip only two components of the tensor are non-zero: parallel and perpendicular to the para-axis:

$$\overline{W}_{11} = W_{11}\cos^2\pi/3 + W_{22}\sin^2\pi/3$$
$$\overline{W}_{22} = W_{22}\cos^2\pi/3 + W_{11}\sin^2\pi/3 \tag{2.27}$$

Allowing the aromatic rings be tilted in the molecular frame we can express the components of the tensor in terms of the angle ε and the torsion angle φ (Fig. 5)

$$W_{\zeta\zeta} = \overline{W}_{11} - (\overline{W}_{11} - \overline{W}_{22})\sin^2\varepsilon - (\overline{W}_{11} + 2\overline{W}_{22})\sin^2\varepsilon\sin^2\varphi \tag{2.28}$$

The experiments performed in this research included the following steps:
- *Determination of the orientational order parameter S*. It was made by observing dipolar splitting of H in positions 9 and 11 in ^{1}H-NMR (when these positions are not substituted). Three spin system formed by a proton H11 and two protons H10 gives in the molecular frame an outer splitting $\Delta\nu_0 = k\,\Delta\nu_0^{(2)}$, where $\Delta\nu_0^{(2)}$ is the splitting in a two-spin system with a field parallel to the vector connecting the protons H10 and H11. The coefficient k depends on the precise geometry of the ring. Neglecting the transversal order parameter D the dipole splitting can be expressed by Eq. 2.12

$$\Delta\nu = \Delta\nu_0\, S(\frac{3}{2}\cos^2\beta - \frac{1}{2}) \tag{2.29}$$

where $\Delta \nu_0^{(2)} = -\dfrac{3K}{r^3}$ with $K = \dfrac{\gamma_i \gamma_j}{2\pi}\hbar$, $\Delta \nu_0^{(2)} = 47.25$ ppm for $r = 2.48$ Å, and

ß regards to an angle between the symmetry axis and the molecular long axis. We also measured shift anisotropy of carbons in positions 9 and 10 (11, 12). If the position 11 was substituted by fluorine, then the order parameter S could be found directly from ^{19}F-NMR measurements. The values of chemical shift anisotropy tensor were taken from literature [54]. Since there are no data on exactly the same molecules we had to choose the molecules with similar groups and substituents. Using their data on shift anisotropy as initial parameters we made refinement also with respect to the geometry of the rings to obtain a better agreement between different methods.

- *The bending angles ε and torsion angles φ for the rings A and B* have been determined from ^{13}C-NMR from the corresponding positions in the rings A and B with a help of Eq. 2.28. If the ring A is fluorinated, the angle ε could be found from the dipolar splitting by the neighboring proton.

2.4.3 Experimental setup

NMR experiments were made using Bruker MSL500 spectrometer operating at 500 MHz for proton resonance. The temperature of the sample was stabilized with an accuracy of 0.1ºC. ^{13}C-NMR spectra were recorded at 125.6 MHz in the isotropic state using pulse excitation together with continuous or WALTZ decoupling method. For the liquid crystalline state cross polarization technique with higher decoupling power was used, however not all lines could be resolved. The order parameters and some conformational features were also estimated on the base of ^{1}H-, ^{2}H-, ^{13}C-, ^{19}F-NMR experiments.
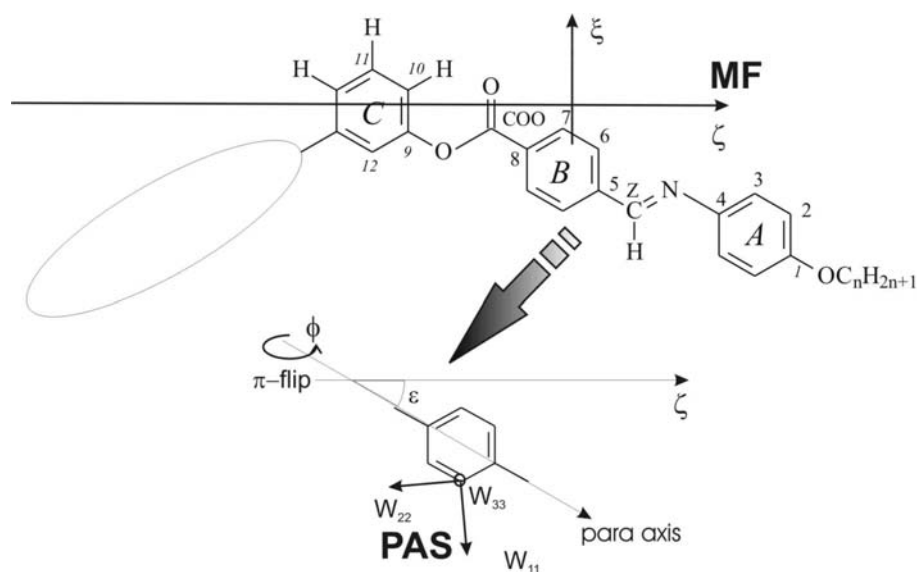
2.5 X-ray diffraction

Fig. 2.5: Co-ordinate frames and the assignment of the atomic positions in a bent-shaped molecule

2.5.1 Theoretical overview

X-ray provides one of the most definitive ways to determine the structure of liquid crystalline phases. This technique has played a key role in the identification of liquid crystalline phases and in quantitative study of several liquid crystalline phase transitions. However, conventional analysis and data interpretation of X-ray crystallography can not be applied to liquid crystals.

In this section we will review some principles of the X-ray scattering especially with application to the fibers of smectic liquid crystals. Usually, the tilt angle of calamitic molecules in the SmC phase can be obtained from the relative positions of the outer-diffuse scattering maxima in the wide-angle region. In case of an oriented monodomain sample these maxima are shifted from the equator if the layer normal is aligned parallel to the meridian and the appearance of the X-ray pattern depends on the orientation of the sample with respect to the beam. Often the experimental conditions do not allow obtaining monodomains with the same direction of the tilt. Instead, the sample is constituted from many domains so that the tilt directions of different domains are often distributed around the layer normal. The X-ray patterns do not change if the sample is rotated around the layer normal. The interpretation of the intensity distribution of the diffuse scattering should be modified in such geometry.

Let us consider "simple" smectic phases, where molecules form liquid-like layers and in direction perpendicular to the layer normal there is no positional correlation between the molecules from different layers. How does the lack of such correlation affect the scattering? The first model which shows some basic features of the scattering by "simple" smectic structure is a stack of crystalline two-dimensional layers. The differential cross-section $d^2\sigma/d\Omega$ of the scattering by potential $U(\mathbf{x})$ per unit solid angle can be expressed in the form [1]:

$$\frac{d^2\sigma}{d\Omega} \sim \frac{2\pi}{\hbar} \left| \langle \mathbf{k} | U | \mathbf{k}' \rangle \right|^2 \qquad (2.30)$$

In the approximation of kinematical scattering it is convenient to use the scattering amplitude [55, 56]

$$F(\mathbf{q}) = \int \rho(\mathbf{r}) e^{i\mathbf{q}\mathbf{r}} d^3 r \qquad (2.31)$$

Then the intensity in the direction of the scattering vector $\mathbf{q}$ will be given by a product (here a constant coefficient – square of the Thomson scattering length is omitted)

$$I(\mathbf{q}) = F(\mathbf{q}) F(\mathbf{q})^* \qquad (2.32)$$

The density of periodically distributed molecules can be expressed in terms of a convolution of the density of a molecule ρ_m with a density of a lattice ρ_l formed by the centers of the molecules (which is a sum of Dirac's delta functions in case of crystals)

$$\rho(\mathbf{r}) = \rho_m(\mathbf{r}) * \sum_i \delta(\mathbf{r} - \mathbf{r_i})$$

Since the scattering amplitude is a Fourier image of the density, the following expression is valid for the intensity

$$F(\mathbf{q}) = \left(\int \rho_m(\mathbf{r}) e^{i\mathbf{q}\mathbf{r}} d^3 r \right) \left(\int \rho_l(\mathbf{r}) e^{i\mathbf{q}\mathbf{r}} d^3 r \right) = F_{mol}(\mathbf{q}) F_{lattice}(\mathbf{q}) \qquad (2.33)$$

It is a product of the Fourier image of the molecule density (molecular form-factor) and the Fourier image of the lattice (structure factor) and the expression for the intensity will yield:

$$I(\mathbf{q}) = F_m^2(\mathbf{q})S(\mathbf{q})$$

A three dimensional lattice relevant to our problem can be modeled as a structure, consisting of points distributed over equidistant parallel planes. Then the number density will have the following form:

$$n(\mathbf{x}) = \sum_{\mathbf{l},p} \delta(\mathbf{x}_\perp - \mathbf{R}_l - \varphi_p)\delta(z - pc) \qquad (2.34)$$

where $\mathbf{x} = \{\mathbf{x}_\perp, z\}$, vectors $\mathbf{R}_l$ define an in-plane lattice, phase φ_p specifies the shift of the origin in different planes, periodically spaced with a period c. The phase φ_p will have a certain value when the molecules in different planes (index p) are correlated. When the correlation disappears the phase takes random values for different planes. Thus, the intensity (in this case equal to the structure function) is

$$I(\mathbf{q}) = \sum e^{-iq_z c(p-p')} e^{-i\mathbf{q}_\perp(\mathbf{R}_l - \mathbf{R}_{l'})} \left\langle e^{-iq_\perp(\varphi_p - \varphi_{p'})} \right\rangle \qquad (2.35)$$

where $\langle \ \rangle$ stands for averaging over the phases φ_p. Since the points in the neighboring planes are not correlated, the phases φ_p will be independent random variables for each plane and the average

$$\left\langle e^{-iq_\perp(\varphi_p - \varphi_{p'})} \right\rangle = \begin{cases} \delta_{pp'} & \text{if } \mathbf{q}_\perp \neq \mathbf{0} \\ 1 & \text{if } \mathbf{q}_\perp = \mathbf{0} \end{cases} \qquad (2.36)$$

In these two cases the structure function can be evaluated giving:

$$I(\mathbf{q}) = \begin{cases} N_\perp^2 N_\parallel^2 \sum_n \delta_{q_z, 2\pi n/c} & \text{if } \mathbf{q}_\perp = \mathbf{0} \\ N_\perp N_\parallel^2 \sum_{\mathbf{G}} \delta_{\mathbf{q}_\perp, \mathbf{G}} & \text{if } \mathbf{q}_\perp \neq \mathbf{0} \text{ for } \forall q_z \end{cases} \qquad (2.37)$$

Thus, the formula 2.38 shows Bragg peaks situated along the z-axis of the reciprocal space and lines parallel to the z-axis, crossing the plane $q_z = 0$ in the points of the reciprocal "in-plane lattice" $\mathbf{G}$ (Fig. 2.6a). Since all directions in the $q_\perp$ plane (due to the liquid nature of the layers) are equivalent the structure factor of the smectics represents a cylinder (Fig. 2.6c). The width of the cylinder in the $q_\perp$ direction is determined by the peculiarities of the short-range order ($\xi_\perp/2$ for the Lorentz line-shape) It is useful to compare this formula with the one of a real three-dimensional crystal consisting of parallel crystalline planes, where the order of the points is strictly correlated in all directions (Fig. 2.6 b). In this case the scattering pattern consists of Bragg reflections situated in the planes of reciprocal space parallel to the plane $q_z = 0$. Thus, the pattern will contain not only the reflections along the z-axis and in the xy-plane, but also cross-reflections (speaking in crystallographic terms hkl reflections with $h, k, l \neq 0$). When we remove the correlation between the planes the cross-reflections will smear and turn into the lines parallel to the z-axis of the reciprocal space; only the reflections along the z-axis will remain. Therefore the cross-reflections indicate the correlations between the molecules from different layers, while (00l) reflections stem from the periodicity of
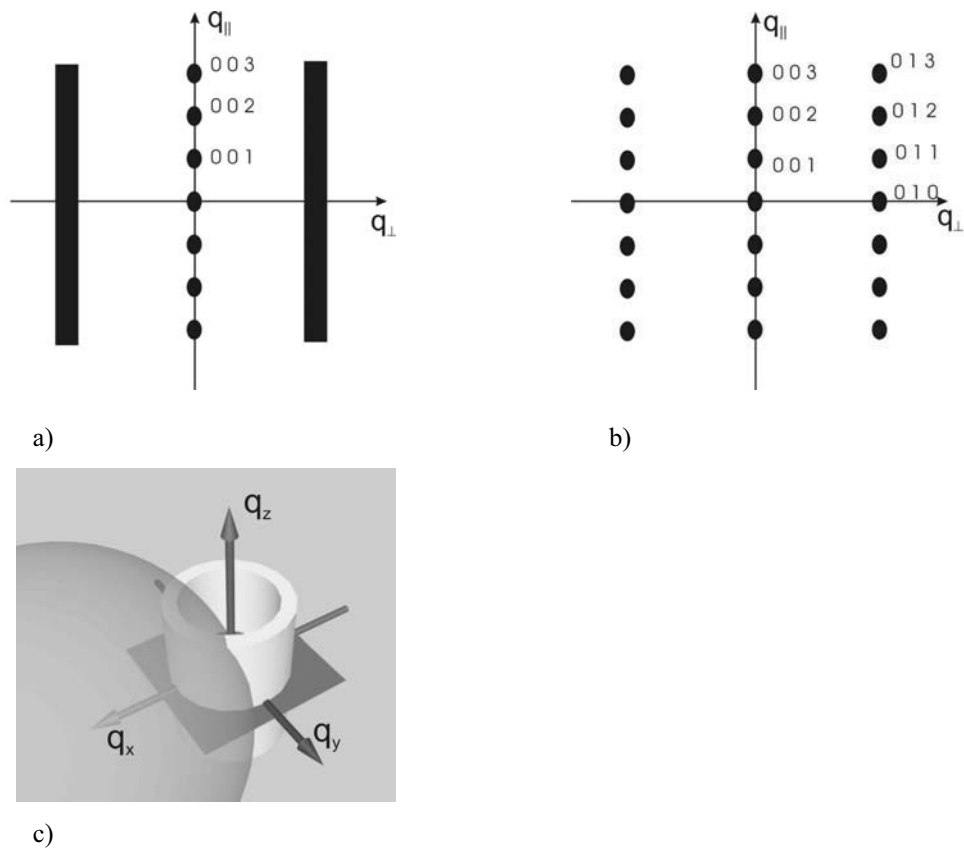
Fig. 2.6: a) Pattern of a structure with uncorrelated layers b) pattern of the crystalline phase (the layers are correlated) c) cylinder of the structure factor crossed by Ewald sphere

layers along z-axis, which remains if the layers are not correlated; and the lines parallel to $q_z = 0$ are just a Fourier image of points in a two-dimensional plane.

2.5.2 Experimental techniques

2.5.2.1 Experiments on non-oriented preparations

The preparation was made by filling up a thin glass capillary (Hilgenberg, Germany) with the liquid crystal compound in the isotropic phase. The thickness of the capillary was from 0.7 till 1.0 mm. The capillaries were put in the holders and then inserted into the ovens. The temperatures were regulated with the accuracy up to 0.1˚C.

The periodicity of the smectic layers has been measured using Guinier camera as well as a Guinier goniometer (Huber Diffraktionstechnik GmbH) (Fig. 2.7). The standard Coolidge tube served as a source of the X-rays. A germanium single-crystal monochromator filters the radiation of the Cu-K_α line ($\lambda = 1.54$ Å). A modified beam-stop enables measurements in the small-angle region up to $\theta = 0.8$ deg. Registration of the scattered radiation was performed using photo film in cylindrical geometry or computer controlled scintillator detector. The accuracy of the detector measurements was 0.001 deg.
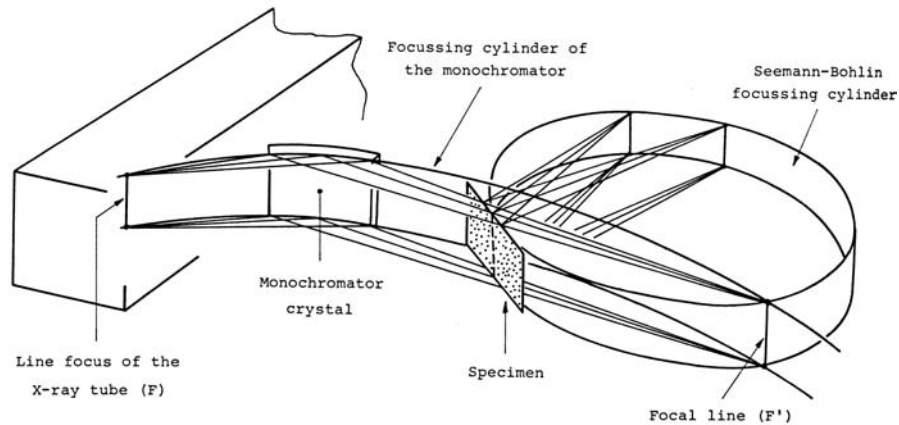
Fig. 2.7: Guinier method

The measurements in the small-angle region (0.6 – 3 deg) have been made using a custom-made small-angle camera based on the Kratky system.

2.5.2.2 Experiments on oriented samples

Oriented samples were obtained by very slow cooling of a drop of the mesogen from the isotropic into the liquid-crystalline state on a glass plate. In this case the smectic layers could be aligned parallel to the substrates and the X-ray beam was incident parallel to the smectic layers. The scattered radiation has been recorded using a 2D detector (HI-Star, Siemens AG).

The incident X-ray beam was parallel to the glass plate, which shadowed the lower part of the reciprocal sphere and an additional analysis was required to obtain the full picture. The experimental curves $I_{meas}(\chi)$ were normalized with a transmission function $t(\chi)$, in order to prevent experimentally caused errors by shadowing the lower part of the reciprocal space. The transmission function $t(\chi)$ was obtained by recording the scattering by the sample in the isotropic phase $I_{isotr}(\chi)$. In this ideal case the
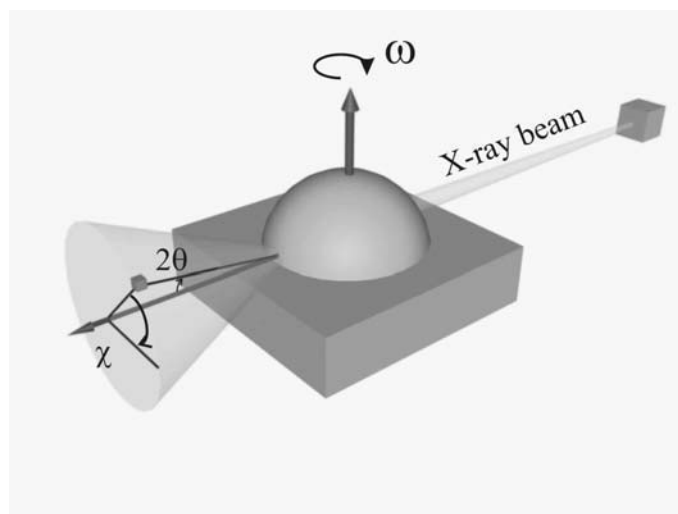

Fig. 2.8: Definition of angles in diffraction measurements on surface oriented samples

intensity of the diffuse scattering is independent of χ. Thus

$$t(\chi) = 1/I_{isotrop}(\chi) \qquad (2.38)$$

Then the corrected distribution of the scattering intensity in the mesophase is

$$I(\chi) = I_{meas}(\chi)t(\chi) \qquad (2.39)$$

The calibration allows a better determination of the positions of the maxima in the wide-angle region.

Chapter 3

Simulation of the X-ray scattering by fiber samples

The influence of the bent and the tilt of the molecules on the diffuse scattering is not trivial according to the present hand-books. In this chapter we will try to develop a model of scattering by fiber samples in order to answer the question: How does the bent shape of the molecules affect the scattering? To start with, the models of structure factors will be discussed. Then we will consider two ways of modeling the molecular form factor: approximating the molecules by rods or expressing the molecular form factor as a sum of the atomic form factors over atomic sites in the molecule. These two approaches will finally be used for developing of a computer program to simulate the scattering. As it has already been briefly outlined before (Chapter 2) the intensity of the scattering can be represented as a product of the structure factor and the molecular form factor. In ordinary smectic phases like SmA or SmC, the smectic layers are not correlated which leads to smearing of the cross-reflections (section 2.6).

3.2 Structure factor

3.2.1 General approach

General approach to build the structure factor is based on using the pair correlation function for the number-density of the particles and the potential of the interactions between them. Defining density-density correlation function [1] as

$$S_{nn} = \left\langle \left[n(\mathbf{x_1}) - \left\langle n(\mathbf{x_1}) \right\rangle \right] \left[n(\mathbf{x_2}) - \left\langle n(\mathbf{x_2}) \right\rangle \right] \right\rangle$$
$$= \left\langle \delta n(\mathbf{x_1}) \delta n(\mathbf{x_2}) \right\rangle \tag{3.1}$$

we obtain the general form of the structure factor

$$S(\mathbf{q}) = \frac{1}{V} \left| \int e^{-i\mathbf{q}\cdot\mathbf{x}} \left\langle n(\mathbf{x}) \right\rangle d^3 x \right|^2 + S_{nn}(\mathbf{q}) \tag{3.2}$$

where

$$S_{nn}(\mathbf{q}) = \frac{1}{V} \int d^3 x_1 d^3 x_2 e^{-iq\cdot(\mathbf{x_1}-\mathbf{x_2})} S_{nn}(\mathbf{x_1}, \mathbf{x_2}) \tag{3.3}$$

is a Fourier image of $S_{nn}(\mathbf{q})$. The information on the role of the intermolecular interactions is confined in the pair correlation function.

There are a few approaches to construct correlation functions. First is the straight-forward approach (which is hardly realizable) when the Hamiltonian of the interaction is substituted into the Gibbs distribution with further integration of the density products over the phase space [57]. Another way, which is a further development of the Gibbs formalism, is to solve the Bogolubov's chain-equations for the pair correlation function having chosen a certain interaction potential. However, this approach can be applied for relatively simple systems such as simple gases, systems with Coulomb interactions such as Debye-Hückel screening). This task can be reduced to a system of integral-differential equations which is usually very hard to solve.

Finally, a widely used method nowadays is molecular dynamics simulations (also Monte Carlo simulations). There the molecules are enabled to move in accordance with laws of Newton's mechanics and to interact with each over by an ad hoc potential [58]. The most burden of the computation in this kind of simulations is carried by computers.

3.2.2 Phenomenological polycrystalline approach: liquid-like order vs. crystalline

In this section we will consider another approach to construct the structure factor of the smectic phases. The structure factor should express the following features of the system:
- liquid-like order (short-range) of the molecules in the smectic plane (XY)
- quasi long-range order in the direction perpendicular to the smectic planes (Z)
- absence of the correlation between the layers

The situation with the last to points is clear. The effect of the short-range order is not trivial and the discussion which will follow is based on the arguments proposed in ref. [59; 56]. It is based on a polycrystalline model where the system is realized as a network (lattice) of points and two kinds of distortions are introduced. The distortions of the first kind do not disturb long range order: the molecules (points) are allowed to fluctuate about the vertexes of the network. When the distortions of the second kind take place the positions of a point is determined by the positions of its neighbors which results in destruction of the long-range order. To illustrate this we will consider a one-dimensional case – a periodic chain. The long-range order is defined by the density of the chain with the period $\bar{a}$

$$n(x) = \sum_k \delta(x - \bar{a}k) \tag{3.4}$$

where k is integer.

The second-kind distortion can be introduced in the following way. Consider the 1st point (molecule) which is fluctuating about, let us say, the 1st vertex and the 2nd point is about the 2nd vertex. Introduce a positional distribution function $H_1(x)$ of the 2nd point when the position of the first one is fixed. Then, the average distance between the molecules will be

$$\bar{a} = \int x H_1(x) dx \tag{3.5}$$

The same distribution function describes the positions of the nearest neighbor of any point in the chain. Then the distribution of the second nearest neighbor will be given as a self-convolution

$$H_2(x) = H_1(x) * H_1(x) \tag{3.6}$$

In the same manner

$$H_m(x) = \underbrace{H_1(x) * ... * H_1(x)}_{m \text{ times}} \tag{3.7}$$

Thus, the density distribution will be the sum

$$n(x) = H_0(x) + \sum_{m=-\infty}^{\infty} \overset{m}{\hat{H}_1}(x) \tag{3.8}$$

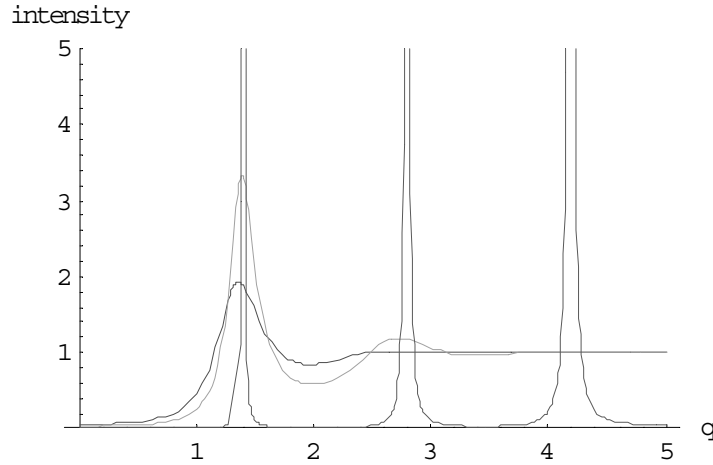The structure function will be obtained by its Fourier transformation which gives

Fig. 3.1: Calculated structure functions for different values of Δ: the red curve 1.1, the green curve 0.8 and the lilac 0.1 Å.

$$I(q) = \frac{1 - |F|^2}{1 - 2|F|\cos\chi + |F|^2} \tag{3.9}$$

where $\chi = q\,\overline{a}$ and $|F| = \Im[H_1(x + \overline{a})]$. As an example, consider a Gaussian distribution for $H_1(x)$

$$H_1(x + \overline{a}) = \frac{1}{\sqrt{2\pi}\Delta} e^{-\frac{1}{2}\frac{x^2}{\Delta^2}} \tag{3.10}$$

The structure function will be an oscillating function dying out at large q. It has maxima at $q = h\frac{2\pi}{\overline{a}}$ and minima at $q = (h + \frac{1}{2})\frac{2\pi}{\overline{a}}$.

The parameter $\varDelta$ is responsible for smearing of the maxima and minima: when $\Delta \to \infty$ only one central maximum remains at $q = 0$, which is characteristic for gases; another opposite limit $\Delta \to 0$, the structure function will consist of equidistant delta functions, which describes crystalline long-range positional order.

For SmA and SmC phases only one broad maxima in the wide-angle region is observed. The Eq. 3.9 can be used to fit the experimental curve where $\overline{a}$ is taken as the average intermolecular distance. From the ratio of the half-width of this maximum to the scattering vector's length measured in the experiments it can be estimated that the typical parameters are $\overline{a} = 4.5\,\text{Å}$ and $\Delta = 1.1\,\text{Å}$. The calculated structure functions for different values of $\varDelta$ are shown in Fig. 3.1. Since we consider the layers with isotropic in-plane distribution of the molecules, the formula deduced for a one-dimensional chain will be applicable as a radial structure function for two-dimensional fluid layers. However, in our calculations a Gaussian shape of the structure factor will be used. Such approximation gives a good qualitative picture of the structure factor in this case.

3.2.3 Notes on layer reflections

In crystalline phase a stack of layers gives a periodic set of delta-functions in the reciprocal space sometimes called "Dirac's comb". The modulation of such structure

factor by a molecular form factor (and further by Debye-Waller factor) would give an experimentally observed intensity distribution of the reflections (see Chapter 1). Thus it seems plausible, that choosing different molecular models it is possible to evaluate them with respect to the intensity distribution they give.

The case of smectic liquid crystals is more complicated. Considering, for instance, the SmA phase the translational order is characterized in the direction z along the layer normal by the density

$$\rho(z) = \frac{2}{d} \sum_{n=0}^{\infty} \tau_n \cos(nq_0 z)$$

$$\tau_n = \left\langle \cos(nq_0 z) \right\rangle$$

(3.11)

where d is the layer spacing and the corresponding wave-vector $q_0 = 2\pi/d$. The quantities τ_n are the smectic order parameters. In the conventional liquid crystals formed by rod-like molecules the main contribution is given only by first harmonic τ_1 (the density modulation is sinusoidal), therefore, the structure factor is not the Dirac's comb any more and only one layer reflection is observed. On the other hand, mesophases formed by bent-shaped molecules (SmCP, B_5) are more "rigid": they usually contain up to five layer reflections. However, generally, the partially ordered system should be described by all order parameters τ_n on which the intensity of the peaks will depend (apart from molecular form factor). Since the information on both conformation and ordering is not available, strictly speaking, it is not possible to estimate conformation from the intensity of the layer reflections. In some cases when the pattern contains many reflections or an unusual (not just monotonically decreasing, see, for example Chapter 9) sequence of the intensities it is possible to make an estimation like it is made in Chapter 9.

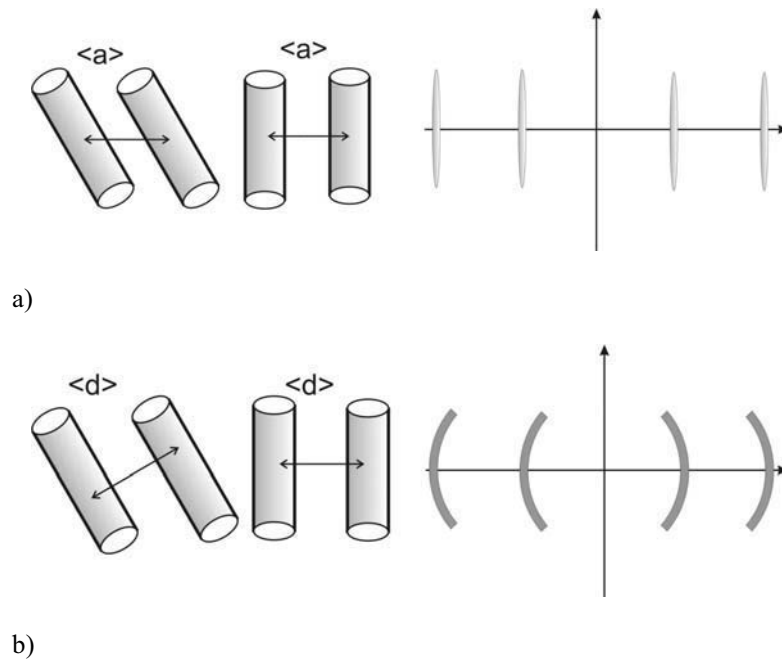## 3.2.4 Models for in-plane distribution of the molecules

a)

b)

Fig. 3.2: Models of the molecular packing in layers: a) model 1 the distance between the centers of the molecules is independent of their tilt; b) model 2 the distance between the long axis is constant

In the SmA phase the centers of the molecules are isotropicaly distributed in a plane with the mean distance $\bar{a}$. Since the smectic layers are not correlated as discussed in Chapter 2, the scattering intensity caused by lateral ordering of the molecules will be an incoherent sum of the intensities of each smectic layer. Then the Fourier transform of the points in the plane gives infinite lines perpendicular to the planes in the reciprocal space. The rest of the pattern is formed by a section of these lines with a molecular form factor, which is a disk, and further cylindrical averaging. It will result in maxima on the equator.

In the SmC phase one can consider two models for the arrangements of the molecules within the layers (Fig. 3.2). The first model assumes that the centers of the molecules in the layers are distributed in random way although the distance between the centers is constant (Fig. 3.2a). The fiber pattern contains two lines perpendicular to the equator. The lines cross the equator at $q = 2\pi / \bar{a}$ in the reciprocal space (Fig. 3.3). Experimentally observed pattern is different. There the diffuse scattering is distributed over arcs not lines. In order to comply with experiment we should review the assumption that the distance between the centers of the molecules is constant. The scattering will be distributed over an arc only in case when the distance between a pair of molecules will depend on their mutual orientation so that the distance between the molecular axis is constant (Fig. 3.2b and 3.4). This condition is equivalent to the model of closely packed cylinder-like molecules. The inclination of the molecules leads to the increase of the distance between their centers Fig. 3.5 in the direction of the tilt. The angular dependence can be easily calculated. The centers are situated in a "smectic" plane which crosses the inclined cylinders. The section of a cylinder by a plane is an ellipse. Then the distance between the centers is $a(\varphi) = 2\bar{a}\sqrt{\dfrac{\cos^2 \varphi}{\cos^2 \alpha} + \sin^2 \varphi}$. The formation of the scattering pattern is shown in Fig. 3.5.
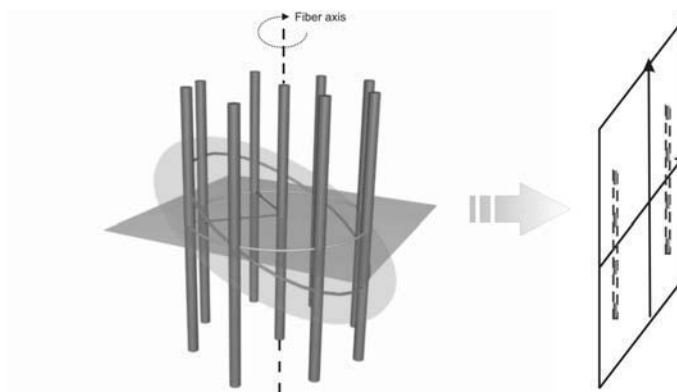
Fig. 3.3: Formation of the X-ray pattern for model 1: the distance between the centers of any pair of molecules is independent of their mutual orientation
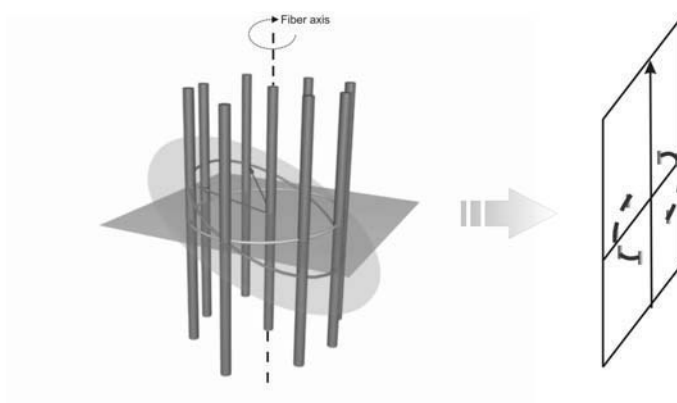

Fig. 3.4: Formation of the X-ray pattern for model 2: the distance between the long axis of the molecules is constant
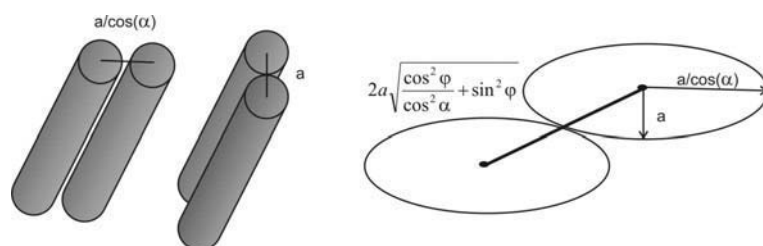

Fig. 3.5: Calculation of the intermolecular distance in the model 2

3.3 Simulation of scattering

A qualitative consideration of the scattering by fibers of orthogonal and tilted molecules we will start with calculation of the scattering by rods. First, we approximate the concerning molecules by rods of uniform density and investigate the problem of scattering off one molecule, which is equivalent to the calculation of the molecular form factor. The aim of this task is to find the main features of the cylindrically averaged molecular form factor of calamitic and bent-shaped molecules, such as directions of scattering intensity maxima.

There are two ways of presenting structure of the molecule. First, a molecule can be defined by the positions of the atoms. The motions of different groups are neglected and it is supposed that the density is localized in the atoms sites. The molecular form factor will be expressed as a sum of the atomic form factors. This approach has some considerable draw backs since we are dealing with large molecules in liquid-like phases and the motions of different molecular units can not be neglected.

Another way is to approximate the molecules by cylinders assuming, that the density is uniformly distributed over the volume of the cylinder. Such approach is very convenient since in the molecules commit motions and averaging is required.

In the following chapter, we shall also proceed with some actual models of molecules created by Cerius2 molecular simulation software.

3.3.1 Modeling of the molecules from atoms

The structure of a molecule can be defined by the positions of the constituting atoms
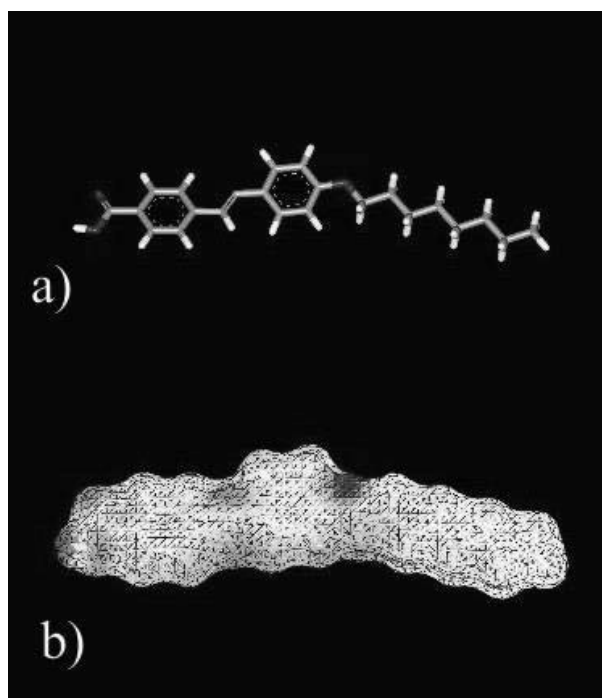

Fig. 3.5: a) Model of a molecule defined by the set of the atom positions and b) its effective volume

(Fig. 3.5). Such option can be offered by some commercial molecular modeling software, for example, Cerius2. Using the algorithms of energy minimization an optimal conformation is calculated giving coordinates of atoms as an input. The program, which

we developed, reads these data and calculates the scattering intensity in different orientations of the molecule. The program estimates the form factor using the analytical expression

$$f(\frac{q}{4\pi}) = \sum_{j=1}^{4} a_j e^{-b_j(q/4\pi)^2} + c \qquad (3.12)$$

where a, d and c are parameters taken from tables [55]. After averaging over rotations around the fiber axis, the transversal intensity distribution has been fitted by the intensity obtained from scattering from the cylinder with the fitting parameter – radius a. Actually the similar modeling of different phases have been done using the models of the molecules and they give very similar results to the scattering from cylinder.

3.3.2 Approximation by cylinders

The simplest case is the scattering by a single rod (cylinder) of the radius a, the length c and a uniform density ρ_0. The scattering amplitude of a single cylinder aligned along the axis OZ is:

$$F_m(q_x q_y q_z) = \int_{-c/2}^{c/2} e^{iq_z z} \int_{x^2+y^2 \leq a^2} e^{i(q_x x+q_y y)} dxdy = 4\pi a J_1(a\sqrt{q_x^2+q_y^2})\frac{\sin(cq_z/2)}{q_z\sqrt{q_x^2+q_y^2}} \quad (3.13)$$

or in cylindrical coordinates

$$F_m(q_\perp q_z) = 4\pi a J_1(a q_\perp)\frac{\sin(cq_z/2)}{q_z q_\perp} \qquad (3.14)$$

Thus, the intensity of the scattering by a single cylinder gives

$$F_m^2(q_\perp q_z) = 16\pi^2 a^2 r_0^2 J_1^2(a q_\perp)\frac{\sin^2(cq_z/2)}{(q_z q_\perp)^2} \qquad (3.15)$$

This formula can serve as a model of a molecular form factor for a rod-like molecule.

3.4 Scattering by rod-like molecules

In order to model the scattering from one layer of the SmA phase the form-factor (3.15) obtained above should be multiplied by the corresponding structure factor discussed in previous chapter. The resulting pattern is shown in Fig. 3.6.

The SmC phase is formed by tilted molecules. The tilt in the real space is equivalent to the rotation in the reciprocal space (see for example [60]). We incline the cylinder in ZOY plane by an angle ψ. A corresponding rotation matrix is:

$$\hat{A}_x^\psi = \begin{pmatrix} 1 & \cos(\psi) & \sin(\psi) \\ 0 & -\sin(\psi) & \cos(\psi) \\ 0 & 0 & 0 \end{pmatrix} \qquad (3.16)$$
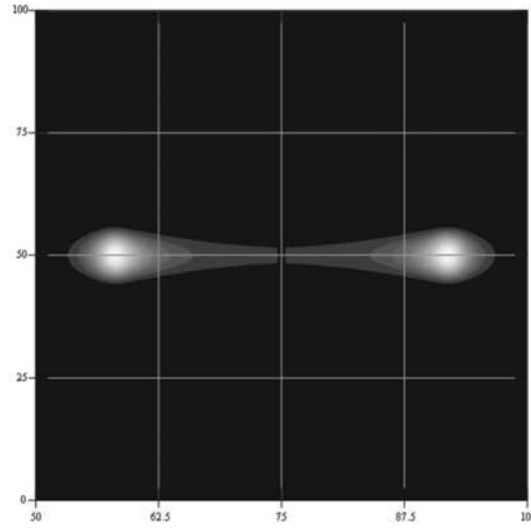
Fig. 3.6: Simulated pattern of the wide-angle scattering in the SmA phase

Using the property of the Fourier transform the molecular form factor can be expressed in terms of rotation in the reciprocal space $\vec{q}' = \hat{A}_x^{\psi} \vec{q}$. We obtain the amplitude $F(\vec{q}')$ which is merely a turned image. Taking the axis OZ as a fiber axis and passing to the cylindrical coordinates $\{q_x, q_y, q_z\} \rightarrow \{q_\perp, \varphi, q_z\}$, the form factor will be expressed

$$F_{inclined\,rod}(q'_\perp, \varphi, q'_z, \psi) = F_{rod}(q'_\perp, \varphi, q'_z)|_\psi \qquad (3.17)$$

where ψ is a parameter – tilt angle.

Before calculation of the total scattering, let us consider the structure factor of two models:

1. the distance between the centers of the molecules is constant and independent of their mutual orientation
2. the distance between the molecular long axis is constant

The structure factor in the first model is independent of the azimuth φ and can be taken out of the product with the structure factor. Then the full intensity gives

$$I(\vec{q}) = \left(\left\langle F_{inclined\,rod}(q_\perp, \varphi, q) \, S(q_\perp) \right\rangle |_\varphi \right)^2 = \left(\frac{1}{2\pi} \int_0^{2\pi} F_{inclined\,rod}(q_\perp, \varphi, q) \, S(q_\perp) d\varphi \right)^2 =$$

$$\left(S(q_\perp) \left\langle F_{inclined\,rod}(q_\perp, \varphi, q) \right\rangle \right)^2 \qquad (3.18)$$

For the second model the structure factor will depend on the azimuth angle and the average of the product will not be equal to the product of the averaged form and structure factors:

$$I(\vec{q}) = \left(\left\langle F_{inclined\,rod}(q_\perp, \varphi, q) \, S(q_\perp, \varphi) \right\rangle |_\varphi \right)^2 \qquad (3.19)$$
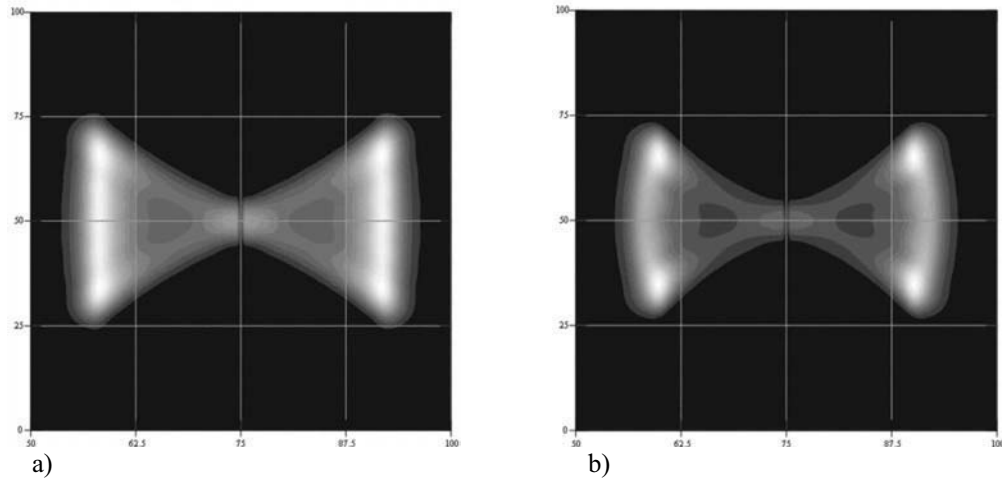
a)   b)

Fig. 3.7: Simulated pattern of the wide-angle scattering in the SmC phase a) model 1 and b) model 2

The patters computed for these two models are shown in Fig. 3.7a and b. There are two maxima below and above the equator of the pattern. In the model 1 the maxima are situated on a straight line perpendicular to the equator and for the model 2 the scattering is distributed over arcs.

3.5 Scattering by bent-shaped molecules

Molecular form factor of a bent-shaped molecule can be expressed using the previous results obtained for cylinders. Consider a model of a bent shaped molecule consisting of a pair of cylinders inclined with respect to the vertical axis as it is shown in Fig. 3.8. This model looks very similar to the model of the SmC phase with molecules arranged in anticlinic fashion. However, this case is essentially different. In case of the SmC phase there is no correlation between the molecules in different layers (except for the z-components along the layer normal) and the molecules scatter incoherently from adjacent layers so that the total intensity is a sum of the intensities scattered from the two parts:

$$I(\vec{q}) = I_{up}(\vec{q}) + I_{down}(\vec{q}) = F_{up}F_{up}^* + F_{down}F_{down}^* \qquad (3.20)$$

where "up" and "down" correspond to the upper and lower cylinders (Fig. 3.8). In bent-shaped molecules the two parts of the molecules are bound together and the interference should be accounted. The formula for the scattered intensity will have another form

$$I(\vec{q}) = (F_{up} + F_{down})(F_{up} + F_{down})^* \qquad (3.21)$$

Scattering amplitudes F_{up} and F_{down} can be evaluated using our previous results. The upper cylinder is obtained by a shift of an orthogonal cylinder along z-axis by $d = 0.5c\cos(\varepsilon)$ and then turned along y-axis by the angle $\varepsilon = (\pi - \alpha)/2$, where α is a bending angle. Thus the scattering amplitude gives:

$$F_{up}(x,y,z) = \frac{4a\,J_1(a\sqrt{x^2\cos^2\varepsilon + z^2\sin^2\varepsilon + xy\sin 2\varepsilon + y^2})\sin(c(z\cos\varepsilon - x\sin\varepsilon)/2)}{(z\cos\varepsilon - x\sin\varepsilon)\sqrt{x^2\cos^2\varepsilon + z^2\sin^2\varepsilon + xy\sin 2\varepsilon + y^2}}e^{-\frac{z\,c\cos(\varepsilon)}{2}} \qquad (3.22)$$
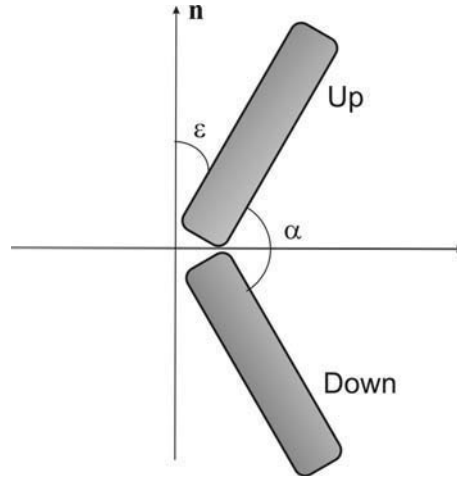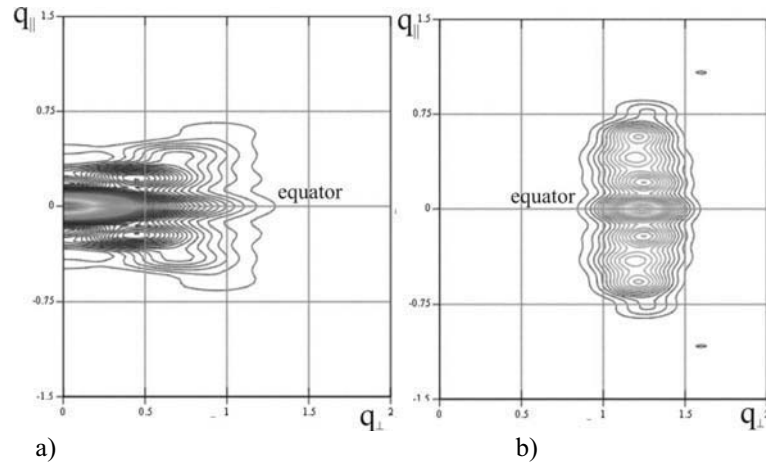
Fig. 3.8: Model of a bent-shaped molecule

a)   b)

Fig. 3.9: a) Simulated averaged form factor of a bent-shaped molecule ($\alpha = 120$ deg) in orthogonal arrangement ($\theta = 0$ deg); b) simulated wide-angle intensity corresponding to the form-factor a) (SmAP phase modeled by cylinders)

a similar expression is obtained for F_{down} by a change $\varepsilon \rightarrow -\varepsilon$ and $e^{-\frac{z\,c\cos(\varepsilon)}{2}} \rightarrow e^{+\frac{z\,c\cos(\varepsilon)}{2}}$. Putting the terms into the expression 3.21 and passing to the cylindrical coordinates we obtain the scattered intensity for the bent-shaped molecule $I(r,\varphi,z)$. Scattering by a fiber of orthogonally aligned molecules will be expressed as an integral:

$$I_{fiber}(r,z) = \langle I(r,\varphi,z) \rangle = \frac{1}{2\pi} \int_{0}^{2\pi} I(r,\varphi,z)d\varphi \qquad (3.23)$$

The Fig. 3.9 below shows an averaged form factor (a) and the intensities (b) calculated for a bent-shaped molecule with a bending angle 120 deg. Using two "equivalent" rod-like molecules inclined by the angle of 120 deg to each other we find that the intensity maxima are above and below the equator (Fig. 3.7b). The effect of the interference is quite large: the intensity is scattered mostly along the equator for the bent molecule and out of the equator for the rod-like molecule. Such pattern corresponds to the SmA or SmAP phase formed by bent-shaped molecules. Similar results were obtained from the
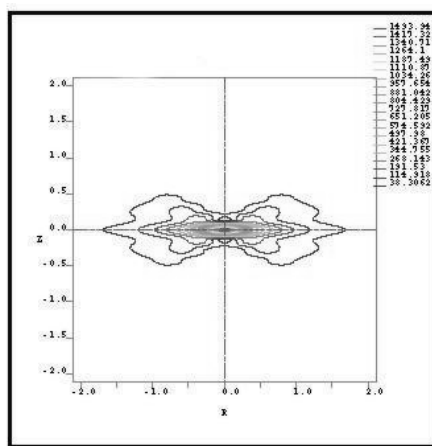
a)
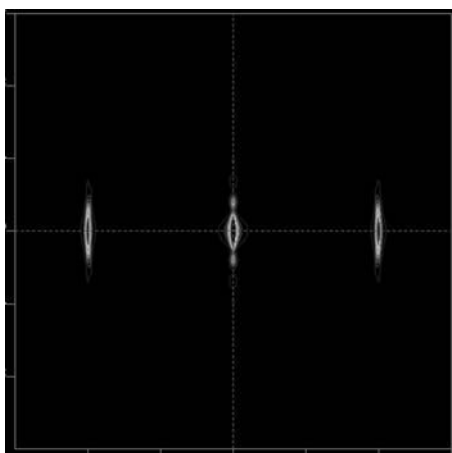
b)

Fig. 3.10: a) and b) are the same as in Fig. 3.9 but molecular models used in Cerius2 software

models in Cerius2 software (Fig. 3.10). The experimental measurements of the diffuse scattering distribution in the SmA and the SmAP phases described in Chapter 5 confirmed these findings.

A tilted smectic phase with a polar order along the layers is called SmCP phase. The rotation of the molecules along the long axis is hampered. The X-ray pattern of such phase can be obtained by an additional tilt of the rods. The inclination of the model of the bent-shaped molecule performed by rotation around the x-axis and further averaging over all possible directions results in scattering out of the equator. The averaged form factor and the calculated pattern (30 deg tilt and 120 deg bending) are shown in Fig. 3.11. The intensity on the equator is quite high which agrees with the experimental observations shown in the following chapters. Some additional modulations seen in the calculated pattern probably appear because of the voids between the two cylinders. The density within a molecule is distributed more smoothly and such modulations are not observed experimentally. The effect of bending on the scattering pattern can be seen from the averaged form factors shown in Fig. 3.13. There the tilt angle is fixed (30 deg) and the bending angle is changing from 90 deg till 180 deg. The intensity on the equator is smaller when the bending angle is larger. Similar
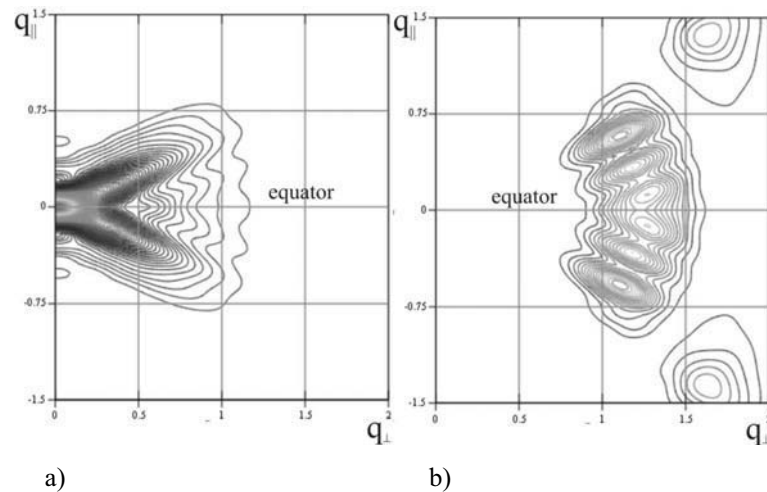
a)   b)

Fig. 3.11: a) Simulated averaged form factor of a bent-shaped molecule (α = 120 deg) in tilted arrangement (θ = 30 deg); b) simulated wide-angle maxima corresponding to the form-factor a) (SmCP phase modeled by cylinders).
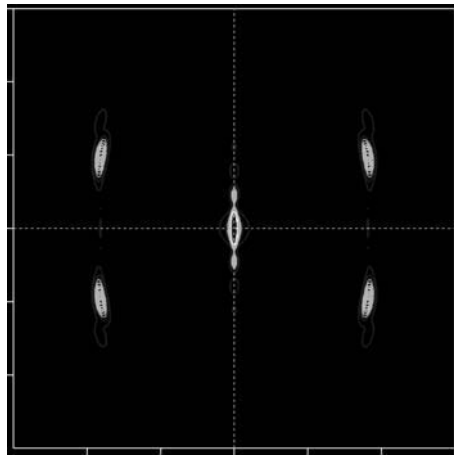

Fig. 3.12: Simulated pattern of the B_5 phase (Cerius softaware) there are maxima out and on the equator.

simulations have been performed on models of molecules using Cerius2 software. These data are in good agreement with the results obtained from cylinders.

Another mesophase formed by bent-shaped molecules is B_5. The molecules form a rectangular network within the layers. Assuming that the intensity of the "structure factor cylinder" has Gaussian distribution we can perform similar calculations to simulate the X-ray pattern. The simulations have been done using Cerius2 software (Fig. 3.12). The characteristic features of these patterns are two peaks out of the equator like in SmCP phase, as well as small peaks on the equator. All three peaks lie on one line. Experimental observations of such behavior are reported in Chapter 9.

3.6 Conclusion

Straight forward calculations show that even in partially oriented SmC samples where the layer normal has a preferred direction while the **c**-director has a random distribution
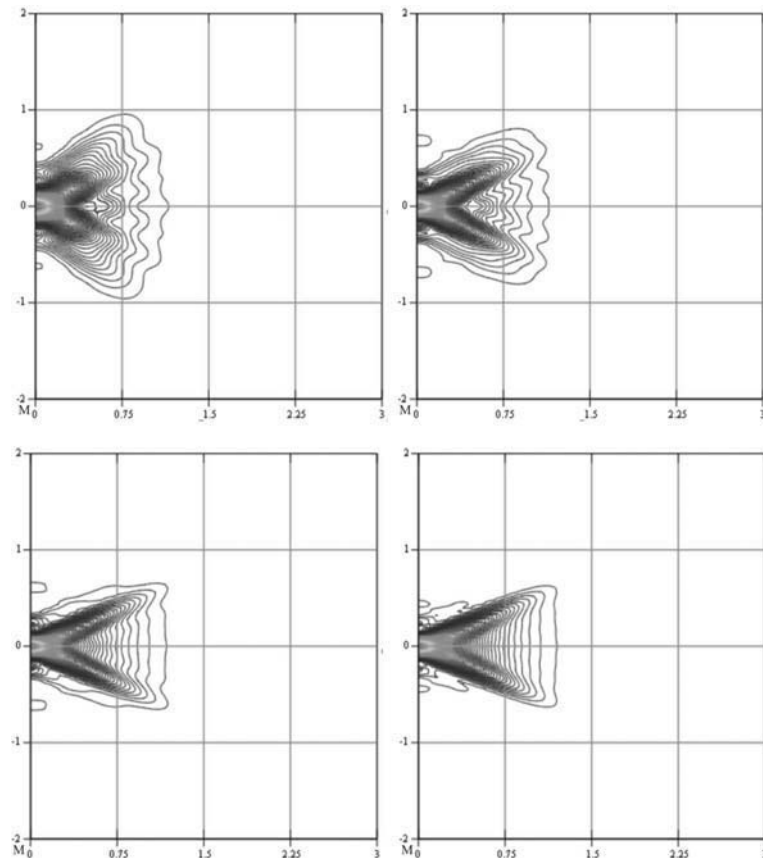
Fig. 3.13: Averaged form factors in the SmCP phase at constant tilt 30 deg and bending angles
a) 90 deg, b)120 deg, c)160 deg, d) 180 deg

perpendicular to the layer normal, the wide-angle scattering possesses two maxima: below and above the equator.

The splitting is visible for angles larger than ~ 8 deg, however it depends on the ratio radius to length of the cylinders as well as on the Debye-Waller factor which was not accounted in these estimations. The intensity is distributed over arcs not stripes indicating the validity of the model 2 for the in-plane distribution of the molecules. This fact follows from the idea of close packing of the cylinders in smectic layers that steric interactions dominate in the stabilization of the smectic A and C phases, which is characteristic for condensed matter systems [1].

In case of bent-shaped molecules the two parts ("wings") equivalent to tilted calamitics molecules are connected in one piece and this situation is not similar to the scattering by an anticlinic SmC phase. Simulations performed on cylinders and models of molecules show the importance of the interference from two "wings" of bent-shaped molecules. In case of the orthogonal arrangement such as in SmA or SmAP phases of the bent-shaped compound, the form factor is "stretched" along the equator (Fig. 3.9). Bending of the molecules will lead to an increase of the scattering along the equator but this effect is quite weak (Fig. 3.13). The influence of bending observed in model calculations is shown in Fig. 3.13. Decreasing the bent angle the intensity on the equator is enhanced (Fig. 3.13c, d)

The tilt of the bent molecules will result in increase of the scattering intensity out of the equator. This process is continuous and the same effect can be obtained either by bending of a tilted molecule or tilting of a bent molecule. Scattering out of the

equator is brought by tilt of the molecules, but an additional intensity on the equator is observed which is mostly controlled by the bending. That means that the tilt of the cylinder leads to splitting of the scattering maxima. An additional bending of the cylinder results in the increase of the intensity on the equator.

These calculations qualitatively agree with the experimental observations. Wide-angle scattering in the SmCP phase has high intensity on the equator. Especially it is pronounced in the B_5 phase where we can see a "cut" of the form factor and can distinguish these three maxima. On the other hand real patterns are also affected by the degree of order, fluctuations as well as by the mozaisity of the sample, therefore, these calculations give just a qualitative picture of the phenomena of scattering by fibers of bent-shaped molecules.

Chapter 4

Spontaneous chiral ordering in the nematic phase

Nematic phases are usually uniaxial. A non-polar biaxial nematic phase, predicted theoretically by M.J. Freiser [61] has been experimentally discovered in lyotropic systems [62] and later in liquid crystalline side-chain polymers [63]. As first discussed by H.R. Brand *et al* [64], bent-shaped mesogens are promising candidates for polar biaxial nematics. Nematic phases of different symmetries have also been predicted in the ref. [6]. Similarly to smectic phases of the same symmetry, polar biaxial nematics should possess ferro-, ferri- or antiferroelectric properties [12]. Recently a number of bent-core mesogens exhibiting the nematic phase has been reported in the literature. Some of these compounds form the nematic phase only [65-67]. Other compounds show the usual smectic and "banana" phases in addition to the nematic phase [23, 68, 69]. Up to now no considerable anomalies have been observed in these nematic phases, probably since in most cases the shape of the molecules can be regarded as approximately rod-like. Furthermore, computer simulations give evidence that bent molecules can form the nematic phase when the bending angle α is above a critical value [10]. It was shown by these simulations that the nematic phase can adopt a helical superstructure near the transition into the polar smectic phase which corresponds to a conical twist-bend deformation.

In this chapter we present a new achiral banana-shaped mesogen exhibiting a nematic phase with unusual optical and electro-optical properties (Fig. 4.1). In addition, an unknown low-temperature phase preliminary designated as X occurs. The compound under study is 4-chlororesorcinol bis[4-(4-n-dodecyloxybenzoyloxy)benzoate].
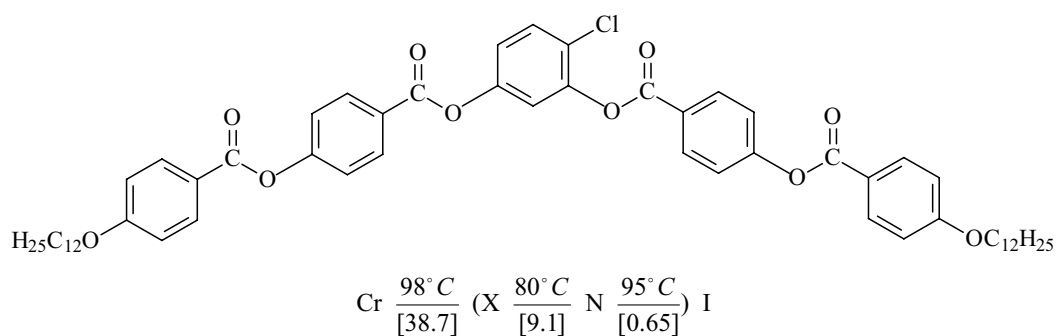

$$\text{Cr} \ \frac{98\,^{\circ}C}{[38.7]} \ (\text{X} \ \frac{80\,^{\circ}C}{[9.1]} \ \text{N} \ \frac{95\,^{\circ}C}{[0.65]}) \ \text{I}$$

Fig. 4.1: Structural formula of the compound IV/**1** (the numbers in square brackets below the transition temperatures denote the transition enthalpies)

In the nematic phase regions with different optical properties have been observed by means of polarizing microscopy over the whole temperature range of the mesophase. Starting from the crossed position of the polarizers and rotating one polarizer clockwise by a small angle (10 – 20 deg) we observed light and dark domains. Rotating the polarizer anticlockwise by the same angle the effect is reversed, that means, the previously dark domains now appear light and vice versa (see Fig. 4.2). In addition, these domains have also been distinguished by illuminating the cell with left or right circular polarized light in the reflection mode of the microscope. The formation of the regions with opposite handedness in the nematic phase can be explain as a result of a
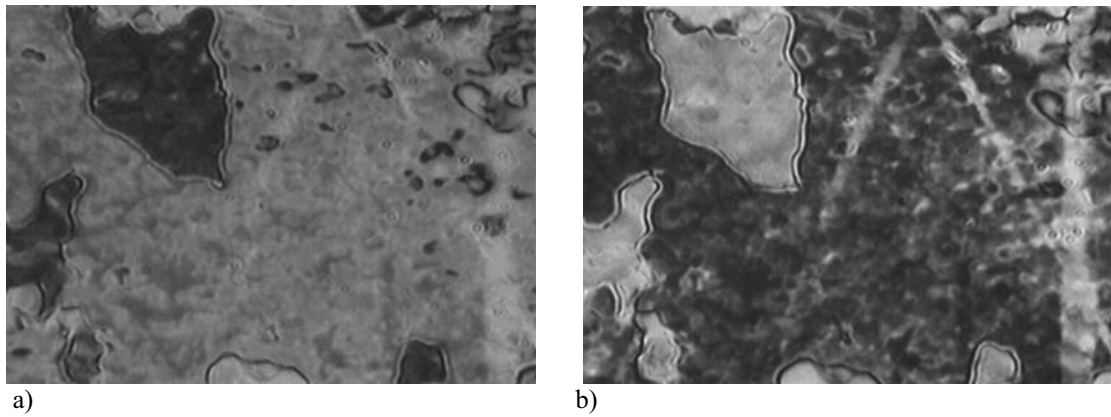
Fig. 4.2: Texture of the nematic phase observed by rotating one polarizer by 15 deg a) clockwise and b) anticlockwise from the crossed polarizer position indicating domains of opposite handedness
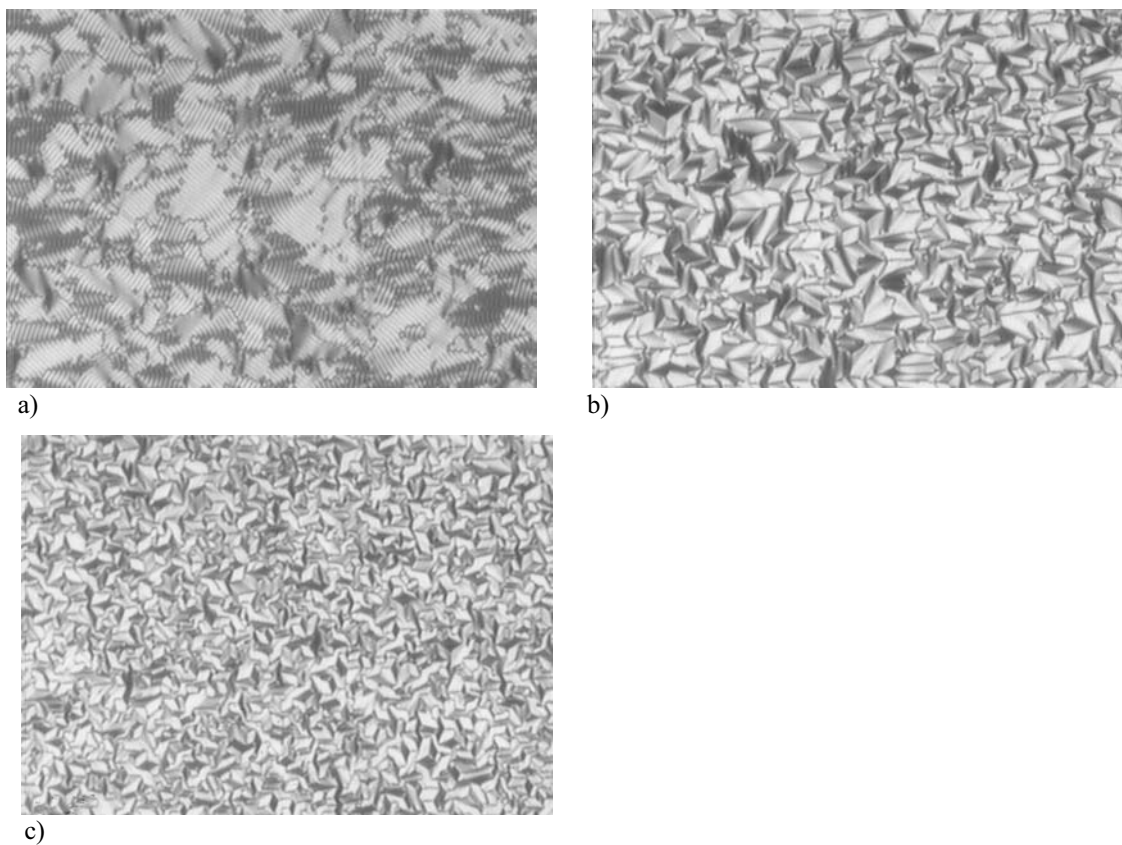

Fig. 4.3: Field-induced texture change of the nematic phase (90°C; cell thickness: 6 μm): a) 17 V, b) 25 V and c) 50 V

spontaneous macroscopic twist. We found that the domains of opposite handedness are formed with equal probability.

It should be noted that these domains occur in random places of the sandwich cell and can be changed by a mechanical stress or by a temperature change. The pitch of the twisted domains seems to be larger than the sample thickness.

The X-ray measurements revealed no layer structure and the presence of the cybotactic groups in well-oriented samples is compatible with the properties of the nematic phase

Another interesting finding should be mentioned in this connection. Applying a d.c. field to the planar oriented nematic phase we observed a domain pattern with equidistant stripes parallel to the original director orientation appears, but this pattern is disturbed by electrohydrodynamic processes as a consequence of the relatively high conductivity. With increasing voltage the long-wave nematic director fluctuations become weaker and a myeline texture with fine equidistant stripes arises (Fig. 4.3a) which transforms into a fan-shaped texture with further increasing voltage (see Fig. 4.3 and 4). This field-induced fan-shaped texture which is reminiscent of a smectic phase is observed in the whole existence region of the nematic phase. If the electric field is removed the texture of the planar oriented nematic phase reappears. Although the field-induced formation of a smectic phase cannot be excluded it is more probable that the original partially twisted sample is deformed by the electric field in such a way that the fan-shaped texture is built up which is also characteristic of a cholesteric phase, but we have no explanation of the mechanism by which such fan-shaped texture can be
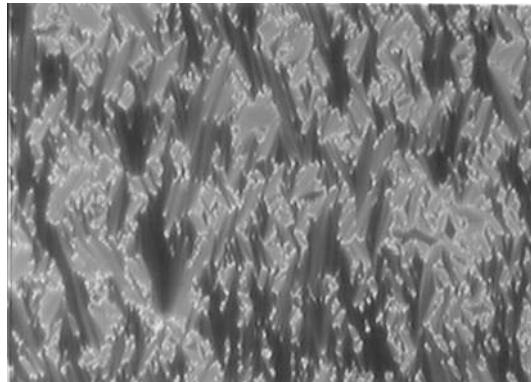

Fig. 4.4: Field-induced fan-shaped texture in the nematic phase (90°C; cell thickness: 10 μm; applied voltage: 100 V)

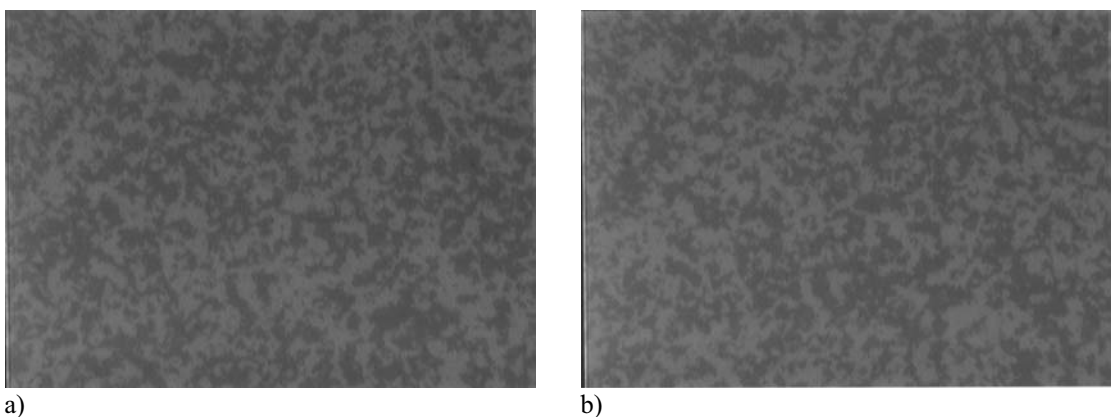a)   b)

Fig. 4.5: Texture of the X phase observed by rotating one polarizer by 8 deg a) clockwise and b) anticlockwise from the crossed polarizer position indicating domains of opposite handedness (75°C; sample thickness: 10 μm)

generated. We were not able to detect a polar switching. Also dielectric measurements gave no evidence for a positive dipole correlation.

Spontaneous twisting has also been found in the low-temperature X phase. This phase is highly viscous and shows complete extinction between crossed polarizers. Closer optical examinations gave evidence that this phase is isotropic. It forms spontaneously domains of opposite chirality which are randomly distributed and visible by rotating of one polarizer from the crossed polarizer position (Fig. 4.5). These domains are much more pronounced if this phase is formed in the presence of an electric field. In the X phase the X-ray pattern displays a closed ring in the small angle region and diffuse scattering in the wide angle region. Although well oriented samples have been obtained in the nematic phase, the alignment get completely lost in the X phase. The full width of half maximum of the inner ring is in between that of the nematic and usual smectic phases (about 4 times the instrumental resolution). It indicates that the structure of the X phase has no long-range order.

The formation of spontaneously twisted structures in the nematic phases of banana-shaped compounds can result form the bent shape of the molecules. Such behaviour has been predicted by computer simulations with banana-shaped molecules according to whose a temperature-driven transition from a uniform nematic to a nematic phase with macroscopic twist can take place [10]. As recently shown by I. Dozov [11] the bent shape of the molecules can induce a local bend of the director giving rise either to a splay-bend deformation or a conical twist-bend helix. The highly viscous X phase possesses an isotropic structure and spontaneously forms chiral domains, which is reminiscent of a cholesteric blue phase.

Chapter 5

Orthogonal phases: SmA and SmAP

5.1 Introduction

Conventional smectic phases, are constituted by stacks of layers in which the molecules are aligned parallel (SmA) or obliquely (SmC) with respect to the layer normal. The SmA phase is optically uniaxial with the local symmetry $D_{\infty h}$; the SmC phase is biaxial with the local symmetry C_{2h}. A biaxial smectic phase may also appear if one of the principal axis of the magnetic susceptibility tensor $Q_{\alpha\beta}$ is parallel to the layer normal but the transversal components of the tensor $Q_{\xi\xi}$ and $Q_{\eta\eta}$, are no longer equivalent [2]. In this case, the molecules are aligned parallel to the layer normal but the properties with respect to the in-plane directions are different. This smectic phase was designated by the code letter C_M , where M refers to McMillan [70,71], who established the first microscopic theory of the SmA and SmC phase. In a theoretical investigation done by H.R. Brand *et al* [72], the inequivalence of the transversal components of Q has been achieved by considering board-like molecules where for steric reasons $Q_{\xi\xi} \neq Q_{\eta\eta}$ and the phase possesses D_{2h} symmetry. Up to now, four liquid crystalline systems have been reported that exhibit a C_M phase [73 – 77].

Another way to obtain $Q_{\xi\xi} \neq Q_{\eta\eta}$ can be realized in the mesophases with bent-shaped mesogens. A sterical moment of the molecules in a smectic phase favors polar packing within the layers [12, 15, 16]. If the alignment of the molecules is orthogonal with respect to the layer planes, a local C_{2v} symmetry results (in contrast to the C_M phase). This phase is similar to the SmA phase since one of the principal axes of Q is parallel to the layer normal. Therefore, it might be better to call such phase SmAP in analogy to the well-known tilted variant designated as SmCP [15]. The tilted switchable phase SmCP or B_2 is well studied, in contrast, the SmAP phase has not been reported before for low-molar bent-core mesogens. Therefore, we have investigated the mesophases formed by 4-cyano-resorcinol derivative fluorinated on the outer rings in position 3 (compound V/**1**) (Fig. 5.1). In this chapter we will give the experimental evidence for the existence of such SmAP phase, which was predicted theoretically by H.R. Brand *et al* [12, 72].
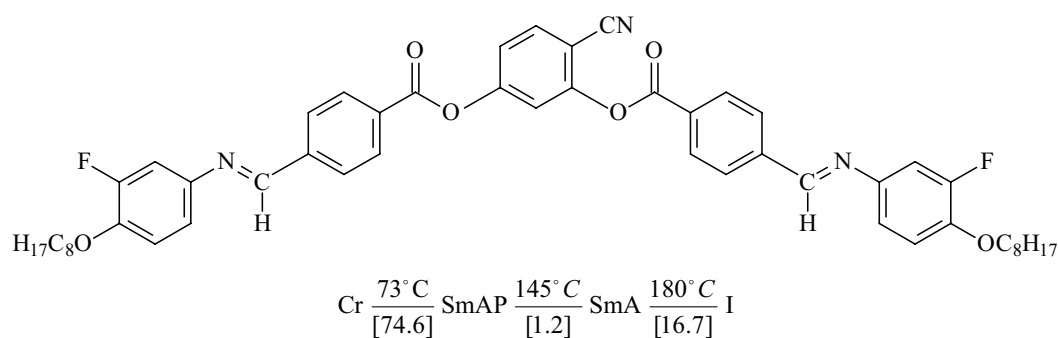

$$\text{Cr} \; \frac{73^\circ C}{[74.6]} \; \text{SmAP} \; \frac{145^\circ C}{[1.2]} \; \text{SmA} \; \frac{180^\circ C}{[16.7]} \; \text{I}$$

Fig. 5.1: Structural formula and mesophase behavior of compound V/**1**

5.2 Optical and thermal behavior

Two mesophases have been clearly detected by calorimetry and polarizing microscopy. From the transition scheme one can see that the transition enthalpy between the two mesophases is quite low (1.2 kJ/mol) in comparison with the SmA-isotropic transition enthalpy (16.7 kJ/mol). The high temperature mesophase exhibits a fan-shaped texture or a homeotropic texture indicating a Sm*A* phase. On cooling, after the transition into the low-temperature phase, the fan-shaped texture remains nearly unchanged. Only some fine irregular stripes parallel to the smectic layers appear on further cooling. However, if the SmA phase shows a homeotropic texture, it transforms into a strongly fluctuating schlieren texture (Fig. 5.2a, b). On further cooling down to room temperature, the texture of the low-temperature phase is not markedly changed: the number of stripes in the fan-shaped texture slightly increases and the schlieren texture becomes more birefringent while the fluctuations completely disappear.

5.3 Electro-optical switching

As it is expected, the SmA phase does not show any field-induced switching. Applying an electric field to the fan-shaped texture of the low-temperature phase, the birefringence (and therefore the interference color) is changed and the stripes within the fans disappear. Furthermore, the texture of the switched states is independent of the polarity of the applied field (Fig. 5.3). At lower temperatures (60 °C), the field-induced switching is considerably delayed and takes some seconds. Two current peaks per half-
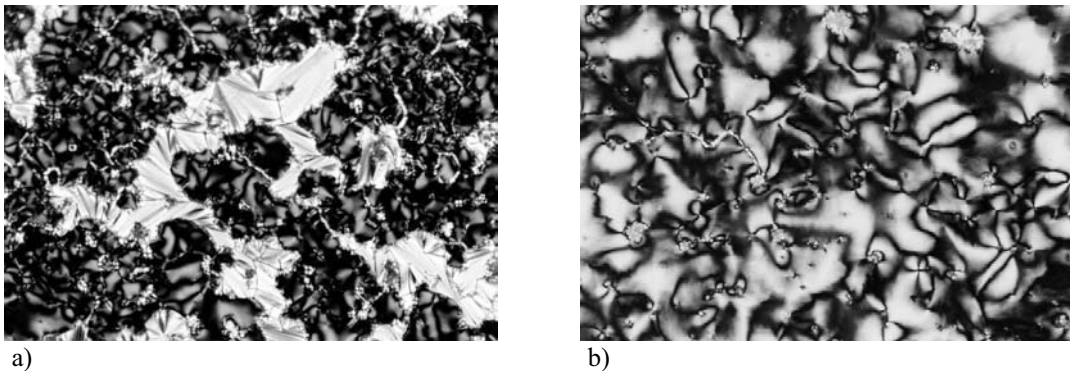

a)   b)

Fig. 5.2: a) and b) fan-shaped and schlieren textures of the SmAP phase

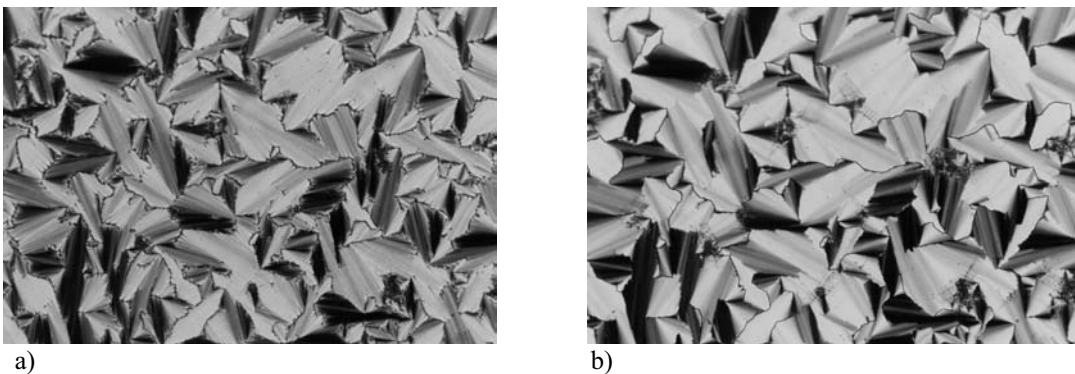a)   b)

Fig. 5.3: Optical textures of the SmAP phase: a) 0 V/µm, b) ±8 V/µm (temperature 138 °C)

period of an applied triangular voltage give evidence for the antiferroelectric nature of this phase. A two-loop antiferroelectric hysteresis curve obtained by integration of the current response is shown in Fig. 5.4. The spontaneous polarization is plotted as a function of the temperature in Fig. 5.5. It is seen from the figure that the polarization is unusually high and reaches values of 1000 nC/cm^2. It is the highest value reported for banana-shaped mesogens so far. Such a high value is obviously a consequence of the high dipole correlation found in this phase.
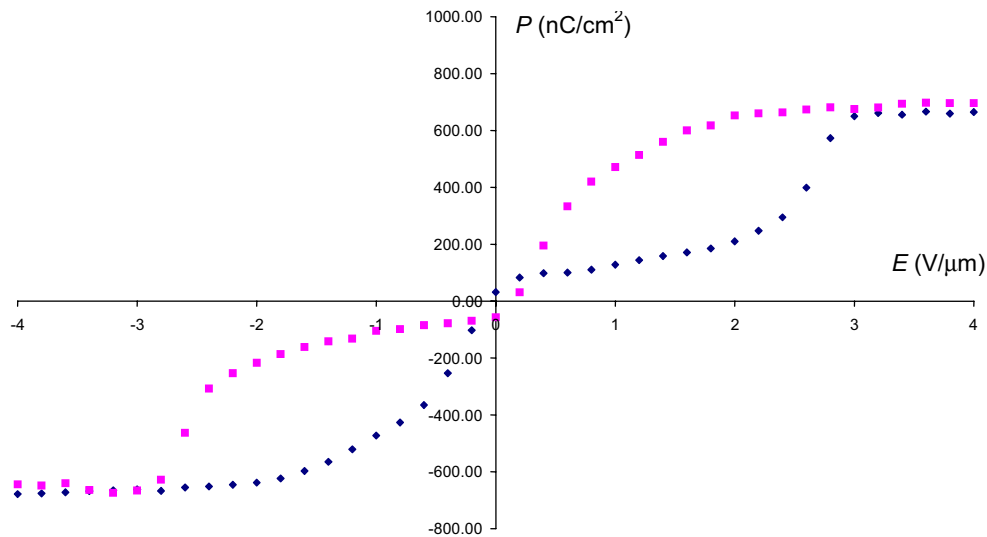
Fig. 5.4: Polarization plotted as a function of the electric field (138 ^{o}C)
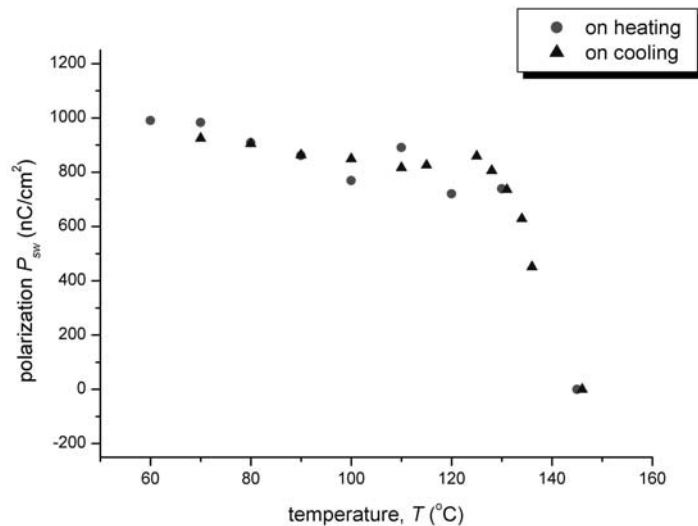
Fig. 5.5: Temperature dependence of the switching polarization

5.4 Structural characterization

5.4.1 X-ray study

The X-ray diagram of the non-oriented samples displays the first three orders of the layer reflections as well as the diffuse outer scattering in a temperature range between 170 and 70 °C (Fig. 5.6). The positions of the quasi-Bragg reflections are nearly independent of the temperature, which means the layer thickness (d = 44.3 Å) remains constant within the limits of 0.2 Å. In the diagrams obtained from the oriented samples, up to three on-the-meridian reflections have also been observed (Fig. 5.7, here the 001 reflection is covered by the beam stop). The X-ray diffraction pattern exhibits an outer diffuse scattering, the maxima of which are clearly positioned on the equator, also in the phase below the SmA phase. No change in the patterns appears down to 45 °C, where the layer reflections become more crescent-like and the outer diffuse scattering splits into a few peaks resulting from the appearance of an in-plane order. But it is clearly seen that these wide-angle reflections still remain diffuse.
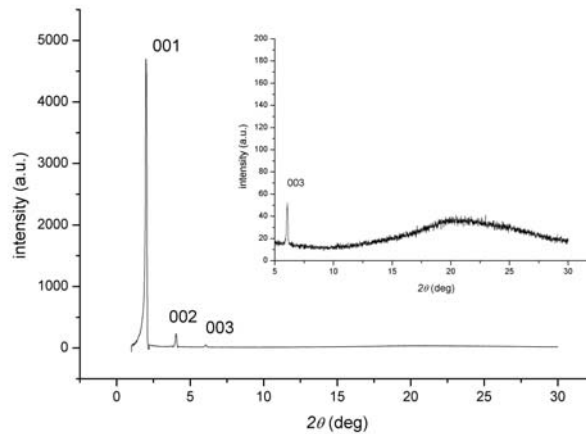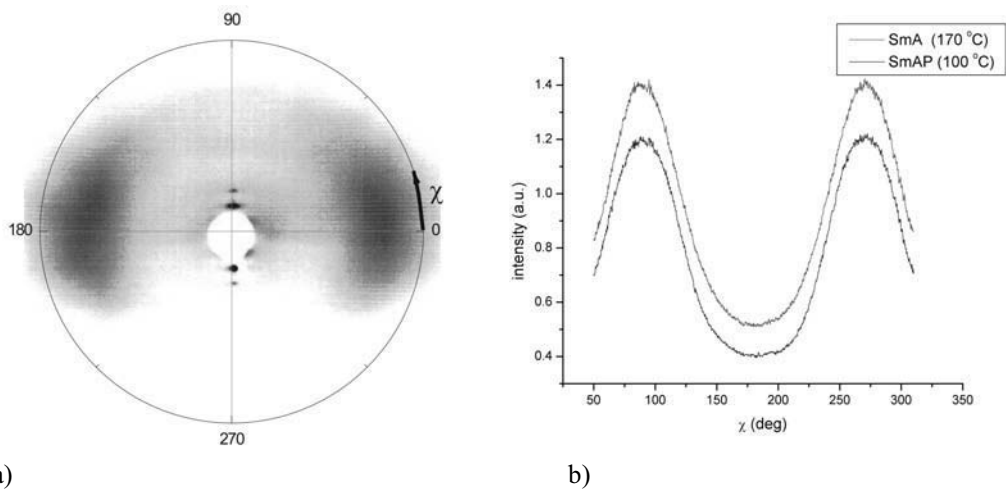

Fig. 5.6: X-ray diagram of a non-oriented sample

a)   b)

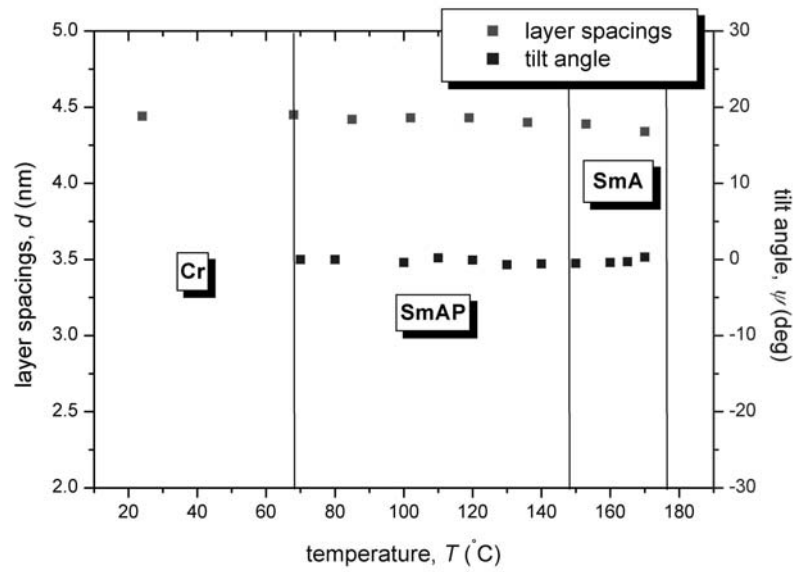Fig. 5.7: X-ray pattern of the oriented sample and b) χ-scans in the SmA and the SmAP phases

Fig. 5.8: Temperature dependence of the layer spacing d and the tilt angle ψ.

The analysis of the diffuse outer scattering intensity has been performed with respect to the θ dependence (θ is the Bragg angle) as well as the χ dependence. The profile of the outer diffuse scattering $I(\chi)$ remains unchanged within the limits of error down to 100 °C. The experimental curves $I_{meas}(\chi)$ have been normalized as it is described in Chapter 2. The function $I(\chi)$ is nearly identical in the SmA and in the low-temperature phase. The derived tilt angle ψ is outlined in Fig. 5.8. It is seen that in both smectic phases (SmA and the low-temperature phase), the molecules are aligned parallel to the layer normal.

5.4.2 NMR study

The assignment of the lines in the ^{13}C-NMR spectra is shown in (Fig. 5.9 a, b). In the liquid crystalline state each position gives a pair of signals, indicating an inequivalence of the right and left "wings" of the molecules. Due to a sterical repulsion caused by an asymmetrical substitution of the central core, the long axis deviates from the symmetry axis of a nonsubstituted molecule (Fig. 5.10). We assume a deviation of 5 deg which reduces the angle β between H10-H11 from 30 to 25 deg. The resolved ^{1}H dipole coupling from these protons gives then the order parameter S according to Eq. 2.29

$$S = \frac{\Delta \nu}{\Delta \nu_0 \left(\frac{3}{2} \cos^2 \beta - \frac{1}{2} \right)}$$

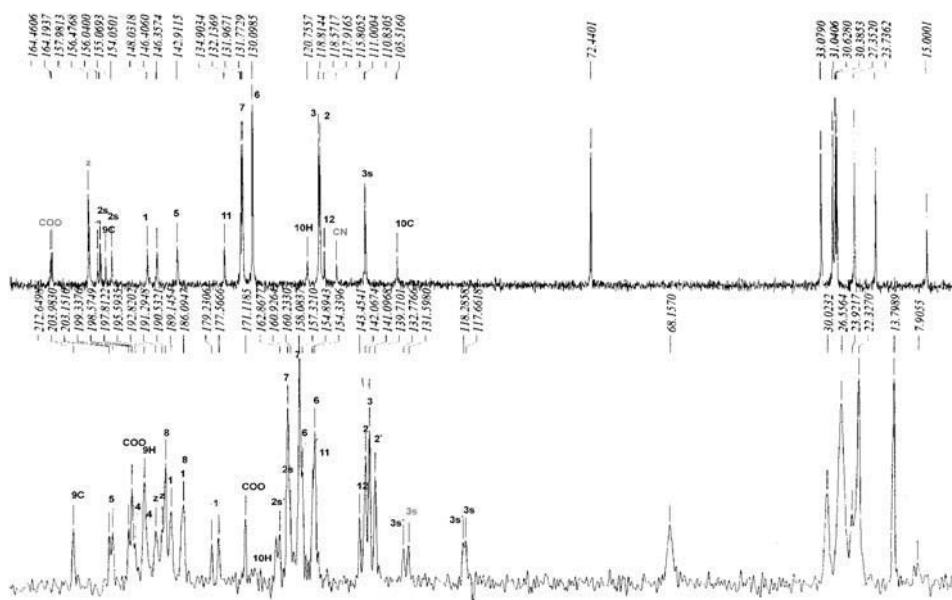where $\Delta \nu_0 = 23.9$ kHz. Here the contribution from D is neglected. The order parameter

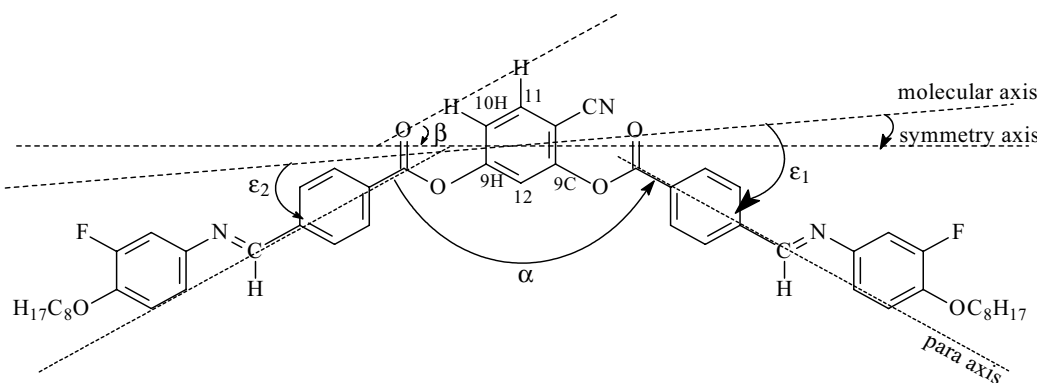Fig. 5.9: ^{13}C-NMR spectra: a) in the isotropic phase, b) in the mesophase
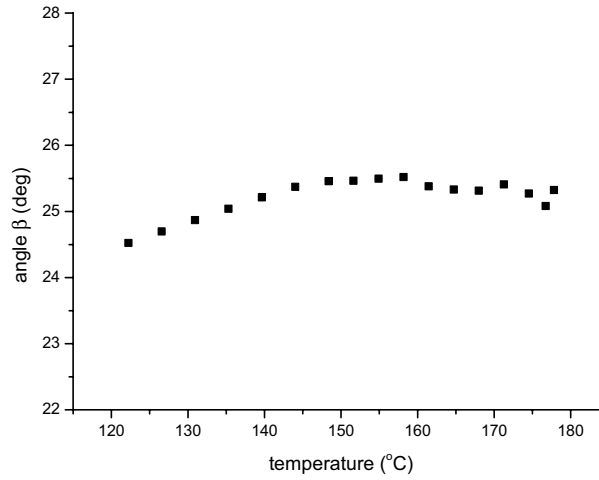

Fig. 5.10: Definition of the angles and atomic positions

Fig. 5.11: Temperature dependence of the angle β

can also be calculated from the measured shift anisotropy tensor in ^{13}C-NMR for the carbons in the central ring (see section 2.5.2). The observed component δ^i_{zz} from the atom in position i, depends on the longitudal and transversal order parameters S and D (Eq. 2.12, 2.19):

$$\delta^i_{zz} = S\,\delta^i_{\zeta\zeta} + \frac{D}{3}(\delta^i_{\xi\xi} - \delta^i_{\eta\eta}) \approx S\delta^i_{\zeta\zeta}$$

Choosing the 4 lines from carbons 9H, 9C, 10H and 10C, which are all resolved in the spectra we calculate their shift ratios $v = \dfrac{\delta^i_{zz}}{\delta^{9H}_{zz}}$. We find that $v_i(T) = \dfrac{\delta^i_{zz}}{\delta^{9H}_{zz}} = \dfrac{\delta^i_{\zeta\zeta}}{\delta^{9H}_{\zeta\zeta}}$ is constant in the SmA phase but varies with temperature in the lower SmAP phase. Agreement with the S from the proton splitting is obtained for $\delta^9_{\zeta\zeta} = 77.5\,\text{ppm}$ and corresponding values : $\delta^i_{\zeta\zeta} = v_i(T)\delta^9_{\zeta\zeta}$, for the others (Table 5.1).

Table 5.1

	9H	9C	10H	10C	CN
$\delta_{\zeta\zeta}$	77,5*	56,1	66,68	67,55	148,82
δ_{11} [1]	91,1	79,2	92	80,3	205
δ_{22} [1]	15	9	15	9	-205/2
β [°]	25	35	35	25	25

The angle β can be found from the anisotropic shift $\delta^{CN}_{\zeta\zeta}$ of the CN carbon since the main frame tensor values ($\delta^{CN}_{11} = 205\,\text{ppm}$) are known from the literature using the formula:

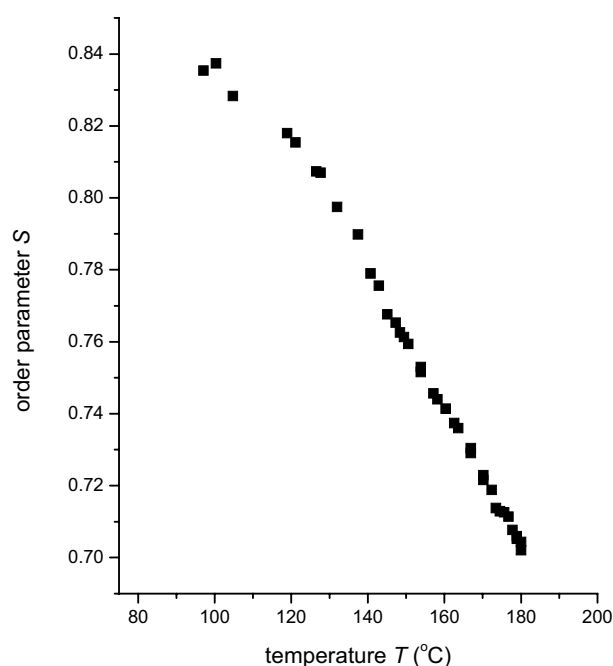$$\delta^{CN}_{\zeta\zeta} = \frac{3\cos^2\beta - 1}{2}\delta^{CN}_{11}$$

Fig. 5.12: Temperature dependence of the order parameter S

The temperature dependence of the angle β can be derived from the shift ratios and is shown in Fig. 5.11. If the molecule were not inclined the angle β should be equal to 30 deg. It is seen from the scatter that the molecule is inclined by the angle $\sim$ 5 deg as assumed above. The scatter of the temperature dependence of the order parameter $S(T)$ is shown in Fig. 5.12. The order parameter is relatively low (0.7) in the SmA phase and it is continuously increasing over the whole temperature range of the mesophases.

Table 5.2

	δ_{11}/ppm	δ_{22}/ppm	ε/SmA	φ/SmA	ε/SmAP	φ/SmAP
C5	93	25	19°	23°	24°	35°
C6	37	72				
C7	39,9	67	22	34°	24°	42°
C8	90	17				
COO						
1	55					
2	35,5					
3	36					
4	77					
F-H	29,5					

The evaluated $S(T)$ is used to calculate $\delta_{\zeta\zeta}^i = \delta_{zz}^i/S$ for all other carbons in the molecule. The values decrease for all carbons with decreasing temperature. The bending angle ε and the torsion angles φ for the rings B and C where found using the 4 resolved lines from the corresponding ring and applying the system of equation $\delta_{\zeta\zeta}^i = \overline{\delta}_{11} - (\overline{\delta}_{11} - \overline{\delta}_{22})\sin^2\varepsilon - (\overline{\delta}_{11} + 2\overline{\delta}_{22})\sin^2\varepsilon\sin^2\varphi$ (see Eq. 2.28). For the solution we need the components of the tensor δ^i in PAS. We estimated the values using results

from simple rod-like molecules (Table 5.2).The angles exhibit a very slight temperature dependence and the bending angle ε is around 19 deg in the SmA phase and 24 deg in the SmAP phase. These data suggest that the overall bending angle α is about ~ 142 – 132 deg.

5.5 Discussion

Summarizing the experimental results, we can see that the low-temperature phase is a smectic phase without in-plane order and with an orthogonal alignment of the molecules, which resembles the SmA phase. But in contrast to SmA, this phase does not form a homeotropic texture but rather a schlieren texture, which mainly displays defects of the strength ± 1 (sometimes also $\pm\frac{1}{2}$). At first sight these findings are compatible with a C_M phase. However, the antiferroelectric switching observed on this compound indicates the presence of the polar axis, which reduces the symmetry of the phase to C_{2v} (different from D_{2h} of the C_M phase). From these results we can conclude that the low-temperature phase is an antiferroelectric version of the SmAP phase discussed by H.R. Brand *et al* [12, 72] and designated as a C_{PA} phase. In this smectic phase, the banana-shaped molecules are packed in the bent direction, which is identical with the polar axis. The smectic layers have C_{2v} symmetry, i.e., a twofold symmetry axis (which coincides with the polar axis) and a vertical mirror plane including the twofold axis and the layer normal. In addition, the polar direction alternates from layer to layer giving rise to the antiferroelectric structure of the SmAP phase. This is suggested by the sporadic occurrence of $s = \pm\frac{1}{2}$ defects in the schlieren texture, which cannot be formed in the ferroelectric SmAP phase. It is known that in smectic phases where the tilt of the molecules or of the mesogenic units alternates in adjacent layers, i.e., in SmC$_A$ phases or in intercalated SmC phases [78 – 80], $s = \pm\frac{1}{2}$ defects can arise by a combination of a disclination and a screw dislocation (dispiration). The same should be true for the SmAP phase under discussion. Further on, in the SmAP or SmAP$_A$ phase, chiral smectic layers cannot exist like in the SmCP phase of banana-shaped compounds, where the bent-shaped molecules are tilted with respect to the layer normal [15]. Therefore,
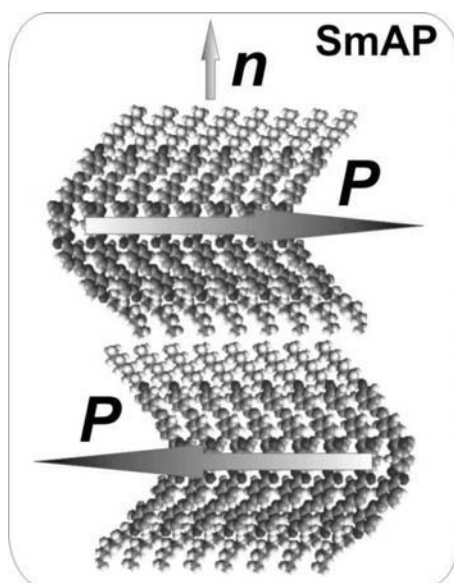

Fig. 5.13: Structure of the SmAP phase

racemic or homogeneously chiral domains cannot be observed in the SmAP phase.

It should be noted that in mixtures of a side-chain polymer and its monomer, a smectic phase with alternating tilt of the mesogenic units has been described [81]. In pyroelectric experiments, this phase shows antiferroelectric properties. Although the structure of this phase is clearly different from that of the $SmAP_A$ phase presented here, the symmetry and the antiferroelectric nature of this phase seem to be the same.

In conclusion it is important to mention that in binary mixtures not only the sequence SmA-$SmAP_A$ is found but also a sequence SmA-$SmAP_A$-$SmCP_A$ [24].

Chapter 6

SmCP phase formed from isotropic or nematic phases

6.1 Introduction

The next step down to lower symmetries leads to the SmCP phase. It is a tilted version of the SmAP phase: the molecules are tilted and packed in a polar fashion so that the polar axis is perpendicular to the layer normal. As it has already been mentioned above, the SmCP phase is one of the most investigated "banana" phases. This chapter focuses on the properties of the SmCP phase which emerges on cooling of the isotropic or nematic phase by means of the first order transition. Some of these features have already been known [82]. Still, the investigation of fluorinated compounds gives some more information on the ordering in the mesophase. On the other hand, nematic phases are very rare among the bent-shaped compounds and potential anomalies in their behavior (see Chapters 1 and 4) can be very interesting.

In this chapter we report two bent-shaped mesogens: VI_**5F** fluorinated in the central core and exhibiting I→SmCP transition (Fig. 6.1a) and VI_**4Cl** chlorine-substituted compound showing N→SmCP transition (Fig. 6.1b). This is the first material where the SmCP phase is formed on cooling the nematic phase [68]. Later such transition has also been reported for six-ring bent-shaped mesogens [69].
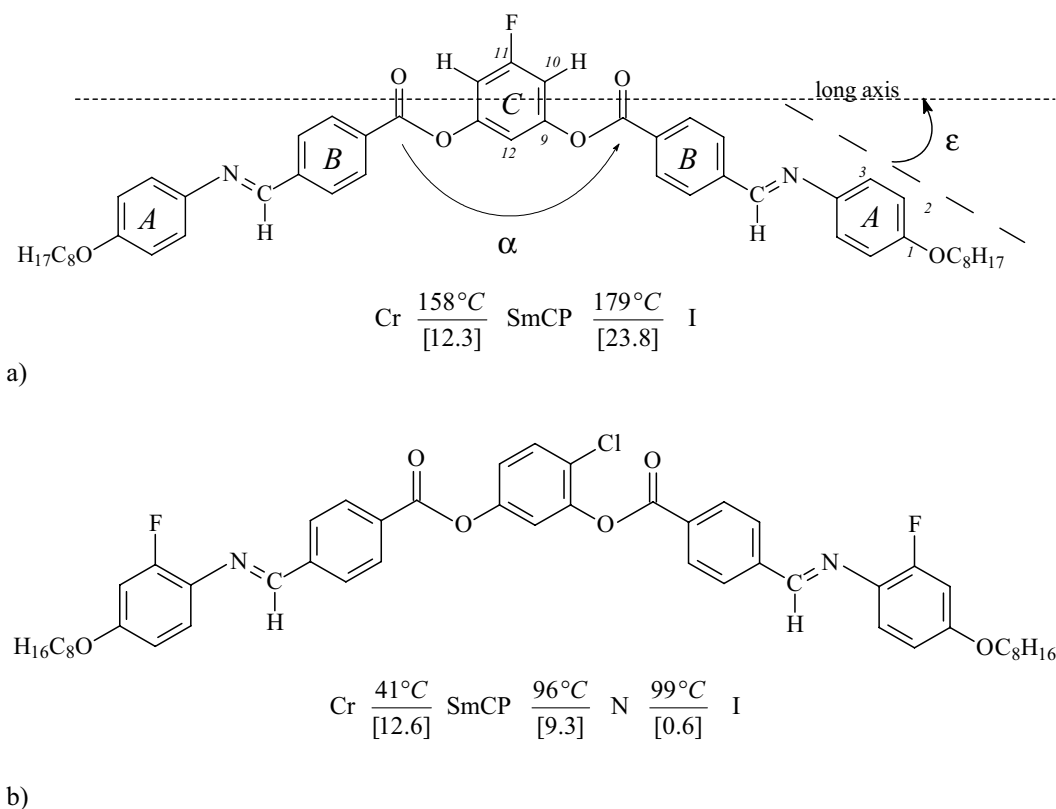

Cr $\frac{158°C}{[12.3]}$ SmCP $\frac{179°C}{[23.8]}$ I

a)

Cr $\frac{41°C}{[12.6]}$ SmCP $\frac{96°C}{[9.3]}$ N $\frac{99°C}{[0.6]}$ I

b)

Fig. 6.1: Structural formula of the compounds a) VI/**5F** and b) VI/**4Cl**

6.2 Microscopical textures and electro-optical switching

The SmCP phase appears from the isotropic phase as a fine grainy texture (compounds VI/**5F**) (Fig. 6.2). When the cooling rate is slow (0.1 K/min) a fan-shaped texture can be observed. The high-temperature nematic phase in the compound VI/**4Cl** exists in a short temperature interval of 3 ˚C and shows characteristic schlieren or marble textures (Fig. 6.3). On cooling the schlieren texture transforms into a fine-grainy one.

Application of an electric field leads to the electro-optical switching. This process has a threshold of about ~1.5 V/µm for compounds VI/**5F** (Fig. 6.4). The switched state is independent of the polarity of the external field. In contrast to the
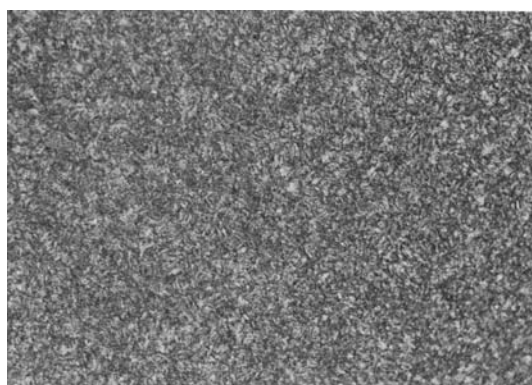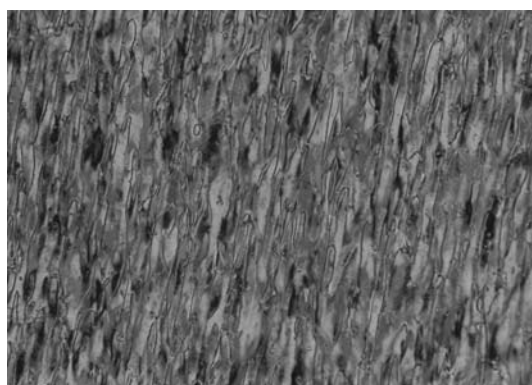

Fig. 6.2: Fine-grainy texture of compound VI/**5F**

Fig. 6.3: Marble texture of the nematic phase (compound VI/**4Cl**)

compounds with I→SmCP phase, the compound VI/**4Cl** shows the electro-optical switching at much higher threshold field of about 100 V/µm, which is the reason why we could not detect the current response in the earlier experiments.
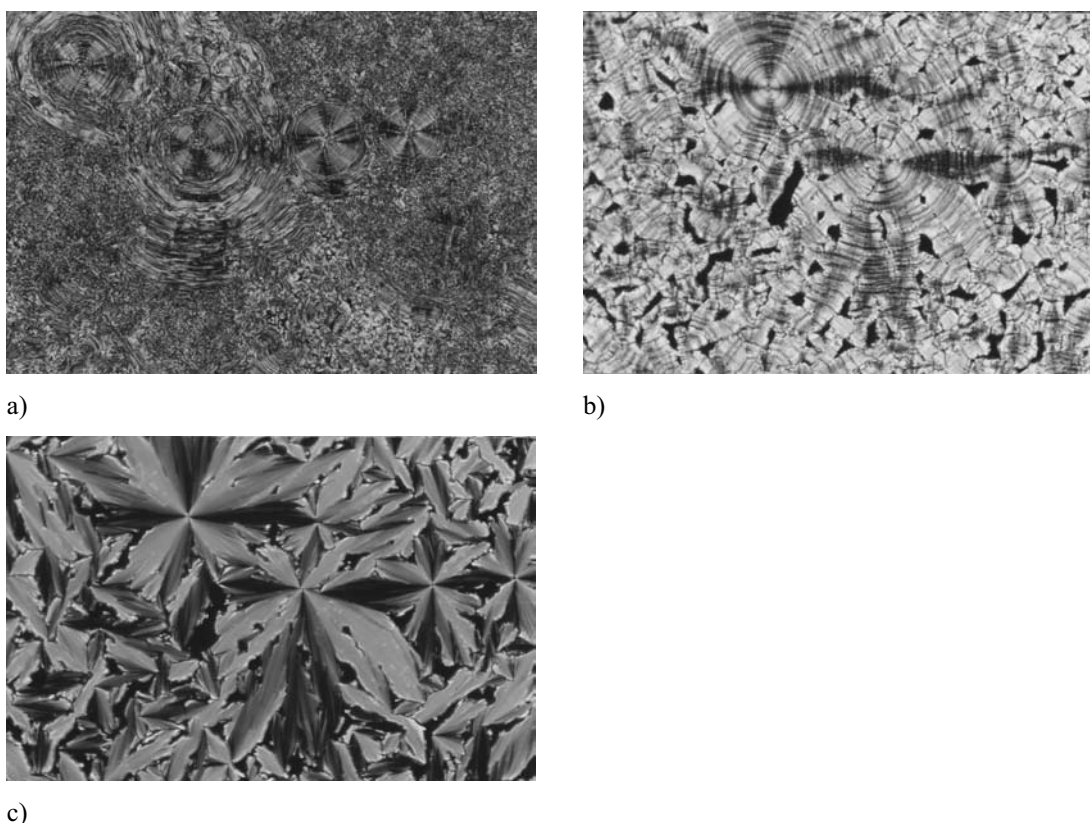
a)

b)

c)

Fig. 6.4: Electro-optical switching in the SmCP phase (compound VI/**5F**): a) $E = 0$, b) $E = 1.2$ and c) $E = 4$ V/μm ($T = 151$ ˚C)

The switching polarization does not show any temperature dependence in the SmCP phase. However, the values of the P_{sw} are quite high for compound VI/**5F** (~ 640 nC/cm^2) and about three times smaller for compound VI/**4Cl** with the nematic phase (~250 nC/cm^2).

6.3 Structure of the phase

6.3.1 X-ray investigation

X-ray measurements on non-oriented samples showed the layer reflections up to the second order and broad diffuse scattering in the wide-angle region. The d-values are temperature independent for all three compounds and are listed in Table 6.1.

Table 6.1

compound	layer spacing d (Å)	molecular length L (Å)
VI/**5F**	37.5	54.0
VI/**4Cl**	35.0	54.0

From Table 6.1 one can estimate an effective molecular length taking an overall bending angle $\alpha = 110$ deg ($\varepsilon = 35$ deg was found in NMR measurements in section 6.3.2) which is equal to 44.2 Å. From the layer spacing and the value of the effective molecular length the tilt angle gives 32 deg.

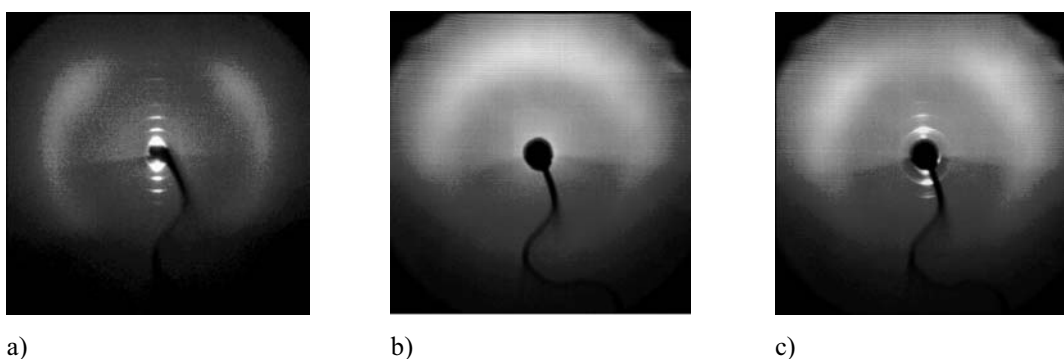a)   b)   c)

Fig. 6.5: X-ray patterns of oriented samples: a) SmCP phase (T = 170 ^{o}C) compound VI/**5F**, b)
         nematic phase of compound VI/**4Cl** (T = 97 ˚C) and d) SmCP phase of compound VI/**4Cl**
         (T = 90 ˚C)
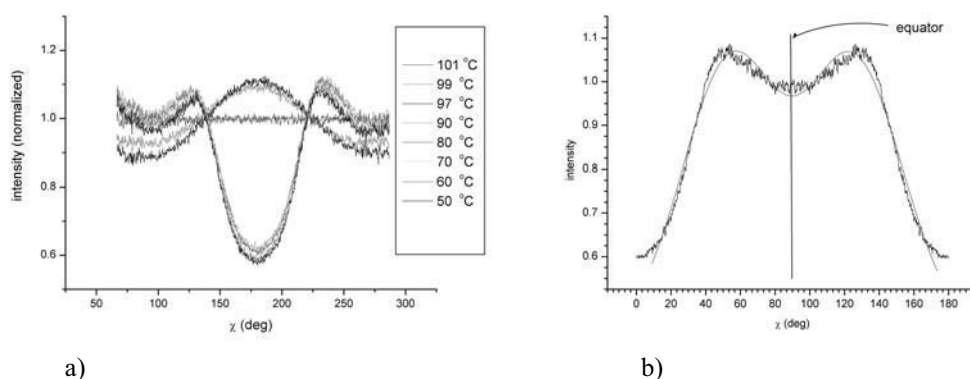

a)   b)

Fig. 6.6: a) Temperature dependence of the χ-scan of the outer diffuse scattering b) reconstructed χ-
         scan of the splitting of the outer diffuse scattering (compound VI/**4Cl**)

Experiments on oriented samples provided us with some more information about the structure of the mesophases. The splitting of the outer diffuse maxima for compound VI/**5Cl** (Fig. 6.5a) indicates a tilted arrangement of the molecules in the smectic layers, which is compatible with the SmCP phase. The splitting does not show any temperature dependence.

Measurements on oriented samples of the compound VI/**4Cl** proved the existence of the SmCP phase as well as the high-temperature nematic phase in this compound. Two kinds of measurements were done: orientation in a thin capillary in a magnetic field and on a glass plate. The first method was of a success since the high-temperature phase is the nematic.

In case of surface oriented samples the analysis of the wide-angle scattering shows a change of the molecular orientation upon the N→SmCP transition. The patterns are shown in Fig. 6.5b and c. In Fig. 6.6 a χ-scan of the diffuse scattering is presented. The normalization technique has been employed to extract the distribution of the scattering. The red curve shows the intensity in the isotropic state and due to the normalization it does not depend on χ. In the nematic phase there is a broad heap in the middle of the scatter which shows that the molecules are mainly oriented parallel to the substrate surface. In the SmCP phase the intensity is distributed mostly at the equator. A

reconstructed plot of the intensity vs. χ is shown in Fig. 6.6b. There are two maxima: above and below the equator corresponding to the tilt of 35 deg, which is close to the value estimated from the layer spacing.

6.3.2 Orientational order and molecular conformation

The NMR measurements have been performed on the compounds VI/**5F** with I→SmCP transitions. The orientational order was investigated by means of ^{13}C- and ^{19}F-NMR. Due to the substitution of the central ring the lines splitting in the ^{1}H-NMR could not be assigned.

6.3.2.1 ^{13}C-NMR

The lines from the ring C have low intensity and due to the dipole interaction between the central fluorine and the carbon C10 the intensity is two times smaller than in the non-substituted ring (Fig. 6.7). It considerably complicates the assignment of the lines in the ring C. From the geometry of the central ring follows that the lines C9, C10 and C12 have a small dipole splitting, whereas, the splitting is large for C11.

The symmetry of the molecule defines the molecular axis ζ perpendicular to the C-F bond in the central ring (Fig. 6.1). The spectra of the central ring provide us with eight parameters: four shift anisotropies and four C-F dipolar couplings. These data are enough to estimate both a transversal order parameter S and the longitudal order parameter D.

Experimental realization is more complicated though. The initial values of the tensor components $\delta_{\zeta\zeta}$ and $\delta_{\xi\xi}$ are different from those used in other bent-shaped compounds. The dipolar splitting has been resolved only for the compound VI/**5F**. Such poor resolution for the positions C9, C10, C12 together with a very strong dependence of the tensor components on the geometry of the ring considerably complicates the exact evaluation of the order parameters (variation of the distance r_{C-F} by 0.02Å has a
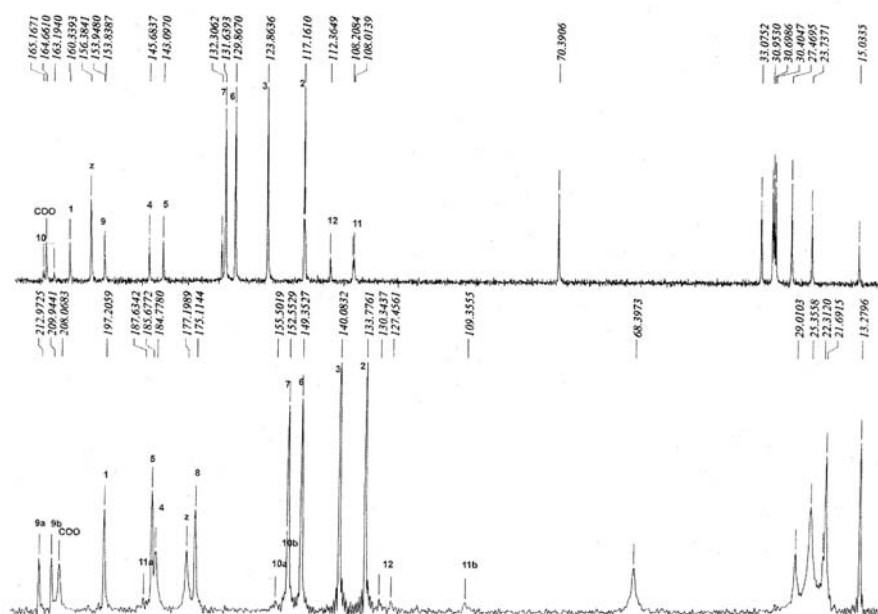

Fig. 6.7: ^{13}C-NMR spectra and the line assignment in the isotropic phase (top) and in the liquid crystalline phase (bottom)

drastic effect). The values of the tensor components for two different values of r_{C-F} are listed in Table 6.2. The calculation is based on Eq 2.12 with account for the scalar spin coupling which takes final form

$$\Delta v^i - J^i = SW_{\zeta\zeta}^i + \frac{D}{3}\left(W_{\xi\xi}^i - W_{\eta\eta}^i\right)$$
(6.1)

The values of the scalar spin coupling are taken from the isotropic spectra. The variation of the r_{C-F} has a large effect on the values of S, at the same time D remains small (Table 6.2). Using the data on shift anisotropy (^{13}C-NMR), dipole coupling C-F and neglecting D, the angles ε and φ can be found using expression 2.28 to be $\varepsilon \approx 35$ deg and $\varphi \approx 44$ deg.

Table 6.2

position	$r_{C-F} = 1.344$ Å		$r_{C-F} = 1.324$ Å	
	$W_{\zeta\zeta}$	$W_{\xi\xi}$	$W_{\zeta\zeta}$	$W_{\xi\xi}$
C11	93.5	-186.10	97.331	-194.662
C10	3.339	-20.874	3.199	-21.123
C9	3.238	-8.098	3.272	-8.21
C12	3.275	-6.550	3.323	-6.646
Order parameters	$S = 0.901$	$D = 0.020$	$S = 0.804$	$D = -0.018$

6.3.2.2 ^{19}F-NMR

The splitting observed in ^{19}F-NMR (470.55 MHz) is governed by the dipolar interactions with the protons C9 and C10. The spectrum is a triplet of doublets (Fig. 6.8). The last doublet splitting is very small about 500 Hz (when the line width is 600 Hz). It was only observed in the compound VI/**5F**. The central line consists of two overlapped doublets. The interaction of the protons between each other has a negligible effect on the ^{19}F-resonance. This additional splitting gives another way to estimate the
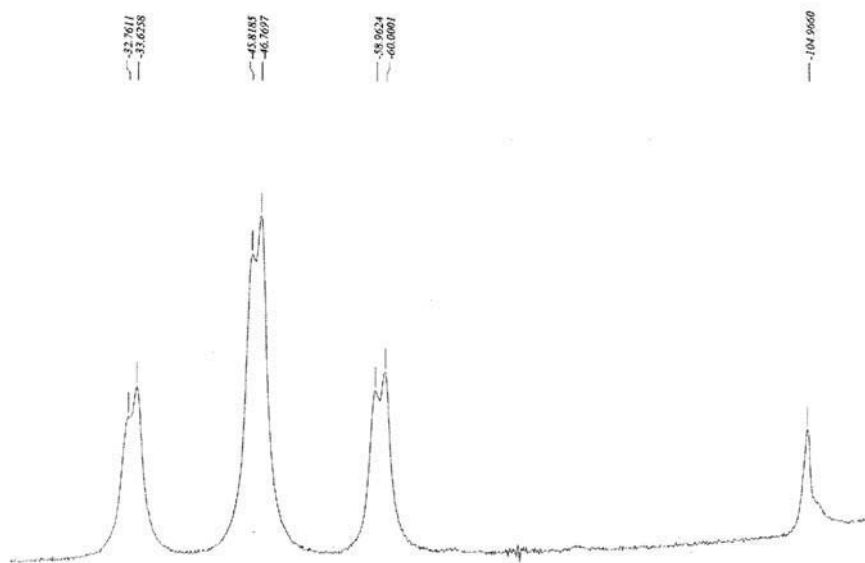
Fig. 6.8: ^{19}F-NMR spectrum in the SmCP phase (compound VI_**5F**)

transversal order parameter. The results are given in Table 6.2. The smallness of the splitting by H12 leads to large systematic errors and the values of D are very different from the ones found in ^{13}C-NMR. Therefore these results will be discarded and the previously found mean values $S = 0.875$ and $D = 0.006$ will be used.

6.4 Discussion

Summarizing the results of this chapter the following characteristic features of the SmCP phase can be outlined. The SmCP phase, has a layer structure with tilted molecules. The polar order of the molecules has been proved by the electro-optical switching found in this phase. In case of the SmCP phases formed by means of the first order I→SmCP and N→SmCP transitions the layer spacing (as well as the tilt angle) has been found to be temperature independent. It is in agreement with earlier reported data on other bent-shaped compounds [16] and the compounds discussed in the proceeding chapters. The same situation has been found in mixtures of the bent-shaped compounds with the first order SmC→SmCP transition reported by M.W. Schröder *et al* [24].

Many bent-shaped compounds showing the SmCP phase has very high values of the switching polarization P_{sw}. The polarization values are much smaller when the phase is formed by cooling of either the nematic or the SmC phase. The latter case is discussed in the further chapters.

Chapter 7

Paraelectric – ferroelectric transition SmC→SmCP

7.1 Introduction

The formation of a polar structure in the SmC phase (resulting in SmCP phase) is promoted by considerable sterical moments of bent molecules. In previous chapters we described transitions of the first order from isotropic or nematic phase into the SmCP phase. Breaking of at least four symmetries (translational, orientational, tilt and polar) results in first order transitions and as NMR measurements have shown there is no change in the bending angle α in the SmCP phase. The strength of the sterical moment promoting polar packing can be assessed by the magnitude of the bending angle. If the angle is large ~180 deg the shape of the molecule is rod-like and paraelectric phases form. Smaller angles ~ 120 deg can be found in compounds showing ferroelectric "banana" phases. Different substituents introduced in the chemical structure of the molecules are aimed to design the compounds with different angles α to find the border when molecular asymmetry and strong sterical moment leads to the new ferroelectric phases. This research led to the synthesis of a few mesogens exhibiting SmC and SmCP phases (as well as SmA and N) [23].

In this chapter, compounds fluorinated on the outer rings and dichloro-substituted on the middle ring (Fig. 7.1) will be discussed. The synthesized homologous compounds show N, SmA, SmC and SmCP phases. The properties of the latter phase are quite different from the SmCP phases discussed in previous chapters. Not only does this phase show a very slight latent heat for the SmC→SmCP transition but also the bending angle α is changing continuously over the whole temperature range of the mesophase existence.
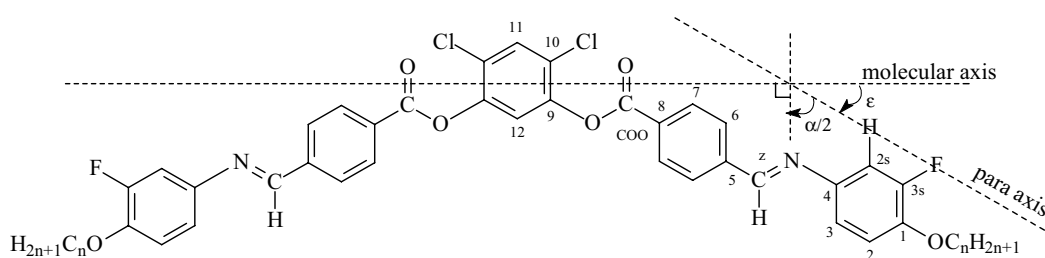

Fig. 7.1: Structural formula and the assignment of the atomic positions

7.2 Thermal behavior

The transition temperatures and the values of the latent heat are listed in Table 7.1. Most of the compounds exhibit the SmA phase and the homologues with short alkyl chains (n = 3, 8) also show the nematic phase. The compounds with longer terminal chains possess the switchable biaxial low-temperature SmCP phase with a small tilt angle. The undecyloxy and dodecyloxy homologues exhibit SmA – SmC – SmCP polymorphism. The SmCP phase is metastable in these compounds and appears only on cooling. It is important to notice that the latent heat of the SmC → SmCP transition measured by DSC technique is very small

and strongly depends on the cooling rate (Fig. 7.2). Such behavior implies the transition be of weakly first order.

Table 7.1

Compound	n	Cr			SmCP			SmC		SmA		N		I
VII/**3**	3	•	179 [75.9]§		-			-		-		(160 [1.3] | •)		•
VII/**8**	8	•	127 [49.0]		(• | 95) [-]		-		•		129.8 [*]	•	130.5 [*]	•
VII/**9**	9	•	113 [44.4]		(• | 100) [0.5]¶		-		•		133 [4.2]	-		•
VII/**10**	10	•	108 [50.5]		(• | 103) [0.7]¶		-		•		137 [5.1]	-		•
VII/**11**	11	•	107 [52.8]		(• | 102) [0.6]¶		•	116 [-]~	•		139 [5.7]	-		•
VII/**12**	12	•	103 [57.1]		(• | 100) [0.7]¶		•	125 [-]~	•		139 [6.1]	-		•

§ In the square brackets the transition enthalpy (kJ/mol) is given

* The calorimetric peaks of SmA-N and N-I transition could not be resolved. The sum of these transition enthalpies: ΔH (SmA-N) + ΔH (N-I) = 2.0 kJ/mol

~The transition is not observable on the DSC

¶ The values show a pronounced dependence on the cooling rate (Fig. 7.2), the giving values correspond to the rate of 5.0 K/min

7.3 Texture observations and electro-optical investigations

Upon cooling of the isotropic liquid, the SmA phase appears either as a homeotropic texture or as a fan-shaped texture. In the SmC phase the schlieren texture becomes broken and a characteristic pattern caused by long-wave director fluctuations is visible. When the phase is formed from the homeotropic texture of the SmA phase, a very weakly birefringent schlieren pattern appears, which indicates that the tilt angle in the SmC phase might be quite small (Fig. 7.3a).
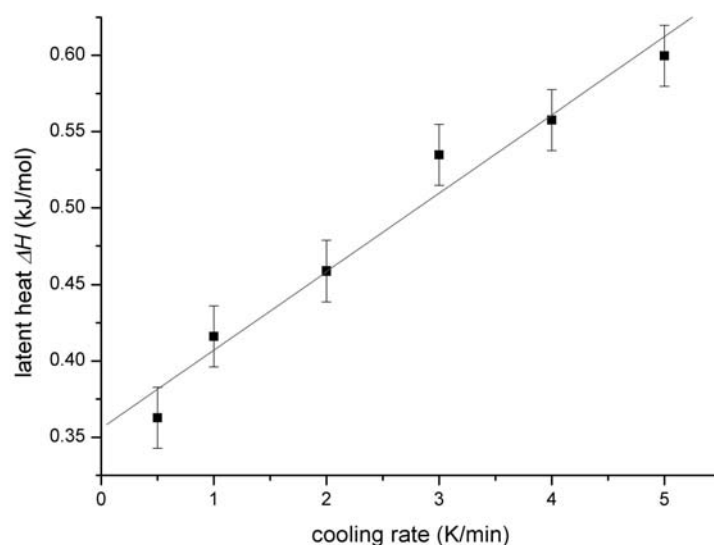

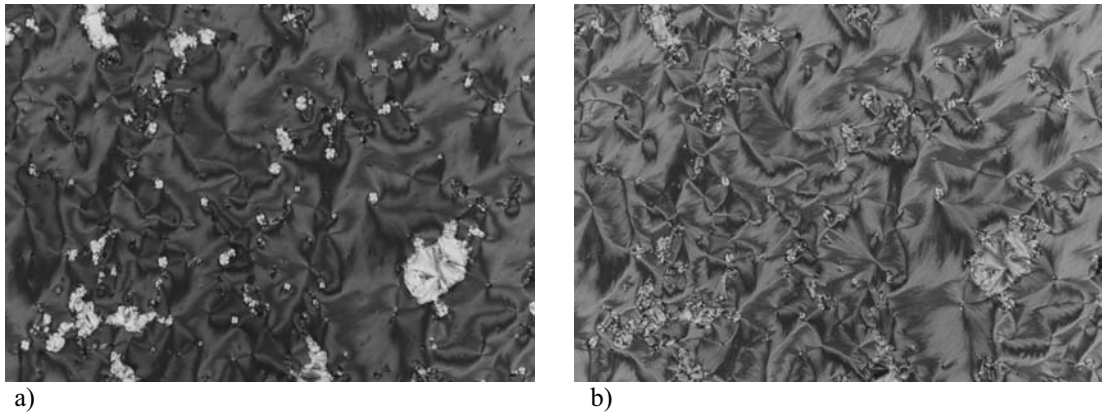Fig. 7.2: Dependence of the transition enthalpy of the SmC→SmCP transition on the cooling rate

a)   b)

Fig. 7.3: a) A weakly birefringent schlieren texture of the SmC phase ($T = 108^{\circ}$C) and b) "frozen"
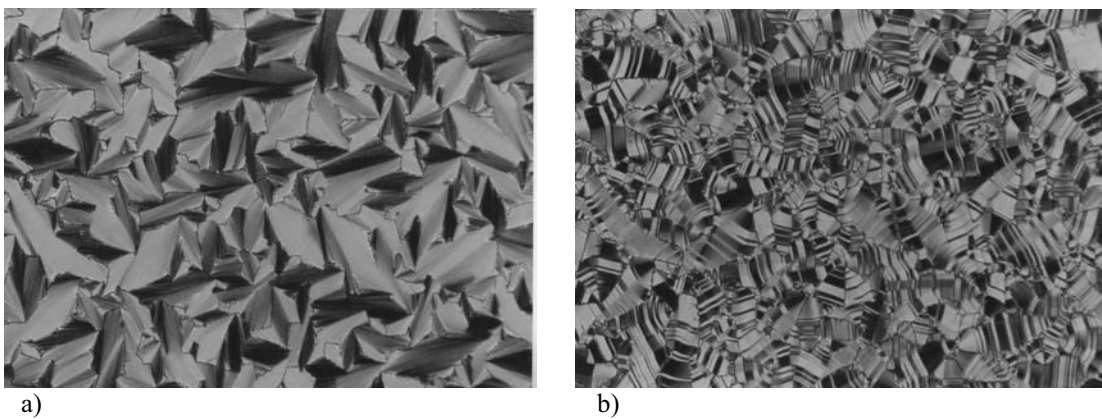schlieren texture in the SmCP phase ($T = 95^{\circ}$C); compound VII/**12**

a)   b)

Fig. 7.4: Microscopic texture of the compound VII/**12** in the SmCP phase ($T = 75^{\circ}$C) a) $E = 0.0$ V/µm
and b) $E = 1.2$ V/µm
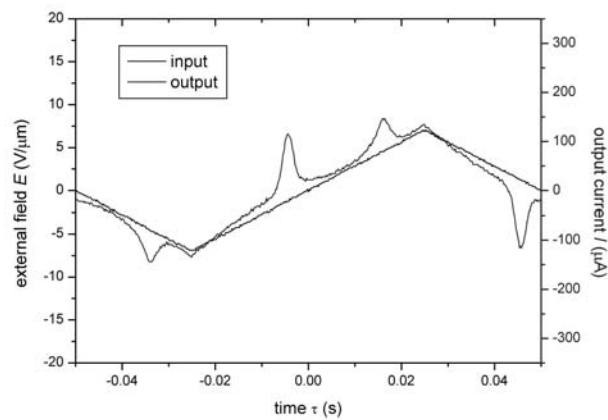
Fig. 7.5: Current response curve to a triangular-wave field $E_{pp} = 5$ V/µm in a 10µm cell ($T = 87\ ^{\circ}$C)
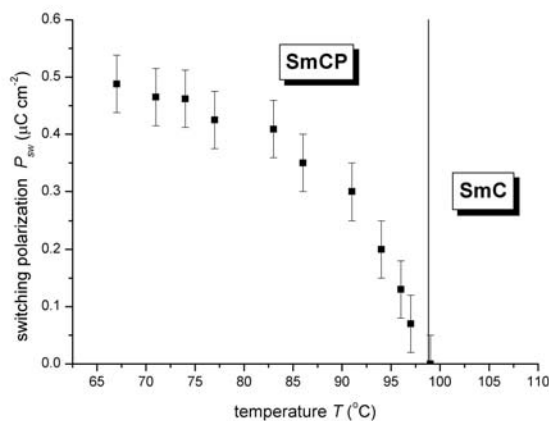
Fig. 7.6: Temperature dependence of the switching polarization for compound VII/**12**

In the SmCP phase the fluctuating schlieren pattern becomes "frozen" and the contrast of the texture increases (Fig. 7.3b). At the same time switching appears in respond to the external electric field. The extinction brushes experience small turns clock- and anticlockwise depending on the polarity of the external field (Fig. 7.4). When the external field goes off the switched state relaxes in the initial state. These findings stand for the antiferroelectric nature of the low-temperature mesophase and the anticlinic $SmC_A P_A$ ground state. A characteristic two peak current response for compound VII/**12** is shown in Fig. 7.5 (triangular-wave technique). In contrast to the compounds with I → SmCP transition where the transition is of the first order, these compounds show a pronounced temperature dependence of the spontaneous polarization in the SmCP phase (Fig. 7.6).

7.4 Structural investigations

7.4.1 NMR measurements

The orientational order parameter S (Fig. 6) has been obtained from the measurements of the shift anisotropy of the atoms in positions 9 and 10 (Fig. 7.7) in ^{13}C-NMR for the compound VII/**12**. The observed anisotropies δ_{zz} of the lines 9 and 10 are proportional to S:

$$\delta_{zz} = S(T)\,\delta_{\zeta\zeta} \tag{6.1}$$

where $\delta_{\zeta\zeta}$ is the shift anisotropy at $S = 1$, in the molecular frame. Using the values reported in the literature for similar compounds and than fitting them to minimize the difference between S obtained from different positions, we arrived to the following values of $\delta_{\zeta\zeta}$: 71.8 ppm for the position 9 and 66.3 ppm for the position 10. We neglect the biaxial term in accordance with our previous experience (Chapter 6).
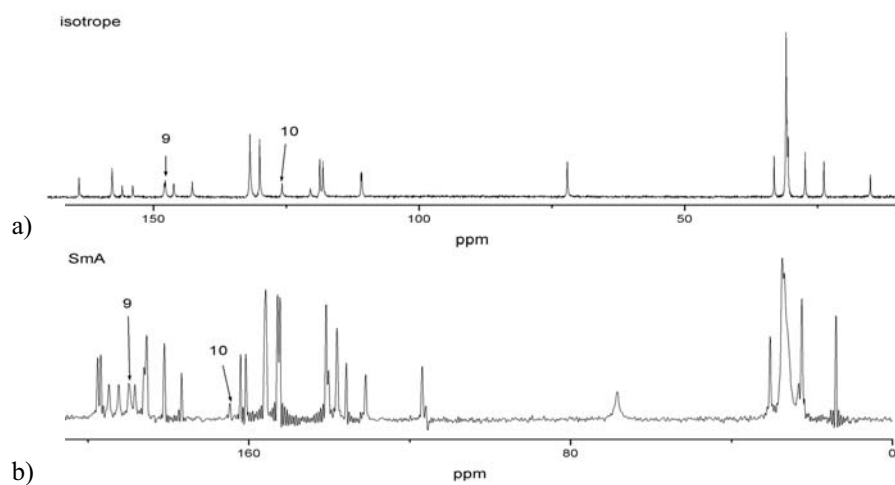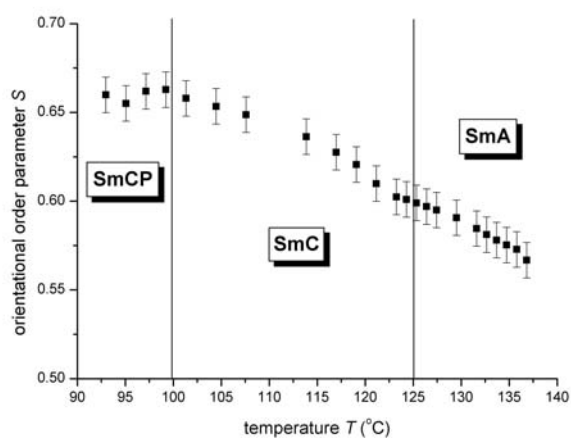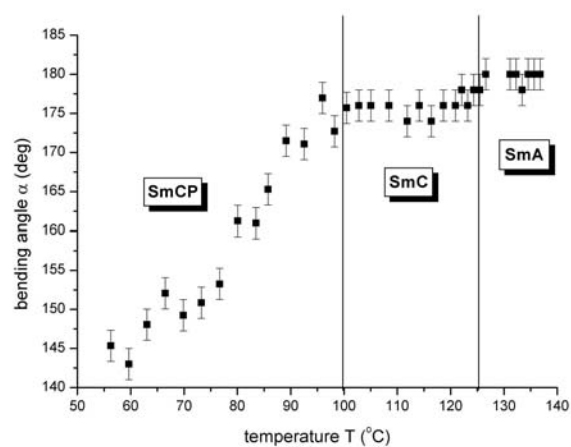
Fig. 7.7: ^{13}C-NMR spectra in isotropic and liquid crystalline states

a)

b)

Fig. 7.8: Temperature dependences a) of the orientational order parameter and b) the bending angle α
       (compound VII/**12**)

There is just a slight temperature dependence of S in the SmA and SmC phases, however, during the transition from the SmC into the SmCP phase the orientational order parameter is essentially constant (Fig. 7.8a).

The bending angle α has been estimated on the base of ^{19}F-NMR measurements. The dipolar splitting of the outer fluorine depends on the angle ε between the long molecular axis and the direction of segment connecting H and F (Fig. 7.1):

$$\Delta \nu = \Delta \nu_0 S(T)(\frac{3}{2}\cos^2 \varepsilon(T) - \frac{1}{2}) \qquad (6.2)$$

where $\Delta \nu_0 = 29.2$ ppm. Finally the overall bending angle is related to the angle ε by the expression $\alpha = 2(\pi - \varepsilon)$ and its temperature dependence is shown in Fig. 7.8b. In the SmA phase the molecule is, actually, stretched: the bending angle is close to 180 deg. There is just a slight decrease of the angle α in the SmC phase and the bending angle decreases considerably in the SmCP phase. This decrease is continuous and over a large temperature interval. At the same time, the minimum value of the bending angle is just around 145 deg, in contrast to the temperature independent α of 120 – 115 deg of the other fluorinated compounds with the I – SmCP transition.

7.4.2 XRD measurements

X-ray diffraction on the oriented and non-oriented samples is an essential tool used for the phase assignment. All three mesophases (except for the nematic) show quasi-Bragg reflections from a layer structure as well as a wide-angle diffuse scattering appearing from the liquid-like order within the smectic layers. The layer spacings measured by Guiner technique exhibit very weak temperature dependence (Fig. 7.9) for all compounds. In the SmA phase the d-values are smaller than the molecular length (Table 7.2). The experimental data can be well fitted by linear function giving the following dependence of the layer spacing on the length of the terminal chain n: $d = 36.08 + 1.12n$ Å. This is smaller than the elongation step of one of the two terminal chains (1.25 Å), which implies that conceivably the molecules in the SmA phase are intercalated.

Table 7.2

compound	layer spacing d (Å)	molecular length L_{str} (Å)	length of the aliphatic chain L_{al} (Å)
VII/**8**	44.8	52.0	10.0
VII/**9**	46.1	55.6	11.3
VII/**10**	47.9	58.0	12.5
VII/**11**	48.3	60.8	13.8
VII/**12**	49.3	62.8	15.0

In the SmC phase the layer spacing slightly decreases by 0.5 – 1 Å depending on the homologue. The absence of a good estimation of the molecular length considerably burdens the investigation of the mesophases with bent-shaped molecules. This decrease might be resulted from a change of the molecular length or tilt or degree of intercalation.
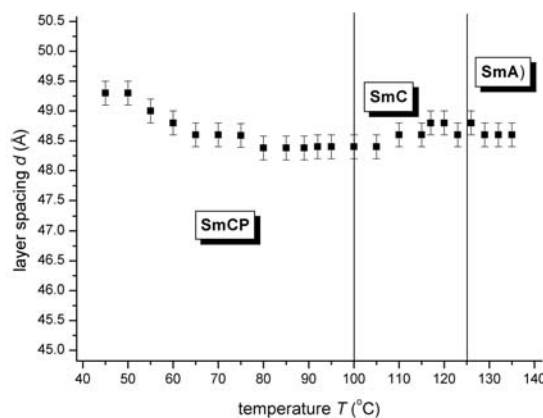
Fig. 7.9: Temperature dependence of the layer spacing (compound **12**)

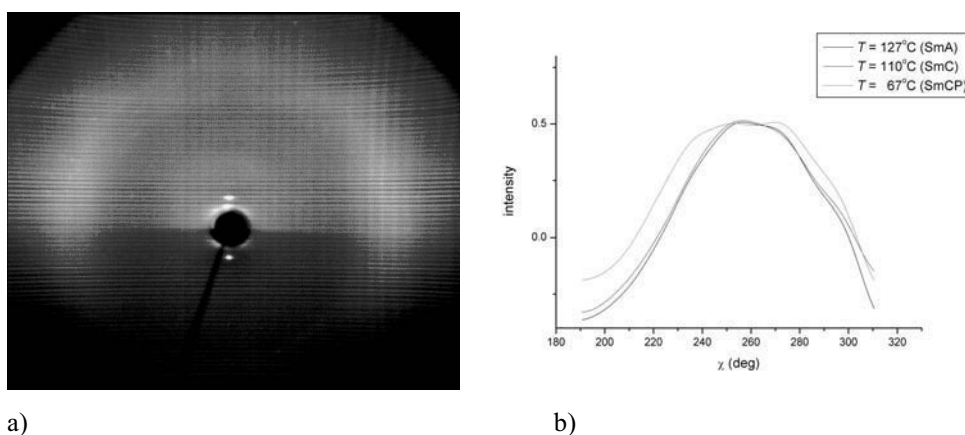a)   b)

Fig. 7.10: a) X-ray pattern of an oriented sample in the SmCP phase (no seeming difference in the appearance of the pattern could be seen in the SmC and the SmA phases) b) χ-scan of the outer-diffuse scattering.

To investigate the effect of the molecular tilt we performed X-ray measurements on the oriented samples. When the smectic layers are oriented parallel to the substrate surface the tilt and bent of the molecules can be detected from the χ-scan of the diffuse scattering. The patterns of all three mesophases SmA, SmC and SmCP look very similar in the case of these compounds (Fig. 7.10a). The χ-scan in the SmC phase is just slightly broader (Fig. 7.10b) than in the SmA phase, which means that the molecular tilt should not exceed 2 – 4 deg. In the SmCP phase the broadening is larger, however, no splitting is observed and the corresponding tilt angle is smaller than about 5 deg.

7.4.3 Dielectric spectroscopy

The temperature dependences of the static dielectric permittivity ε_0 and its high/low frequency limits (ε_1 and ε_2) are shown in Fig. 7.11a. In the SmA and the SmC phase we observed a continuous increase of the permittivity ε_0, which has a sharp λ-like maximum at the transition SmC → SmCP. In the SmCP phase the dielectric response does not show any considerable temperature dependence.
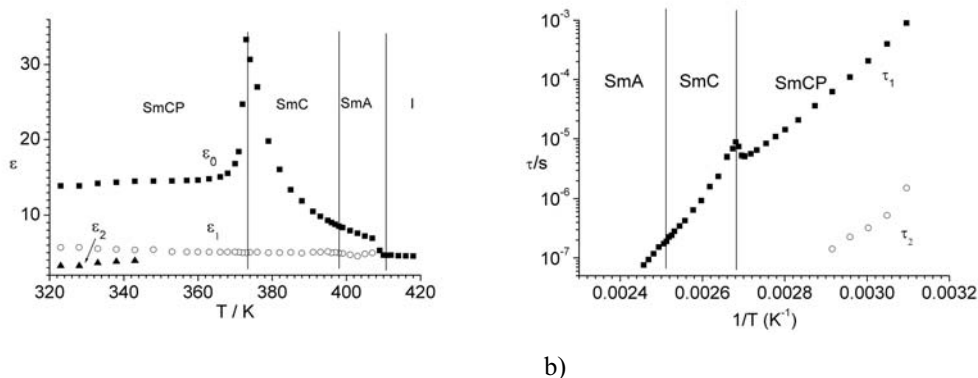
a)

b)

Fig. 7.11: a) Temperature dependences of the static dielectric permittivity ε_0 and its high/low
frequency limits (ε_1 and ε_2) b) relaxation times τ_1, τ_2 and their dependence on the
inversed temperature.

The relaxation times are given in Fig. 7.11b. Two relaxation processes
have been observed. The first one, a slow process characterized by τ_1 can be seen
in the SmA and SmC phases. The relaxation time τ_1 can be interpreted as
collective motion of ordered dipoles. It is growing rapidly with decreasing
temperature indicating that the collective motion of the dipoles becomes more and
more correlated. This process is very fast in the SmA phase and much slower in
the SmCP phase experiencing a small jump on the SmC → SmCP transition.

Another process characterized by the relaxation time τ_2 is fast and
observed only in the SmCP phase. This process is connected with the
reorientation of the dipoles about the long axes and becomes partially collective
due to the strong steric interaction of the lateral dipoles.

Comparing these results with the dielectric response of the "classical"
compounds with I → SmCP transition (first order), we found that in the latter case
the static dielectric permittivity is rather temperature independent and the λ-like
peak was observed only in compounds with the SmC → SmCP transition. In both
cases the two relaxation processes were observed, however, usually the growing
rate of the τ_1 is slower and τ_1 is of order 10^{-4}.

7.5 Discussion

The employed experimental techniques can give a reasonable picture of the SmC
→ SmCP transition. The X-ray measurements show quite a small tilt angle in the
SmC and the SmCP phases. In accordance with our simulations (Chapter 3) the
diffuse scattering should not show any splitting when the tilt is smaller than ~ 5 –
7 deg. The shrinkage of the layer spacing is less than 1% at the tilt of 7 deg and
together with an unknown molecular length and the degree of intercalation the
layer thickness can not be considered. Even in case of the compound VII/**12** the
estimated bending angle α gives 2 Å smaller molecular length and can be well
overcome by a change of the intercalation degree. The assumption of a smallness
of the tilt angle also follows from the weakness of the birefringence of the
schlieren texture in the SmC phase. Thus, summarizing the results we can
conclude that the molecules are slightly tilted in the SmC and SmCP phase and
intercalated in all three phases.

The order in the SmC phase can be described by at least three order
parameters. Non-vanishing value of the orientational order parameter, a tensor of

the second rank Q_{ij}, comes from breaking of rotational symmetry. Breaking of the translational symmetry gives a scalar parameter τ. The tilt of molecules is described by another scalar order parameter – the tilt angle ψ.

The sterical moments of the bent-shaped molecules favor a polar packing in the SmCP phase. The preferred orientation is in the direction of the bows of the molecules and can be described by a vector parallel to the smectic layers and associated with each molecule (in contrast to the board-shaped molecules where the two orientations of the boards are indistinguishable). In case of such symmetric bent-shaped compounds there is a non-zero component of the dipole moment in the same direction. Therefore, the polar ordering in the SmCP phase may be described in terms of the order parameter – spontaneous polarization (or staggered polarization for the antiferroelectric phase), providing, that the molecules are rigid and the magnitude of the dipole moment does not change (which actually means that the conformation does not considerably change and the molecules are rigid). In this case the expansion of the time average charge density of such rigid molecules will have only one harmonic (of cylindrical symmetry) in the high-temperature paraelectric phase. In the SmCP phase the polar order disturbs this symmetry and a non-zero dipole term appears. More general approach is to expand mass distribution in multipoles, however, under assumption of the rigid and symmetrical molecules this approach should give a similar result.

Concerning the other order parameters the NMR experiments do not show any strong change in the orientational order. From the similarity of the X-ray patterns it follows that the parameters τ and ψ are nearly constant. At the same time the switching polarization appears in the SmCP phase. It increases continuously with decreasing the temperature from zero in the SmC phase. The transition is of weakly first order. Thus the free energy expansion can be approximated by L.D. Landau expansion only in powers of **P** as it was firstly made by V.L. Ginzburg in 1945 [28]. Taking the direction OZ along the electric field one obtains:

$$\Phi(P_z) \approx \Phi_0 + AP_z^2 + BP_z^4 - E_z P_z - \frac{E^2}{8\pi} \qquad (7.1)$$

where $A = a(T - T_c)$ and T_c is the transition temperature. In this expansion the sixth power term is disregarded, which is valid far from the tricritical point [28a]. Minimizing the Eq. 7.1 with respect to P_z the following relation can be obtained:

$$2AP_z + 4BP_z^3 = E_z \qquad (7.2)$$

This gives a paraelectric phase with $P_z = 0$ at $T > T_c$ and the susceptibility increases infinitely when the temperature reaches the transition T_c

$$\chi = 1/2a(T - T_c) \qquad (7.3)$$

and dielectric permittivity near the transition is

$$\varepsilon = 1 + 4\pi\chi \cong 2\pi/a(T - T_c) \qquad (7.4)$$

In the ferroelectric phase at $T < T_c$ the Eq. 7.2 gives a two time smaller permittivity for the same value of $|T_c - T|$ in sufficiently weak fields

$$\chi = \left(\frac{dP_z}{dE_z} \right)_E \quad \text{and} \quad \varepsilon \cong \pi / a (T_c - T) \tag{7.5}$$

Qualitatively, it appears that the transition from the paraelectric SmC phase into the ferroelectric SmCP phase should be accompanied with a discontinuity of the dielectric permittivity. Similar behavior has been found in our compounds illustrated in Fig. 7.11a.

However, this simplified approach is made under assumption that the sterical moments can be substituted by the dipole moments of the molecules, which is possible when the conformation and the electron density do not change with the temperature. In our case the bending angle is changing and the relation between the polarization and the sterical moment should depend on the bending angle. Although for small variation of the bending angle it is plausible to assume a linear dependence of the polarization on the bending, which also leads to a Weiss-like behavior of the dielectric permittivity (like in Eq. 7.5).

It should be noticed that despite that the transition is of weakly first order, the latent heat is very small and the Landau expansion still gives qualitatively reasonable results. Another similar paraelectric – ferroelectric transition in bent-shaped mesogens has been investigated by our group [14] (Chapter 5). In that case the transition from an orthogonal apolar SmA phase into the polar SmAP phase was also accompanied by a strong increase of the dielectric permittivity and further decrease. The curve looks different from the one in Fig. 7.11. The reason is that the transition SmA → SmAP was of first order and a similar Landau expansion breaks down.

Chapter 8

Polymorphic SmCP phases

8.1 Introduction

A new 2-methyl-resorcinol derivative is presented (Fig. 8.1) which shows some polymorphic variants of the SmCP phase[1]. Two versions of this compound have been used in the experiments: with a protonated core (compound VIII/**1**) and with a partially deuterated core in positions 4 and 6 (compound VIII/**2**) [82].

Despite that all these phases have quite similar X-ray patterns, the behavior of their orientational order observed in NMR shows considerable anomalies. This compound also exhibits a higher ordered B_5 phase, where an additional density modulation in the smectic layers perpendicular to the layer normal have been observed. This phase has already been described earlier [16, 17] and the in-plane ordering was attributed to rectangular network in the short-range order. Electro-optical switching and the microscopic textures are very similar to the ones of the SmCP phase which complicates preliminary phase assignment and X-ray measurement are usually required to differentiate between the phases.

Another interesting phase exhibited by this compound is a low temperature B_X phase. It shows a crystalline state and electro-optical switching.

8.2 Polarizing microscopy and electro-optical investigations

The B_2 phase appears on cooling of the isotropic liquid exhibiting a grainy or fan-shaped texture (Fig. 8.2a). At the transitions $B_2 \rightarrow B_2{}^{/}$ the texture does not change, whereas at the transition $B_2{}^{/} \rightarrow B_2{}^{//}$ paramorphotic smooth fan-shaped textures arise (Fig. 8.2b). The transition into the B_5 phase is accompanied by a minor change of the texture – by a small change of the birefringence and by the formation of irregular stripes perpendicular to the fans (Fig. 8.2c). The transition into the low-temperature phase B_X could not be recognized by polarizing microscopy.
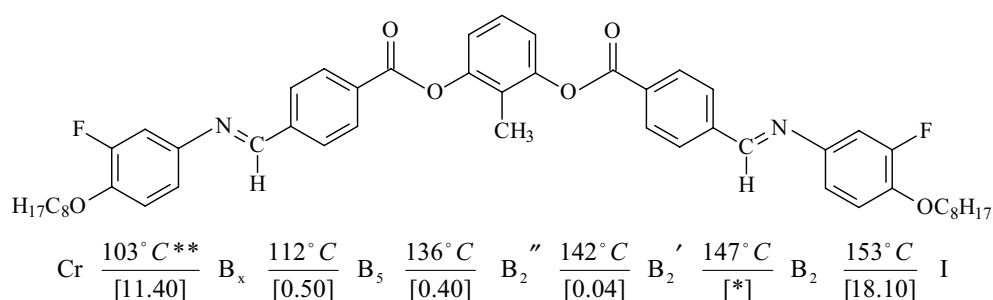

$$\text{Cr} \; \frac{103°C**}{[11.40]} \; \text{B}_x \; \frac{112°C}{[0.50]} \; \text{B}_5 \; \frac{136°C}{[0.40]} \; \text{B}_2{}'' \; \frac{142°C}{[0.04]} \; \text{B}_2{}' \; \frac{147°C}{[*]} \; \text{B}_2 \; \frac{153°C}{[18.10]} \; \text{I}$$

Fig. 8.1: Structural formula of compound VIII/**1** and VIII/**2**, in the latter case the central benzene ring is deuterated in positions 4 and 6

---

[1] . In order to save space we will use designation B_2 for the SmCP phase
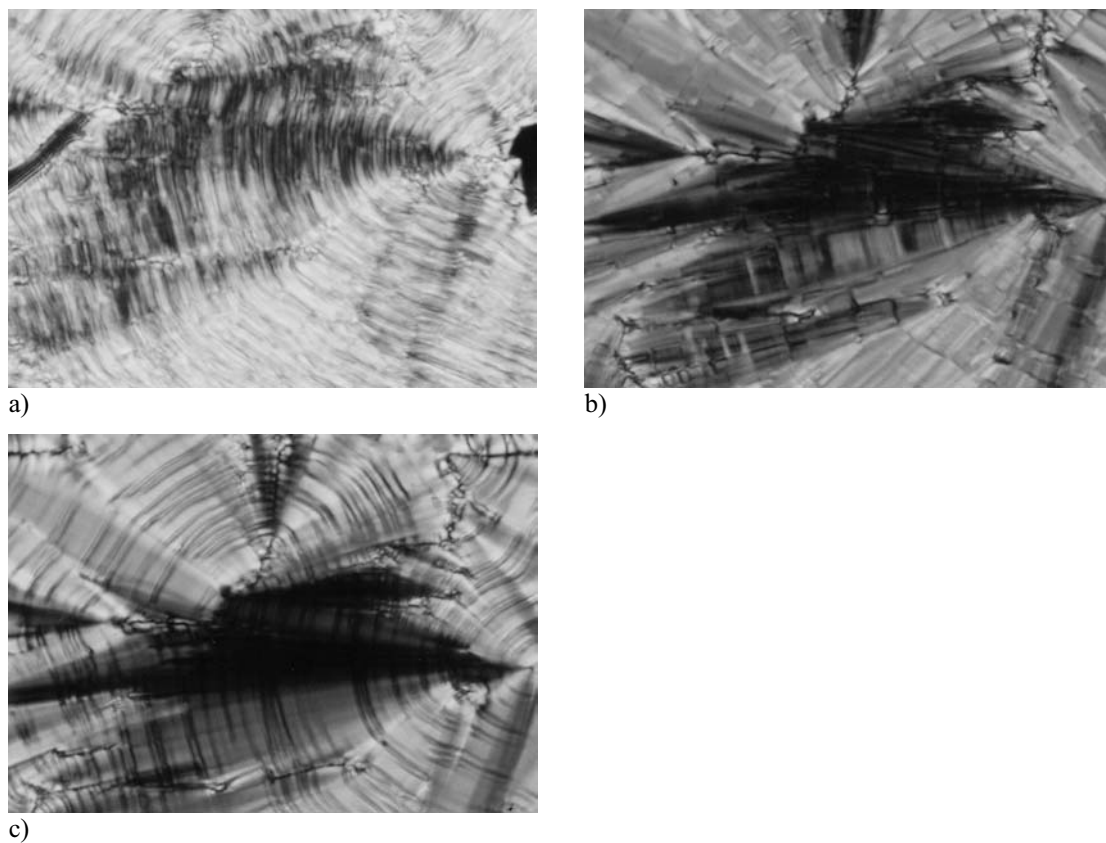
a)

b)

c)

Fig. 8.2: Optical textures a) of the B_2 phase (148ºC); b) the $B_2^{//}$ phase (140ºC) and c) B_5 phase (130ºC)
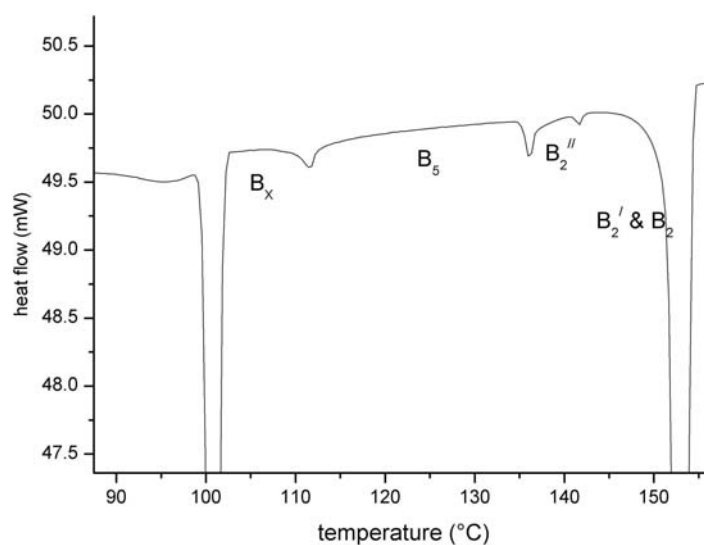

Fig. 8.3: DSC curve

With exception of the phase transition $B_2 \rightarrow B_2^{/}$, which has been observed in NMR and XRD experiments, all transitions have been detected by differential scanning calorimetry technique (Fig. 8.3). It is remarkable that the clearing enthalpy is higher
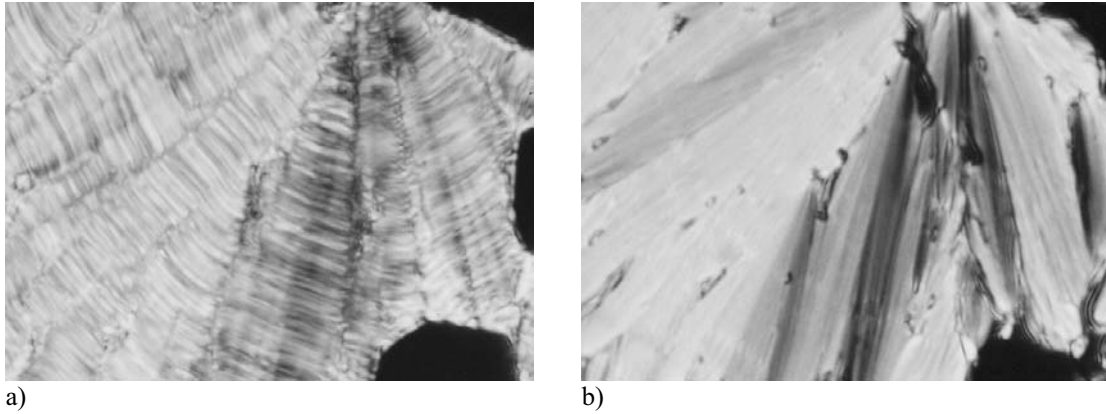
a)   b)

Fig. 8.4: Field-induced texture change of the $B_2^{/}$ phase a) field-off state; b) ± 2.8 V µm^{-1} (cell thickness
          10 µm; temperature 143ºC)

a)   b)
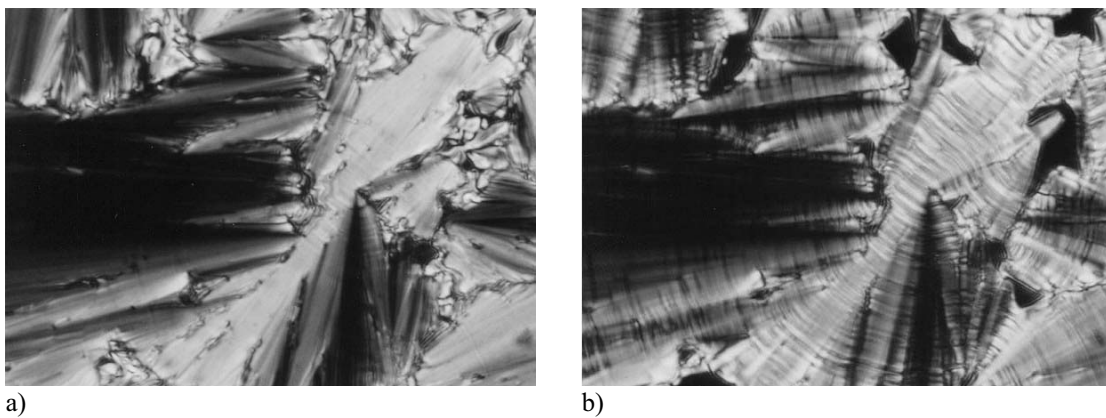
Fig. 8.5: Field-induced texture change of the B_5 phase a) field-off state; b) ± 4.8 V µm^{-1} (cell thickness
          10 µm; temperature 132ºC)

than the enthalpy of melting. On the other hand, the transition enthalpies between the B phases are rather low (0.02 - 0.5 kJmol^{-1}).

All four phases showed similar electro-optical responses to the applied d.c. electric field. The initial fan-shaped texture transformed into a smooth SmA-like fan-shaped texture at the field higher than a threshold 0.5 - 0.8 V/µm for the mesophases B_2, $B_2^{/}$, $B_2^{//}$ and B_5 (Fig. 8.4 and 8.5). The textures relaxed into their initial state when the external field was removed (at $E = 0$).

The current response to the applied triangular-wave voltage contains two peaks of the repolarization current (Fig. 8.6a). From this finding and the observation of the relaxation of the polarized state into the initial state in the experiments with d.c. voltage, we can assume an antiferroelectric (AFE) ground state of the mesophases. However the two current response peaks were observed at considerably low frequencies 1.0 – 0.5 Hz, only one peak could be observed at higher frequencies (Fig. 8.6b). The repolarization signal have also been found when we applied a square impulse varying from $E > E_{th}$ till $E = 0$. If the relaxation time of the field-induced ferroelectric state (FE) into the AFE state is larger than the period of the applied field a direct switching between two FE states occurs. In this case only one current peak can be observed. This phenomenon has been shown by J. Lee *et al* [83] for the chiral antiferroelectric SmC_A^* phase where only one current response peak was observed at high frequencies. Recently, J.P. Bedel *et al* [84] found a similar effect on "banana" phases.
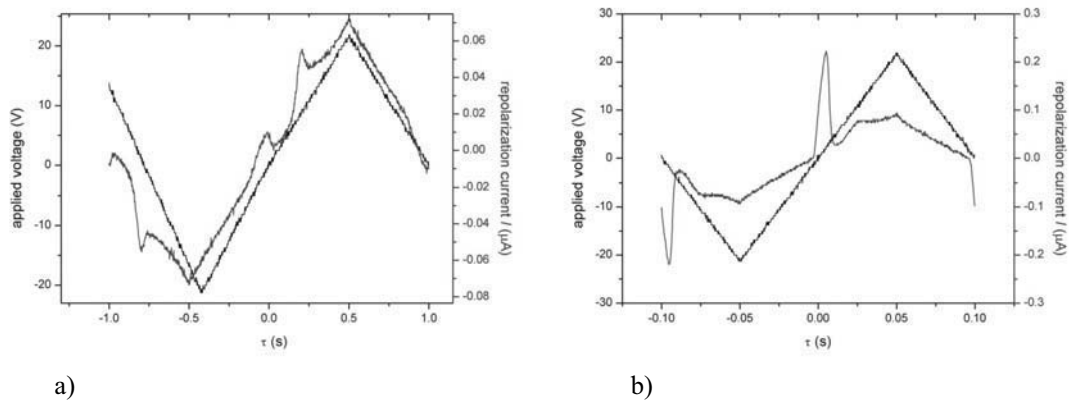
a)   b)

Fig. 7.6: Switching current response of the $B_2^{//}$ phase to an applied triangular wave field at $T = 141°C$ a) $f = 0.5$ Hz, $E_{pp} = 4.0$ V μm^{-1}; b) $f = 5$ Hz, $E_{pp} = 4.0$ V μm^{-1}

The temperature dependence of the spontaneous polarization reaches 800 nCcm^{-2}. At the transition into the low-temperature phase B_X the threshold significantly increases. The relaxation from the polarized state into the ground state is quite slow, probably due to high viscosity of the sample. But the switching behavior is quite similar to that of the B_5 phase.

8.3 X-ray diffraction measurements

The X-ray diffraction patterns of the three high-temperature phases show equally spaced Bragg reflections indicating a layer structure. The layer spacing does not change markedly over the whole temperature range of these phases and is equal to 40.8 – 41.6 Å.

The patterns of oriented samples display some further details (Fig. 8.7). The high temperature phase exhibits a pattern typical for a tilted smectic phase without in-plane order like SmC or B_2 (the latter has been confirmed by the electro-optic technique): the layer reflections are observed on the meridian of the pattern; the maxima of the broad outer diffuse scattering are situated out of the equator (Fig. 8.7a) indicating an inclination of the molecules and the absence of the long-range positional order within the layers. From the χ-scan the tilt angle of about 25 deg has been derived. On cooling the sample into the $B_2^{/}$ phase the meridian reflections reproducibly split up into pairs (Fig. 8.7b), as can be seen from the enlarged profile shown in the inset of Fig. 8.7b. This splitting corresponds to an angle ~ 6 deg between the layer normal and the fiber axis (Fig. 7.8). This additional tilt is too small to be detected from the wide angle diffuse outer scattering. However, this change conforms with alterations in the NMR spectra. The split peaks merge again on the meridian at the transition into the $B_2^{//}$ phase at 142°C. Below 135 °C another mesophase appears where, in addition to the diffuse wide-angle scattering, two stripes perpendicular to the equator are observed (see the equatorial scan in Fig. 8.7c). The continuous stripes express the fact that there is no positional correlation between the molecules from different layers. Thus, the scattering diagram can be described by the formation of a two-dimensional rectangular cell within the layers on a short-range scale, which is characteristic of a B_5 phase (see ref. [17]). The intensity profile along the stripe has a maximum on the equator as well as above and below it. With decreasing temperature, the intensity on the equator becomes more and more pronounced.
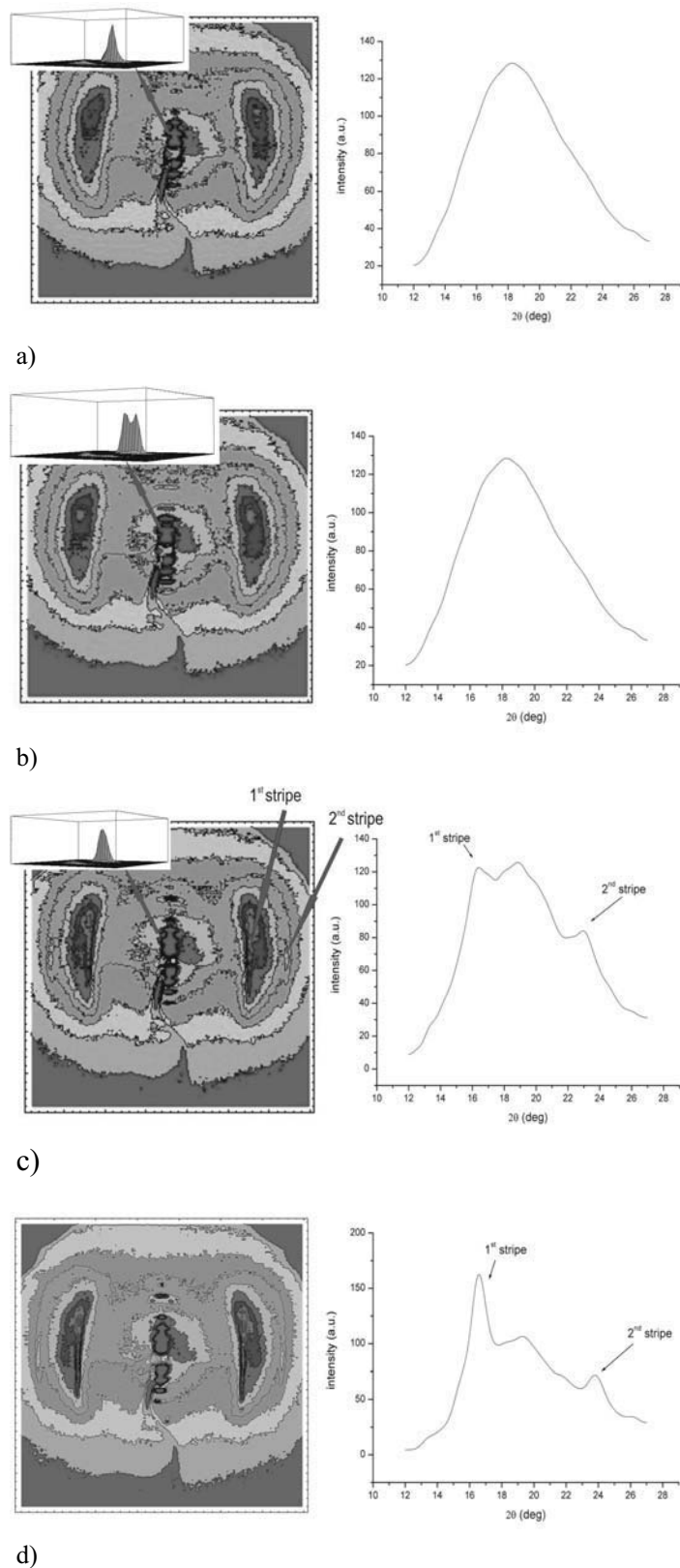
Fig. 8.7: X-ray patterns of oriented samples and their equatorial intensity scans, the inset picture show a three-dimensional profile of the meridian (001) reflection a) B_2 phase (T = 149ºC), b) $B_2^/$ phase (T = 145ºC), c) B_5 phase (T = 120ºC), d) B_X phase (T = 110ºC)

a)   b)
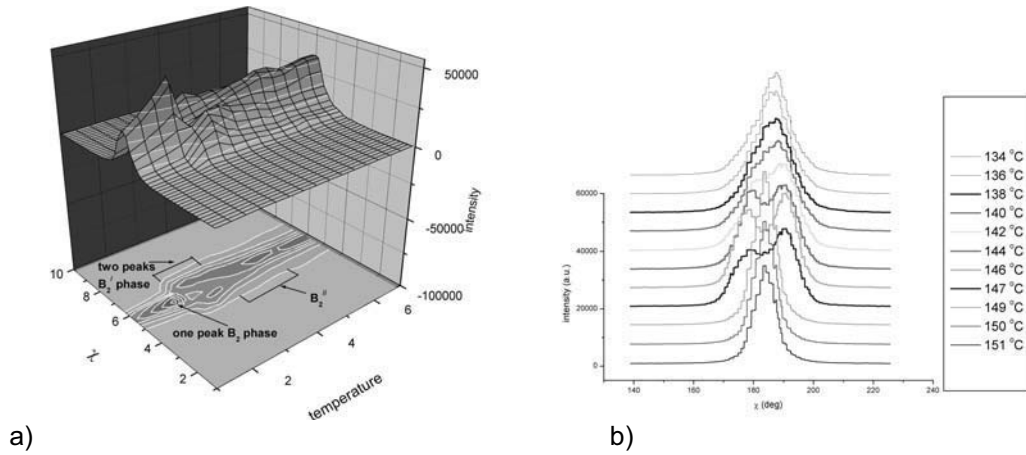
Fig. 8.8: Temperature behavior of the first meridian reflection a) a three dimensional plot in $\chi - T$ co-ordinates (relative units); b) scatters of the χ-scans corresponding to a)

The pattern of the B_X phase is characterized by the appearance of distinct spots on the *hk* rows, which indicates the positional correlation of the molecules in adjacent layers (Fig. 8.7d). With respect to this, the phase can be considered as a three-dimensional crystalline one, although the remaining diffuse scattering implies a large amount of disorder in this phase. Form the position of the spots (perpendicular to the equator of the pattern) an in-plane organization of the molecules described by an orthorombic cell can be inferred. But some satellites around the *00l*-reflections (out of the meridian) stand for a more complex structure (perhaps a helical superstructure), which cannot be resolved at present. The next change of the X-ray pattern takes place below $T \cong 102$ °C. The scattering radiation condenses to a lot of Bragg-reflections corresponding to a true crystalline phase.

8.3.1 Dielectric spectroscopy

The frequency dependence of the real and imaginary parts of the dielectric permittivity $\varepsilon^{/}$ and $\varepsilon^{//}$ are given in Fig. 8.9.

The experimental points of $\varepsilon^{/}$ and $\varepsilon^{//}$ were fitted using the model described by Eq. 8.1 consisting of two Cole-Cole mechanisms (term 2 and 3), a conductivity contribution (term 4) and term 5 accounting for the capacitance of the ionic double layer appearing on the surface of the electrodes at low frequencies:

$$\varepsilon^* = \varepsilon_2 + \frac{\varepsilon_0 - \varepsilon_1}{1 + (j\omega\tau_1)^{1-\alpha_1}} + \frac{\varepsilon_1 - \varepsilon_2}{1 + (j\omega\tau_2)^{1-\alpha_2}} - \frac{jA}{f^M} + \frac{B}{f^N} \tag{8.1}$$

where ε_i - low and high frequency limits of the dielectric permittivity, $\omega = 2\pi f$ (f - frequency), τ_i - relaxation times, α_i - Cole-Cole distribution parameters, the conductivity term A ($\kappa = 2 \cdot A \cdot \pi \cdot \varepsilon^0$, $\varepsilon^0 = 8.85 \cdot 10^{-12}$ As/Vm, if M = 1) as well as M, B and N are fit parameters responsible for the slope of conductivity and capacity of the double layer.
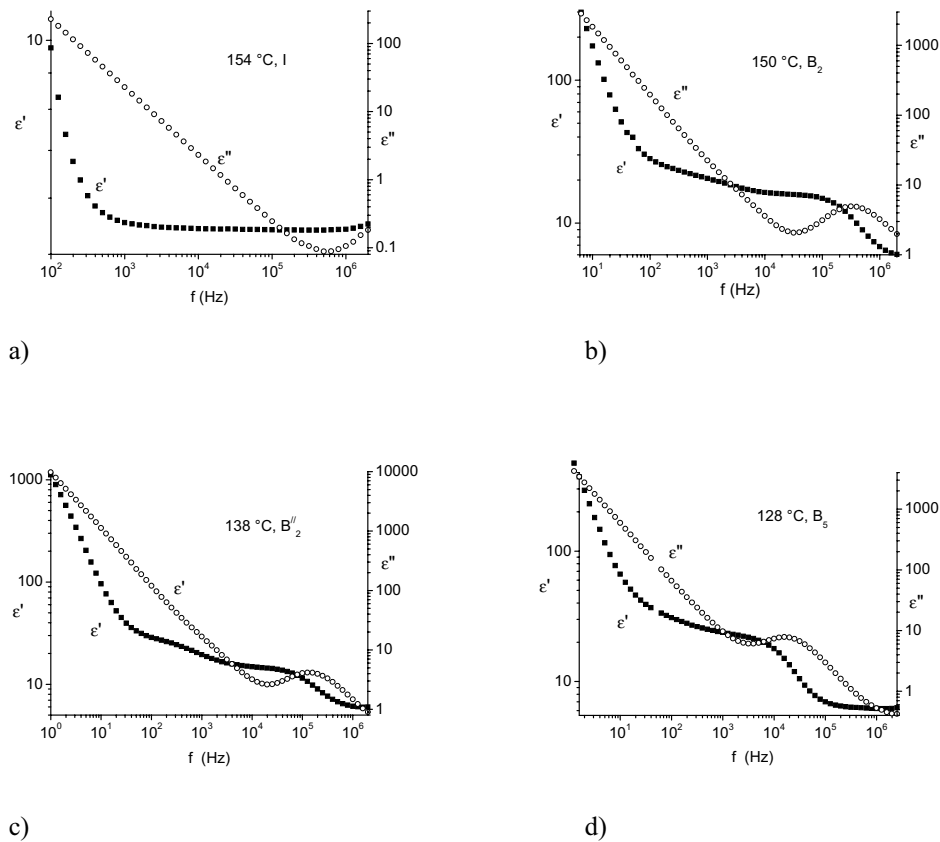
Fig. 8.9: The real and imaginary part of the dielectric permittivity (ε', ε'') as a function of the
frequency a) isotropic phase (154 ºC); b) B_2 phase (150ºC); c) B_2'' phase (138 ºC); d) B_5
phase (128 ºC)

The data acquired in the isotropic phase up to 50 kHz can be well described by use of the first and the last two terms. It is not necessary to consider a relaxation term since no dispersion of the dielectric permittivity was observed (Fig. 8.9a). Data at $f >$ 600 kHz which have been affected by beginning of the absorption at high frequencies and by a standing wave between the capacitor plates were not used in fitting. In the B_2 phases two absorption bands have to be taken into account for the data interpretation [85]. Thus, for the B_2 modification a high frequency process at about 300 kHz and a low frequency one at 500 Hz (Fig. 8.9b), for the B_2'' phase at 150 kHz and 300 Hz (Fig. 8.8c) have been found. The limits of dielectric permittivity calculated from the experimental data according to Eq. 8.1 are shown in Fig. 8.10. Confidence intervals for the dielectric permittivity given in Eq. 8.1 of $\Delta\varepsilon_0 = \pm 2.0$, $\Delta\varepsilon_1 = \pm 1$, $\Delta\varepsilon_1 = \pm 0.3$ as well as a relative error of the relaxation times τ_1 of $\pm 25\%$ and of τ_2 of 10% were calculated. Since the error $\Delta\varepsilon_0$ increases with decreasing temperature, no data of ε_0 and τ_1 are given in the Fig. 8.9 and 8.10 for the temperatures below 136 ºC. The dielectric permittivity ε_1 reflects nearly all phase transitions found by microscopic measurements and indicated by vertical lines. It should be noted that the dielectric increment $\Delta_2 = \varepsilon_1 - \varepsilon_2$ changes significantly at the I/B_2, B_2'/B_2'', and B_2''/B_5 transitions. A relatively high Δ_2 in the B phases in comparison with the isotropic liquid points to a strong positive dipole correlation. The decrease of Δ_2 at the B_5/B_X transition may be connected either with a
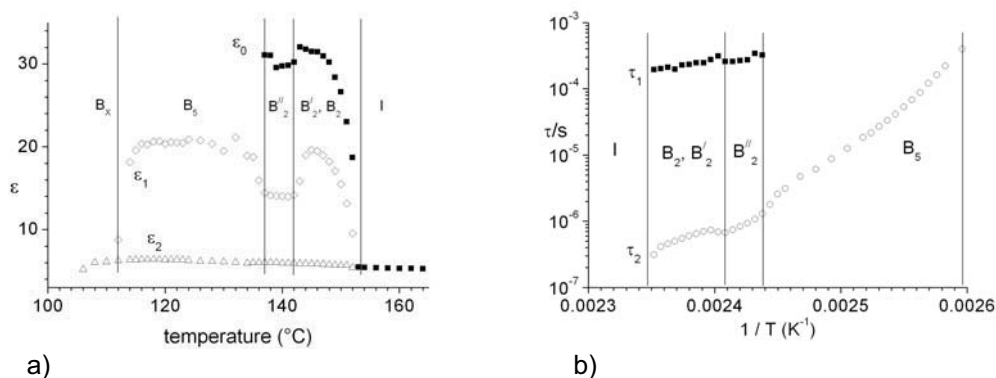
Fig. 8.10: a) Limits of the dielectric permittivity in the isotropic, B_2, $B_2^/$, $B_2^{//}$, B_5 and B_X phase; b) relaxation times τ_1, τ_2 in dependence on the inversed temperature in the B_2, $B_2^/$, $B_2^{//}$ and B_5 phase

complete disappearance or a stepwise decrease of the relaxation frequency of some decades (phase transition into a highly ordered solid-like B phase). The Cole-Cole distribution parameter was calculated to be α_2 = 0,01±0.01 in all phases which corresponds to a classical Debye-mechanism. For the low frequency absorption Cole-Cole distribution parameters α_1 = 0.32±0.03 (B_2) and 0.25±0.03 ($B_2^/$) were obtained, pointing to a distribution of the relaxation times.

The relatively high value of ε_2 = 6 in the B_X phase indicates a modification in which a fast dynamics of the polar end groups and probably also that of local motion within the core takes place. This phase transforms at about 102 °C slowly into a solid phase in which a partial reorientation of dipoles occurs, therefore ε_2 decreases by further cooling to temperatures below 100 °C to about 4 (not shown in Fig. 8.10).

The relaxation times are given in Fig. 8.10. Within the error there is no difference between the data of τ_1 in phases B_2 and $B_2^/$. A mean activation energy of E_A = (56±10) kJmol^{-1} was calculated. We interpret this process as a collective motion of antiparallel ordered dipoles [86]. The faster process characterized by τ_2 is connected with the reorientation of the dipoles about the long axes. This process becomes partially a collective character due to the strong sterical interaction of the lateral dipoles among themselves [86]. The step of τ_2 at the $B_2^//B_2^{//}$ transition is outside of the experimental error. The decrease of the parameters Δ_2 and of τ_2 at the $B_2^//B_2^{//}$ transition may indicate that in the $B_2^{//}$ phase the interaction of the dipoles is reduced with respect to that in the $B_2^/$ phase and gives an argument for a phase transition. The mean activation energies of $E_A(B_2)$ = (130±15) kJmol^{-1}, $E_A(B_2')$ = (180±30) kJ mol^{-1} and $E_A(B_5)$ = (270±20) kJ mol^{-1} were calculated. The detected high increment Δ_2 is in the same order of magnitude as that of the B_2 modification and indicates a strong positive dipole correlation in the B_5 phase.

8.4 Investigation of the orientational order

8.4.1 Order parameter form the dipolar splitting

The temperature dependence of the orientational order parameter $S(T)$ has been measured using ^{1}H-NMR on compound VIII_**1** as it is described in Section 2.5.2. The splitting of the protons in the positions 9 and 11 in the central ring (Fig. 2.5) is
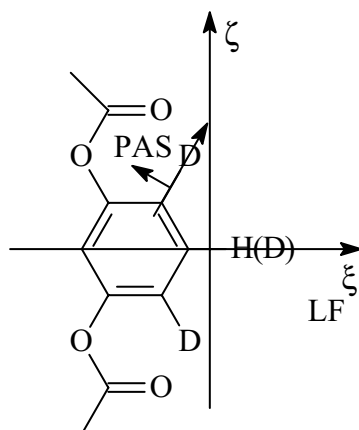
Fig. 8.12: Deuterated central core of compound VIII_**2**

proportional to *S*. Unfortunately, the factor of the splitting magnitude strongly depends on the geometry of the ring C, which considerably complicates the determination of the absolute values of *S*. The central phenyl ring is substituted by the methyl group resulting in its slight deformation. However, the calculations of the order parameter have been performed under the assumption of a regular geometry of the central ring and the corrections on the deformations have been made comparing these results with the order parameters obtained by other methods (^{2}H-, ^{13}C-NMR).

8.4.2 Order parameter from quadrupolar splitting

Partial substitution by ^{2}H in the position 10 of the compound VIII/**2** (Fig. 8.12) allows obtaining both longitudinal order parameter *S* and transversal order parameter *D* using ^{2}H-NMR spectra. The principle axis of the quadrupole tensor is aligned along the C-H bond. The quadrupole coupling tensor $\widehat{W}$ can be expressed in the principle axis frame as a traceless diagonal 2nd rank tensor:

$$\widehat{W} = W_0 \begin{pmatrix} -\dfrac{1-\eta}{2} & 0 & 0 \\ 0 & -\dfrac{1+\eta}{2} & 0 \\ 0 & 0 & 1 \end{pmatrix} \tag{8.2}$$

where the asymmetry factor $\eta = 0.04$ and $W_0 = 277.5\,\mathrm{kHz}$. The quadrupole splitting of ^{2}H10 is very sensitive to the angle between the C-H bond and the direction of the magnetic field. Using the angle φ between the bond direction and the molecular long axis (Fig. 8.12), we obtain the quadrupole splitting in the director frame:

$$\Delta v^i = W_0 \left[S \left(\frac{3}{2}\cos^2\varphi + \frac{\eta}{2}\sin^2\varphi - \frac{1}{2} \right) + \frac{D}{3} \left(\frac{3}{2}\sin^2\varphi + \frac{\eta}{2}(\cos^2\varphi + 1) \right) \right] \tag{8.3}$$

Assuming regular geometry of the central core, we find the angle φ be equal to 30 deg for the position 10 and 90 deg for 11. The spectra resolution is much affected by the orientation of different domains in the magnetic field. The averaged molecular long axis is oriented along the magnetic field and the layer plane is tilted. Thus, two pairs of lines can be seen on ^{2}H-NMR spectrum, corresponding to the two quadrupole splittings (Fig.
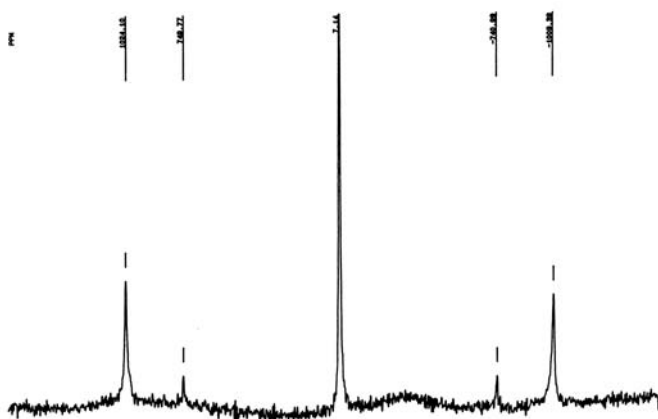
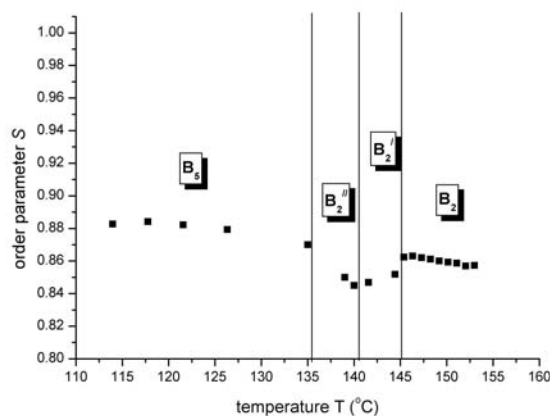Fig. 8.13: ^{2}H-NMR spectrum of the deuterated compound VIII_**2**

Fig. 8.14: Order parameter S obtained under assumption that the molecules are oriented along the magnetic field

8.13): from the positions 10 and 11, which enables us to calculate both parameters S and D. The absolute values depend on the deformation of the central ring and the orientation of the molecular long axis.

8.4.3 Results of the NMR measurements

The order parameter S in the high-temperature B_2 phase was obtained using both ^{1}H-NMR and ^{2}H-NMR techniques under the assumption that the molecules are oriented parallel to the magnetic field. Three regions can be distinguished in the temperature interval of the B_2-like phases (152 ˚C – 136 ˚C) (Fig. 8.13). The first interval between the clearing point and ~145 ˚C where the splitting is almost independent of the temperature, then the splitting experiences a jump and again a small plateau till 142 ˚C. This region we designate as the $B_2^{/}$ phase. The transition into the $B_2^{//}$ phase is accompanied by a small latent heat detected on the DSC curve. The proton splitting is monotonically increasing with decreasing temperature and at 136 ˚C it reaches saturation upon the transition into the B_5 phase. However, the two methods, based on the assumption about the regular geometry of the central core, give slightly different

results. If we account for the small distortion of the ring (Section 8.3.1) with $\varphi^{10} = 29.1$ deg, than with $k = 1.012$ and $\Delta\nu^{(2)}{}_o = 47.25$ ppm it results in $\Delta\nu_o = 47.8$ ppm.

In the temperature region of the B_2 phase one obtains two well resolved line pairs in the ^{2}H-spectra of the compound VIII_**2**. Below 145°C the line pair from ^{2}H10 broadens considerably, but the sharp lines from ^{2}H11 are further observed. With the same angle $\varphi = 29.1$ deg we calculated S and D for the high temperature region, the resulting D is very small ($D < 0.01$). To interpret the data at the lower temperatures, we assumed the same small values of D and calculated S only from the splitting of ^{2}H11 over the whole liquid crystalline temperature region.

8.5 Discussion

A discontinuous decrease of the splitting upon the transition $B_2 \rightarrow B_2{}^{/}$ (145˚C) is unusual. The jump of the splitting value can be interpreted in two ways: either by a discontinuity of the order parameter S or by a change of the orientation of the central core with respect to the magnetic field (due to a conformational change, or the tilt of the molecules). Furthermore, most lines broaden below the transition. It seems more realistic to assume a change in the conformation of the molecule or in the structure of the phase.

The broadening of ^{2}H10 line pair below the transition at 145 ˚C is so strong, that the lines vanish in the noise whereas the lines of ^{2}H11 remain sharp. Similarly, most lines in the ^{13}C and ^{19}F spectra are broaden. The same behavior is observed for both deuterated and nondeuterated materials. The broadening depends on the anisotropy of the observed interaction and the orientation of the principle-axis system of the interaction tensor. One explanation may be given by an inclination of the director with respect to the magnetic field due to a rotation about the x-axis (parallel to the ξ-axis). Further remains the onset of a tilt between the long axis and the plane of ring C by a rotation around the ξ-axis through ^{2}H11. The tensor components along the molecular axis are unchanged for the nearly axialsymmetric tensor of ^{2}H11.

We expect that the director frame for banana-shaped molecules with high viscosity, large order and low molecular mobility is strongly anisotropic. This is described by two order parameters P and C as demonstrated in the equation

$$W_{xx} - W_{yy} = P W_{\zeta\zeta} + \frac{1}{3} C (W_{\xi\xi} - W_{\eta\eta})$$

$$C = \left[(S^x_{\xi\xi} - S^x_{\eta\eta}) - (S^y_{\xi\xi} - S^y_{\eta\eta}) \right], \quad P = (S^x_{\xi\xi} - S^y_{\xi\xi})$$

(8.4)

Since $S = S^z_{\zeta\zeta}$ is large we expect a small P. Than the anisotropy in the director system is proportional to the anisotropy in the molecular system. From the anisotropic packing of the bended molecules in the tilted layers we estimate a preferential orientation of ξ parallel x and η parallel y. That gives a $C/3$ near 1. More exact values could be obtained from measurements with the director axis perpendicular to the magnetic field.

The observed change in the X-ray scattering in the second phase will be discussed below, but this supports the variation in the director orientation. Conformational changes should not be visible by X-rays. Such rotation around the central axis should be accounted in our formulae for the order parameter. Assuming the angles of rotation around the horizontal x-axis is $\Delta\psi$, the interaction tensor is given by

$$W_{zz}(\Delta\psi) = W_{zz}(\frac{3}{2}\cos^2\Delta\psi - \frac{1}{2}) - \frac{1}{2}\frac{C}{3}(W_{\xi\xi} - W_{\eta\eta})\sin^2\Delta\psi$$

$$(W_{\xi\xi} - W_{\eta\eta}) \approx \frac{1-\cos^2\Delta\psi}{\cos^2\Delta\psi - 1/3}W_{\zeta\zeta}$$

(8.5)

For an axialsymmetric phase (N, SmA) the reduction in the tensor component along the magnetic field is proportional to W_{zz} and $P_2(\psi)$. In the biaxial phase the second term exists which is proportional to the molecular asymmetry. Deuterium in position 11 ($\varphi = 90$ deg) has the largest molecular asymmetry and that compensates the first term. W_{zz} does not depend on the angle. The formula explains very well the different line width in the spectra below the high temperature phase.

We explain the observed decrease of the quadrupole splitting below the high temperature phase by a small but abrupt jump of the tilt angle $\Delta\psi$. Let us assume that the order parameter is monotone without a jump. Taking the angle $\varphi = 30$ deg (regular conformation of the central ring), we find the angle $\Delta\psi$ of the rotation along the horizontal axis if we assume certain values for C. The experimental value gives $W_{zz}(\Delta\psi = 0)/W_{zz}(\Delta\psi) = 1.025$ which corresponds to an angle ~ 7 deg, for $C/3 < 1$ the angle increases.

In fact, we observe line broadening and not a shift of the sharp lines. The state of the lowest energy is when the director is parallel to the strong magnetic field. On heating the sample from the crystalline phase the orientation moment is too small to overcome the high friction due to the high viscosity. The same behavior exists on cooling. The tilt of the molecules in the layers changes in the new phase, but the director cannot reach the new equilibrium value. So we observe a director distribution, visible as line broadening. Probably the tilt jumps to smaller values approaching the B_5 phase without tilt discontinuity.

The transition into $B_2^{/}$ phase is accompanied by the splitting of the meridian reflections in the X-ray patterns of the oriented samples, however, no extra reflections have been observed. The behavior obtained from NMR spectroscopy also indicates a phase transition. The results of the XRD measurements can by interpreted by a deformation or a break of the smectic layers and the layer normal takes two directions with an angle ~ 12 deg between them. A similar interpretation might be applied to our NMR results.

The splitting of the meridian reflections merges at $T = 142$ °C, however they still remain quite broad. On the DSC diagram there is a small peak which corresponds to a phase transition. The clear evidence of the phase transition has been given by dielectric spectroscopy. The decrease of the relaxation time τ_2 and the decrease of the parameter Δ_2 found by the dielectric measurements indicate that in this phase the dipole interaction is reduced. In view of similarity of the X-ray pattern of this phase and B_2 phase we name it $B_2^{//}$.

The mesophase which arises on cooling the $B_2^{//}$ phase could be identified as the B_5 phase. The additional diffuse scattering maxima on the equator of the X-ray pattern point to the continuous formation of a positional order in the smectic layers but the order is still restricted to the short range region. We were able to perform quantitative electro-optical investigations on a B_5 phase, for the first time.

From X-ray investigation follows that the low-temperature phase, preliminary designated as B_x, is a three-dimensional solid-like phase. Surprisingly this phase shows

an electrical switching at sufficiently high electric field (10-20 V/μm). In contrast to the B_2, $B_2^{/}$, $B_2^{//}$ and B_5 phases the switched state slowly relaxes to the ground state when the field is switched off. The B_x phase is the first switchable highly ordered "banana phase".

It should be noted that in 1999 H.T. Ngyuen *et al* [87] first presented bent-core mesogens with fluorine substituents on the outer rings. These compounds exhibited four tilted antiferroelectric smectic phases without in-plane order. However, no details about the structure of the mesophases were reported.

Chapter 9

Polymorphic B$_5$ phases

9.1 Introduction

In this chapter we present two homologous five-ring bent-core mesogens with lateral fluorine substituents on the central core and on the outer rings [88]. These compounds exhibit not only a B$_2$ phase but also several switchable higher ordered "banana phases". The structural characterization was performed by X-ray diffraction measurements completed by NMR and electro-optical investigations. Since the compounds contain fluorine substituents on the central core and the outer rings the orientational order parameter and the conformation of the molecules in the liquid crystalline state could be studied in one experiment using ^{19}F-NMR. Besides antiferroelectric B$_5$-like phases, we have been able to detect a low-temperature B$_5$ phase which possesses a ferroelectric ground state and shows a bistable switching.

Two homologous bent-core compounds have been investigated (Fig. 9.1).In the following transition scheme the transition temperatures and enthalpies are presented:
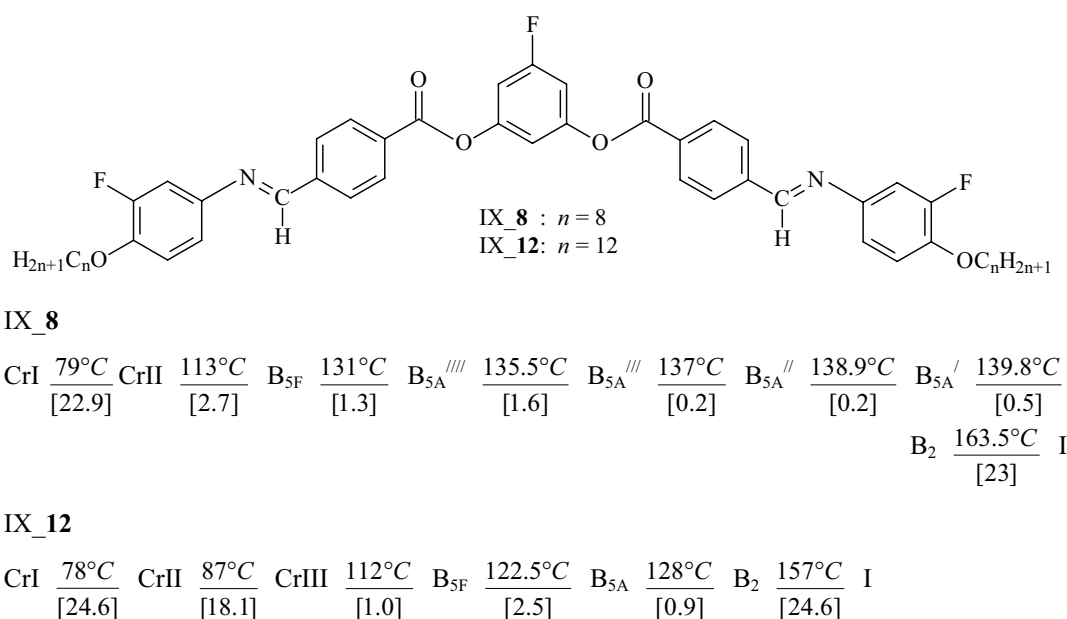

IX_**8** : $n = 8$
IX_**12**: $n = 12$

IX_**8**

CrI $\dfrac{79°C}{[22.9]}$ CrII $\dfrac{113°C}{[2.7]}$ B$_{5F}$ $\dfrac{131°C}{[1.3]}$ B$_{5A}^{////}$ $\dfrac{135.5°C}{[1.6]}$ B$_{5A}^{///}$ $\dfrac{137°C}{[0.2]}$ B$_{5A}^{//}$ $\dfrac{138.9°C}{[0.2]}$ B$_{5A}^{/}$ $\dfrac{139.8°C}{[0.5]}$

B$_2$ $\dfrac{163.5°C}{[23]}$ I

IX_**12**

CrI $\dfrac{78°C}{[24.6]}$ CrII $\dfrac{87°C}{[18.1]}$ CrIII $\dfrac{112°C}{[1.0]}$ B$_{5F}$ $\dfrac{122.5°C}{[2.5]}$ B$_{5A}$ $\dfrac{128°C}{[0.9]}$ B$_2$ $\dfrac{157°C}{[24.6]}$ I

Fig. 9.1: Structural formula and the transition schemes for compounds IX_**8** and IX_**12**

The symbol B$_5$ is used here as a common designation for all phases which exhibit the structural properties of the B$_5$ described earlier [17].

## 9.2 Calorimetric and microscopical investigations

As shown in the DSC-curve of compound IX_**12** and IX_**8** all phase transitions (also for mesophases with a small range of existence) have been detected by calorimetry (Fig. 9.2). It is noteworthy from the transition scheme that the transition enthalpies between these phases are rather low (0.2 - 2.5 kJmol^{-1}) in comparison with the clearing enthalpy.

On cooling the isotropic liquid the B$_2$ mesophase appears as a non-specific grainy texture. A kind of schlieren texture could be obtained by shearing the sample. At the transitions into the low-temperature phases the texture does not markedly change. Nevertheless, for a fast heating or cooling rate these phase transitions have also been recognised by a minor change of the paramorphotic textures.

As it will be discussed later, fan-shaped domains have been obtained using a sufficiently high electric field. At the transition B$_2$ →B$_5$ the fan-shaped texture became more flat. A considerable change was observed at the transition into B$_{5F}$ when a constriction of the texture has been seen and the fans became broken, but there was no change in texture at the transition into the solid state.
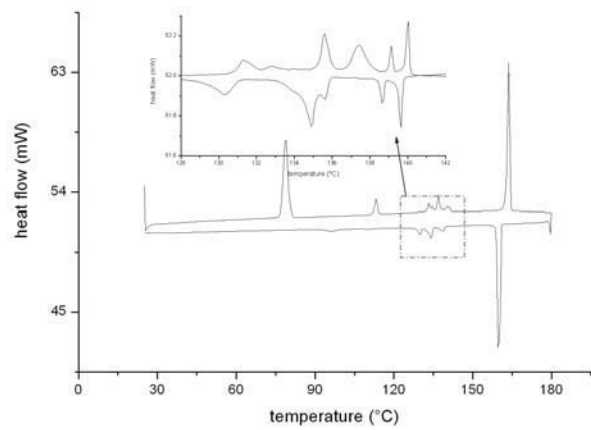
a)
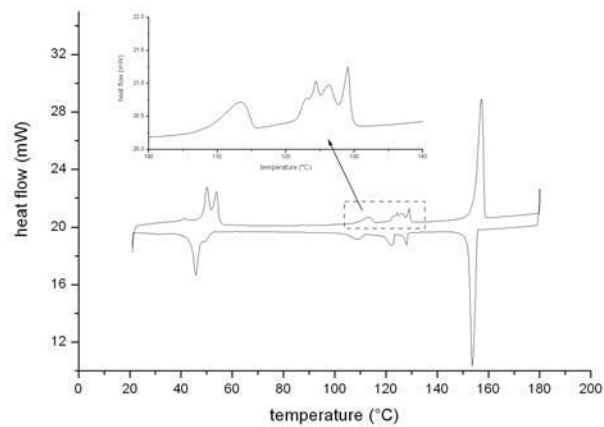
b)

Fig. 9.2: DSC thermogram of compounds a) IX/**8** and b) IX/**12** (heating and cooling run, rate 5.0 K min^{-1}; enlarged region made at the rate 1.0 K min^{-1})

9.3 Structural investigations

9.3.1 Orientational order and molecular conformation

^{19}F-NMR spectra of the compounds in the liquid crystalline phase consist of a triplet representing the dipole interaction of the fluorine atom on the central ring with the two neighbouring protons and a well separated doublet caused by dipole splitting of the fluorine on the ring *A* (Fig. 9.3). The order parameter *S* can be obtained from the triplet separation. Neglecting the transversal order parameter *D* (Chapter 2 and 6), the splitting can be written as

$$\Delta v_{\xi\xi}^{F} = \Delta v_{C}^{F}\, S \tag{9.1}$$

where $\Delta v_{C}^{F} = -15.08$ ppm is an interaction constant defined by the geometry of the ring *C*.

We assume that the ring *C* is deformed by the fluorine substituent. In order to get an agreement between the results obtained from different techniques (^{13}C- and ^{1}H-NMR) the following interatomic distances have been used $r_{CF} = 1.344$ Å, $r_{CH} = 1.09$ Å.

The interaction of the fluorine with the hydrogen in position 12 is weak and appears as a small splitting of the triplet lines. The angle ε between the molecular long axis and a *para*-axis of the ring *C* was calculated from the splitting of the fluorine in position 2. In this case the splitting depends on the order parameter *S* as well as on the
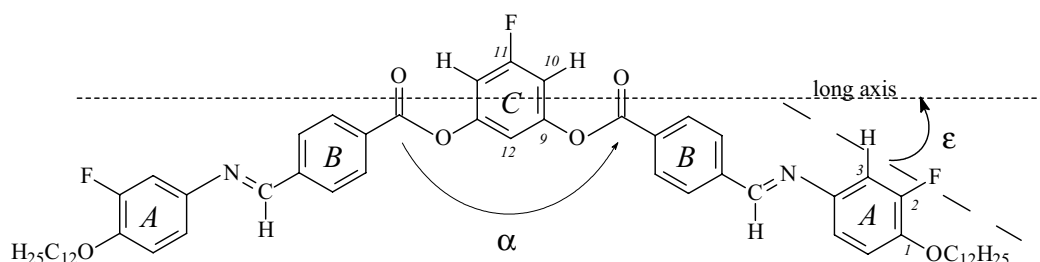

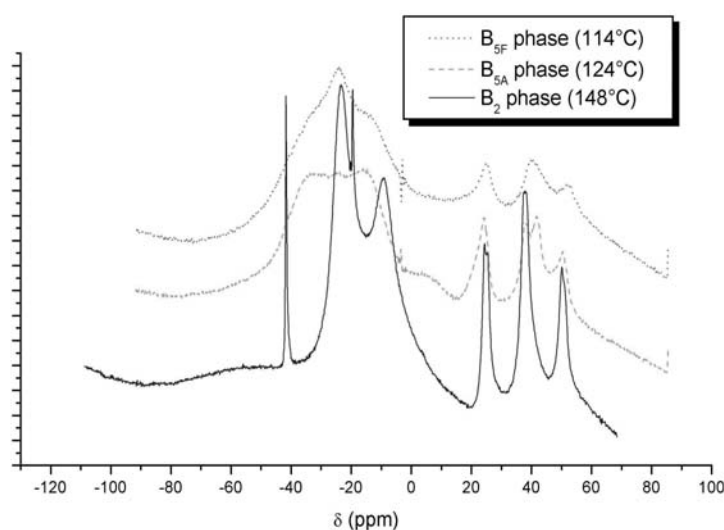Fig. 9.3: Angles and definition of the atom positions in the molecule

Fig. 9.4: ^{19}F-NMR spectra of the B$_2$, B$_{5A}$ and B$_{5F}$ phases of compound IX/**12**

orientation of the *para*-axis of the ring *A*:

$$\Delta\nu_{\xi\xi}^{F} = \Delta\nu_{A}^{F}\, S\,(\frac{3}{2}\cos^{2}(\varepsilon)-\frac{1}{2})$$ (9.2)

where the splitting constant $\Delta\nu_{A}^{F} = -28.0\,\mathrm{ppm}$. The shape of ^{19}F-NMR spectra changes considerably upon the B$_2 \rightarrow$ B$_{5A}$ and B$_{5A} \rightarrow$ B$_{5F}$ phase transitions (Fig. 9.4). Sharp peaks could be observed only in the high temperature phase B$_2$. After the transition into the B$_{5A}$ phase the splitting of the fluorine in position 2 broadens because of poor orientation which complicates the determination of the angle ε. The observed tendency of the splitting enables us to assume that the angle ε in low temperature phases has similar values to those in the high temperature phase (Fig. 9.5). The angle ε was found to be 31-32 deg, which corresponds to a bending angle α (the angle between the wings of the molecule) of 116-118 deg. As shown in Fig. 9.5 the order parameter *S* is nearly temperature independent in the B$_2$ phase. At the transition into the B$_{5A}$ phase *S* slightly increases. In the B$_{5F}$ phase *S* reached a value of about 0.9.

9.3.2 X-ray investigations

Although the compounds under investigation possess quite a large number of mesophases, only two kinds of X-ray patterns could be observed: one typical of the SmC or B$_2$ and the other one typical of the B$_5$ phases. The appearance of the X-ray patterns of both compounds is similar and they will be described for compound IX_**12.** In the first, high-temperature phase, up to six orders of layer-reflections have been seen from the diagrams of the surface-oriented samples where the third order reflection is of extreme low intensity (not detectable). In the wide-angle region there is a diffuse scattering with a maximum off the equator indicating liquid-like order within the smectic layers and the tilt of the molecules characteristic for SmC or B$_2$ phase (Fig. 9.6a).
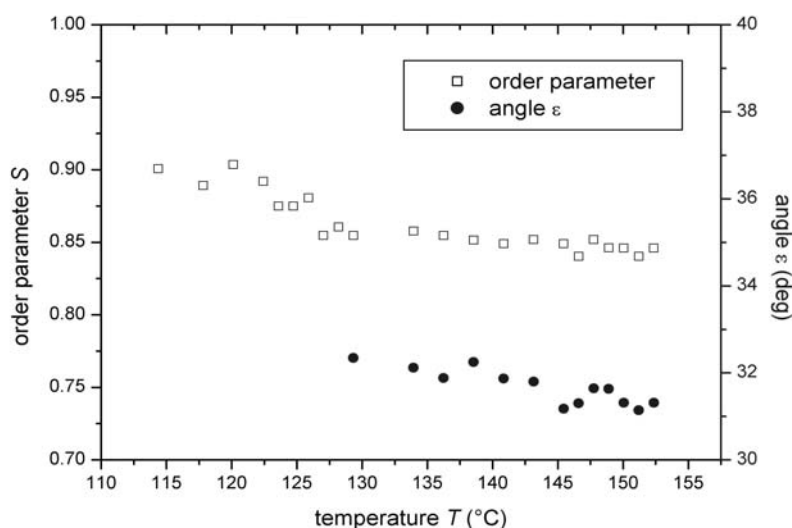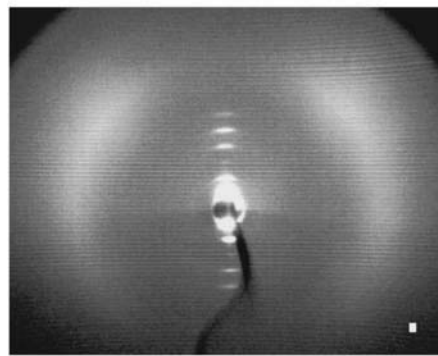

Fig. 9.5: Temperature dependence of the orientational order parameter *S* and the angle ε in the mesophases of compound IX_**12**

A polar order of the phase has been proved by electro-optical measurements, which indicates that the phase is, actually, B$_2$. The tilt angle ψ estimated from the
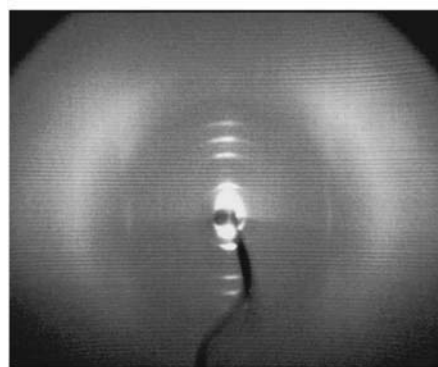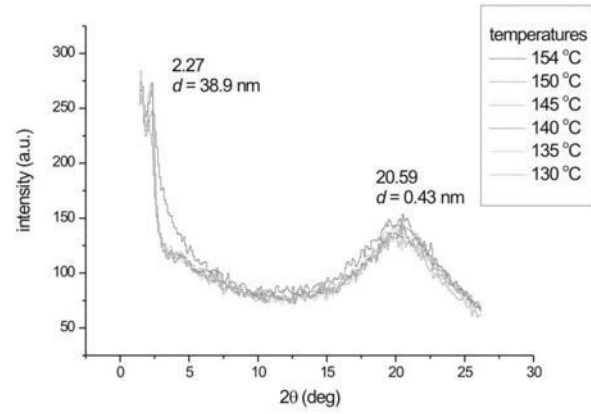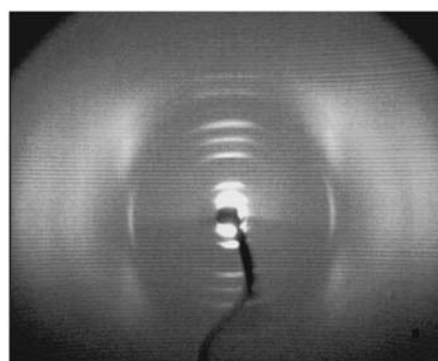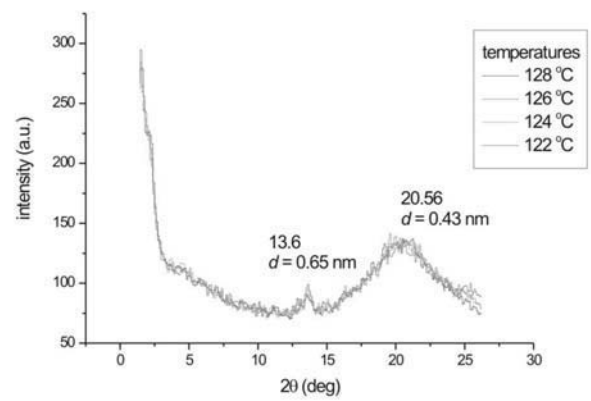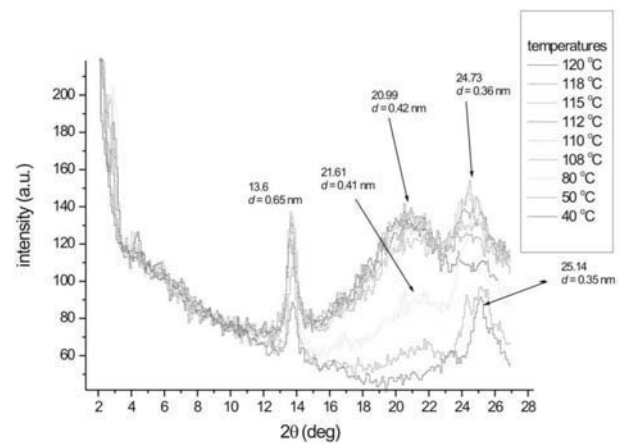

a) SmCP phase (135 °C)

b) B$_{5A}$ phase (124 °C)

c) B$_{5F}$ phase (115 °C)

Fig. 9.6: X-ray patterns of oriented samples and the equatorial scans a) B$_2$ phase (135ºC), b) B$_{5A}$ phase (124ºC) and c) B$_{5F}$ phase (115ºC) compound IX/**12**
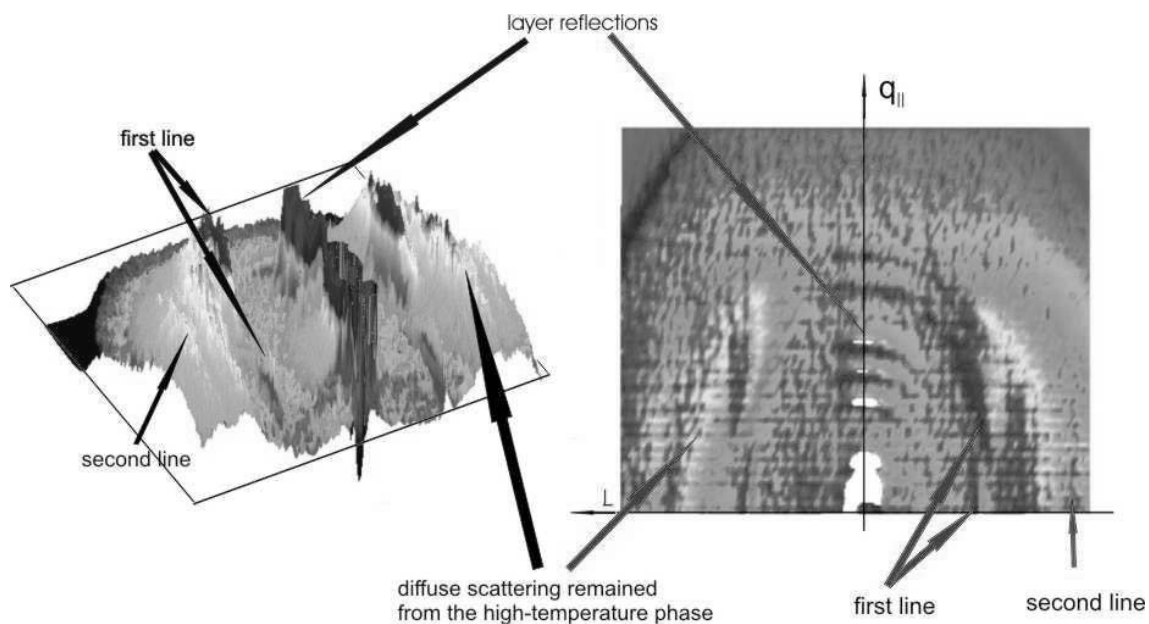
Fig. 9.7: Three-dimensional plot of an X-ray pattern in the B$_{5F}$ phase (115ºC): a) perspective view, b) view from top (only upper half of the scattering sphere).

positions of the diffuse maxima is 38 ± 3 deg for the compound IX/**12**. The equatorial scan for this compound shows only one broad maximum at a scattering angle of $2\theta \cong$ 20.6 deg in the diagram of the B$_2$ phase. Upon the transition from the B$_2$ phase into the lower-temperature phase, a narrow line perpendicular to the equator appears (Fig. 9.6b and 9.7). However, the diffuse scattering remains showing a considerably high amount of disorder in the phase. During cooling, an additional maximum becomes visible at a scattering angle around $2\theta \cong 24.7$ deg (Fig. 9.6c). Those lines indicate an additional order within the smectic layers, which can be described by a rectangular centrated lattice with the parameters a $\cong$ 12 Å and b $\cong$ 7 Å. Thus, we observed that there are two kinds of scattering centers in the low-temperature phases: ordered in a rectangular two-dimensional lattice (the molecules from different layers are not correlated) and disordered centers which give a broad diffuse halo. Such behavior is characteristic for B$_5$ phases. No discontinuous change has been seen at the phase transition temperatures observed in the DSC below the B$_2$ phase. The same situation has been observed for both compounds IX/**12** and IX/**8**. The layer spacing d, obtained from the powder samples is nearly independent of the temperature for the compound IX/**8**, whereas in the compound IX/**12** a slight temperature dependence of the d-values has been found (Fig. 9.8).
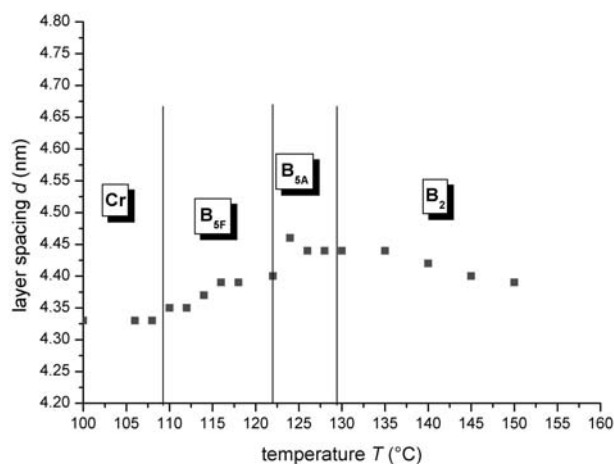
Fig. 9.8: Temperature dependence of the layer spacing of compound IX/**12**

After crystallization the diffuse scattering is absent, and only the reflections along the two lines remain. However, in the crystalline phase the intensity of the lines is modulated due to the positional correlation between the molecules from different layers.

9.4 Electro-optical investigations

Above the threshold the initial bright birefringent ribbon texture of the B$_2$ phase transforms into a smooth SmA-like fan-shaped texture. When the field is removed, the texture switches back into the initial state. The textures of the switched state are independent of the sign of the applied field, which points to a racemic ground state. At the transition from the B$_2$ into the B$_{5A}$ phase the threshold slightly increases from 0.6 V/µm till 1.3 V/µm, however the change of the textures on switching looks similar to the case of the B$_2$ phase (Fig. 9.9).

The electric response in the B$_2$ phase is quite unusual for both compounds IX/**12** and **8**: it consists of a peak at low field and a double peak in a high-field region (Fig. 9.10a). The second high-field peak is broader than the first one, it broadens at lower temperature and completely disappears upon the transition into the B$_{5A}$ phase (Fig. 9.10b).

A drastic change of the electro-optical behavior has been observed in the low-temperature phase designated as B$_{5F}$. As seen from Fig. 9.10c, at the transition from B$_{5A}$ into B$_{5F}$ a third current peak appears between the two peaks of the antiferroelectric B$_{5A}$ phase; the latter diminish and disappear. Simultaneously, the single peak in the B$_{5F}$ phase shifts towards higher values of τ which corresponds to an increasing threshold field (Fig. 9.10d). Furthermore, the texture of the switched states does not relax or change anyway when the external field is removed.

The switching into another polarized state takes place only when the field of opposite polarity (higher than the threshold field) is applied. In contrast to the B$_2$ and B$_{5A}$ phases, the textures of the switched states are different for opposite signs of the electric field, that means, dark domains became bright and vice versa (Fig. 9.11).
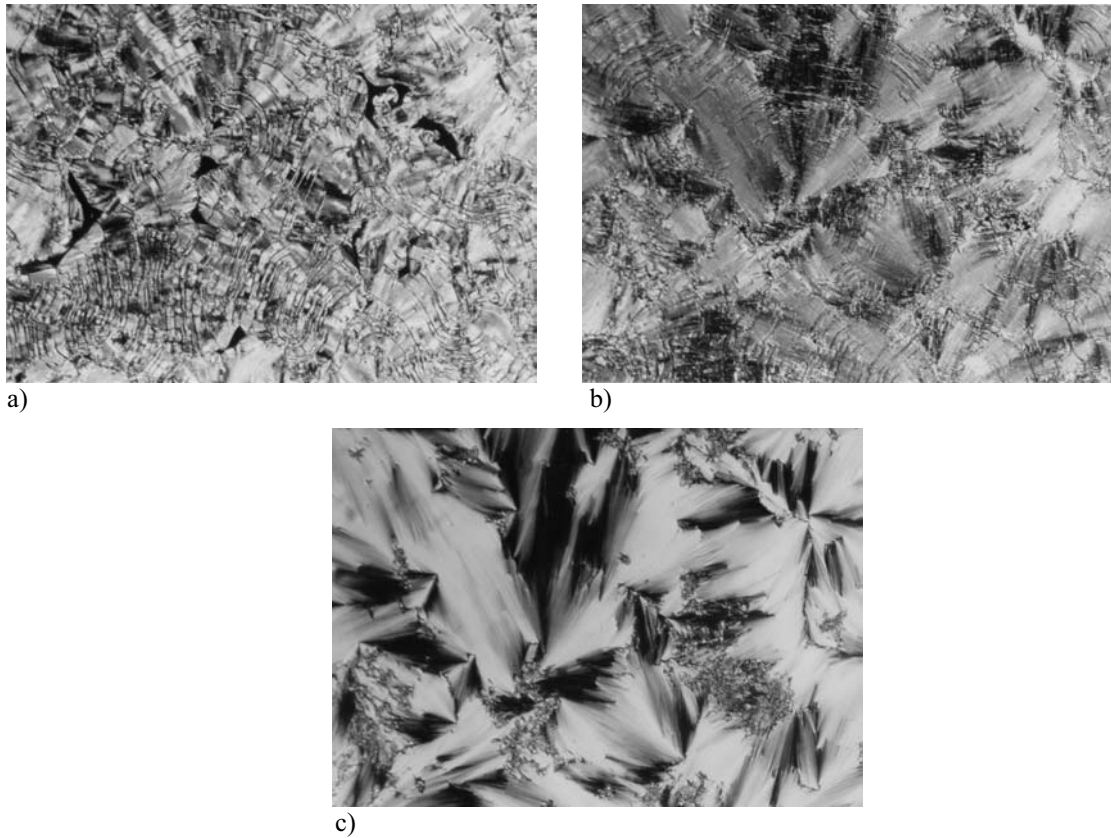
Fig. 9.9: Optical textures of the B$_{5A}$ phase of compound IX_**12** at 125ºC: a) $E = 0$ V μm^{-1}, b) $E = 0.6$ V μm^{-1}, c) $E = 1.6$ V μm^{-1}

The brushes in the extinction cross in circular domains turn to an angle about 65 deg, which corresponds to the double of the director tilt angle. There is a remarkable difference between the appearance of the antiferroelectric B$_{5A}$ phase on cooling and heating. On heating from the B$_{5F}$ phase, some homochiral domains remain, where the texture is different for an opposite sign of the applied field. In contrast, on cooling from B$_2$ the B$_{5A}$ phase appears as a racemic one. In the B$_2$ phase only a racemic ground state has been observed.

Considering all experimental findings we can assume that the low temperature phase B$_{5F}$ is ferroelectric. The hysteresis curves of the B$_{5A}$ and the B$_{5F}$ phases acquired by integration of the current response curves are shown in Fig. 9.12. The spontaneous polarization does not change considerably between the B$_2$, B$_{5A}$ and B$_{5F}$ phases (Fig. 9.13). On average there is no difference in the values of P_{sw} between the compounds IX/**12** and IX/**8**. The low-temperature phase of the compound IX/**8** also has one-peak current response curve, although, the polarized state slowly relaxes after the field is removed.
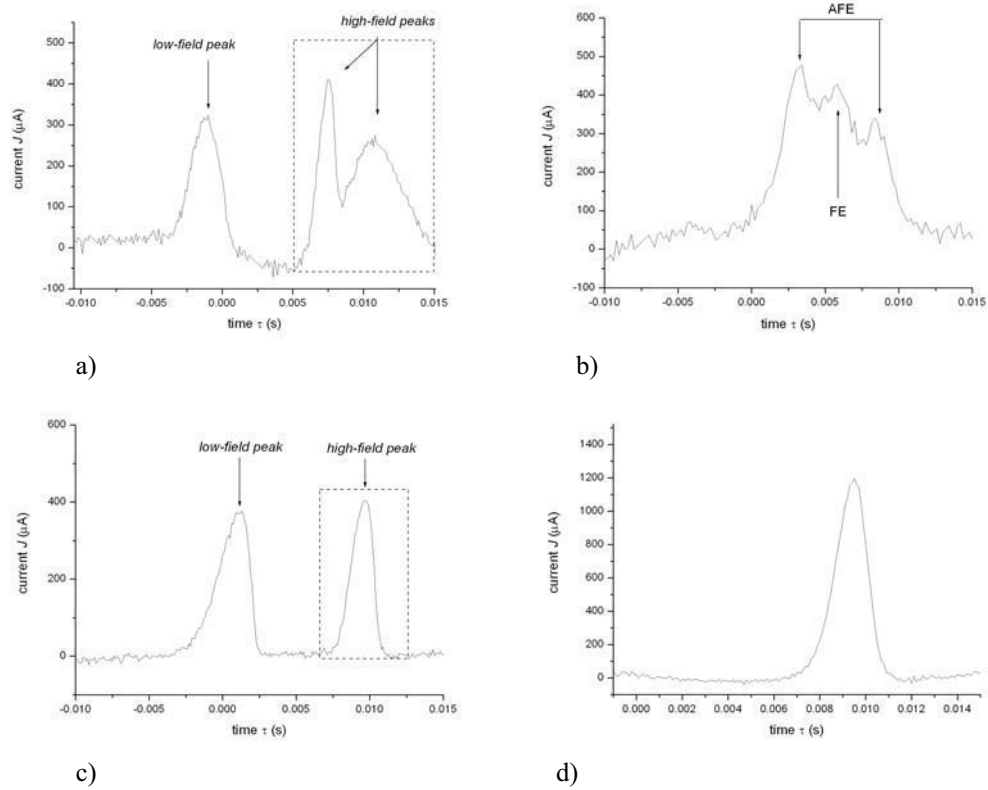
Fig. 9.10: Repolarization current of a) the B$_2$ phase (136ºC), b) the B$_{5A}$ phase (124ºC), c) at the transition B$_{5A}$→B$_{5F}$ (122ºC), d) the B$_{5F}$ phase (117ºC) of compound IX/**12**
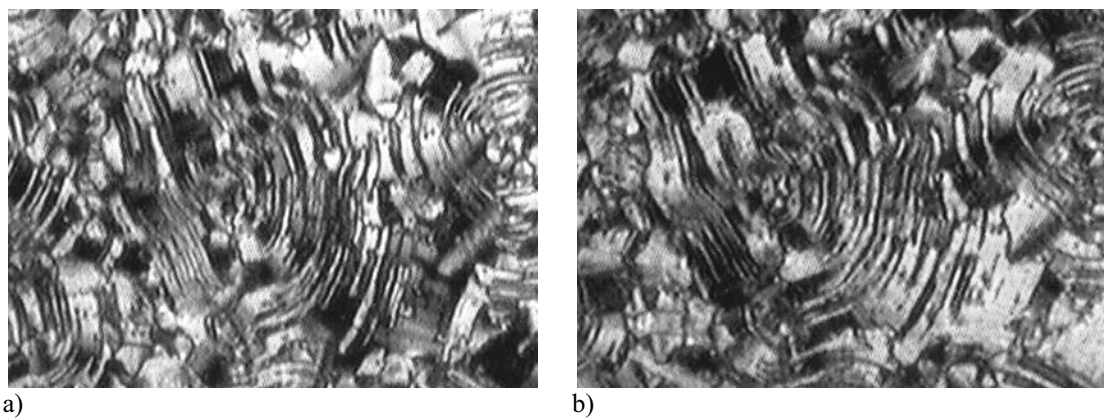

Fig. 9.11: Field-induced optical textures of the B$_{5F}$ phase at 112ºC: a) $E = +7.0$ V μm^{-1}, b) $E = -7.0$ V μm^{-1}
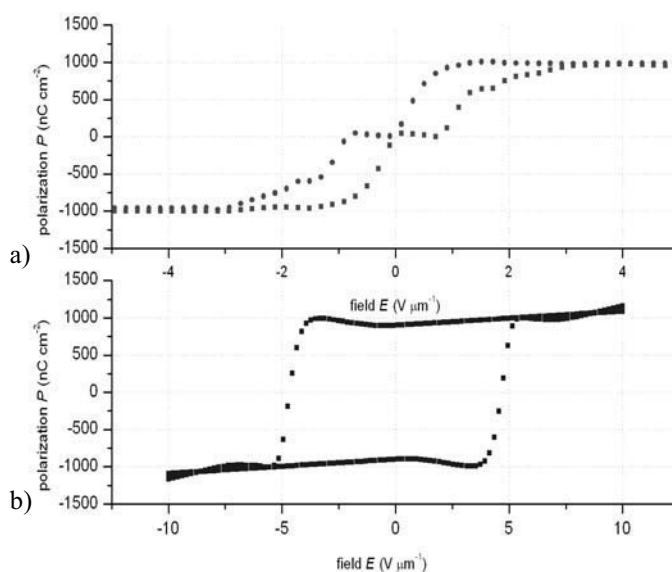
Fig. 9.12: Hysteresis curves $P(E)$ in a) the antiferroelectric B$_{5A}$ phase and b) the ferroelectric B$_{5F}$ phase
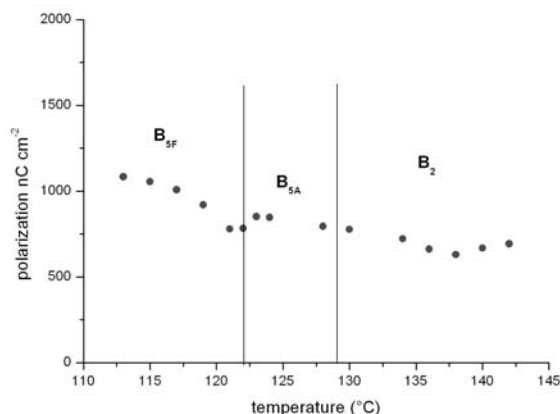

Fig. 9.13: Temperature dependence of the spontaneous polarization of compound IX/**12**

9.5 Discussion

To analyze the experimental results of the X-ray investigation four arrangements have been modeled. A model of a molecule of compound IX/**12** in an energy-minimum conformation was put into an orthorhombic body centered lattice. For the four structures: AFE synclinic { (x, y, z,) (-x, y, 1/2z) }, AFE anticlinic { (x, y, z) (-x, -y, 1/2z) }, FE synclinic { (x, y, z,) (x, y, 1/2z) }, FE anticlinic { (x, y, z,) (x, -y, 1/2z) } the X-ray patterns have been simulated (the terms synclinic and anticlinic correspond to the molecular tilt in neighboring layers and are expressed by the sign of the y-coordinate, whereas AFE/FE order is expressed by the sign of the x-coordinate). An example of AFE synclinic structure is shown in Fig. 9.14 and 9.15. Despite that the calculations were done on the crystalline structures, they still show the main features of the
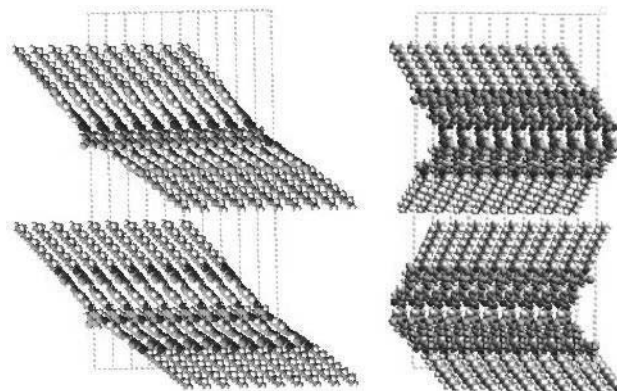
Fig. 9.14: Structural models a) front view of an AFE synclinic packing, b) side view of an AFE synclinic packing
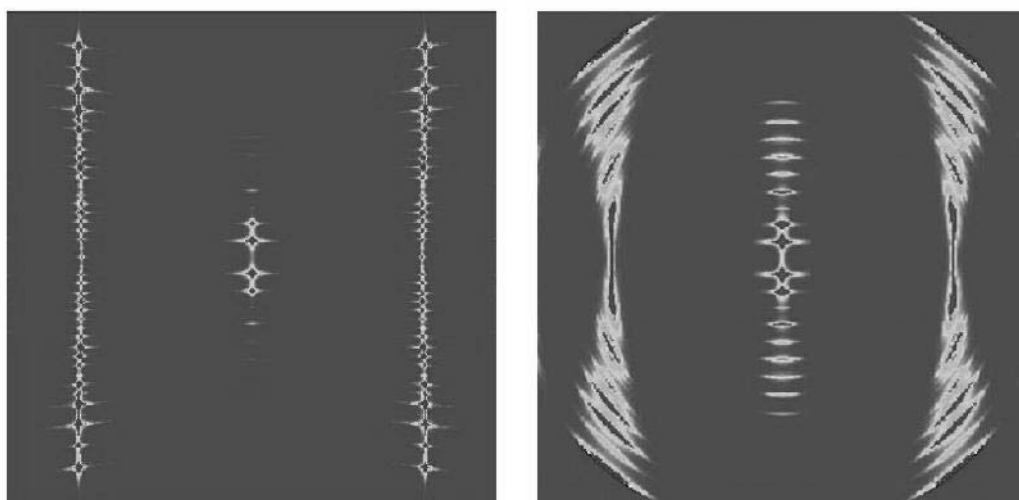

Fig. 9.15: Simulated pattern of the AFE synclinic structure a) without mosaicity, b) with mosaicity 5 deg
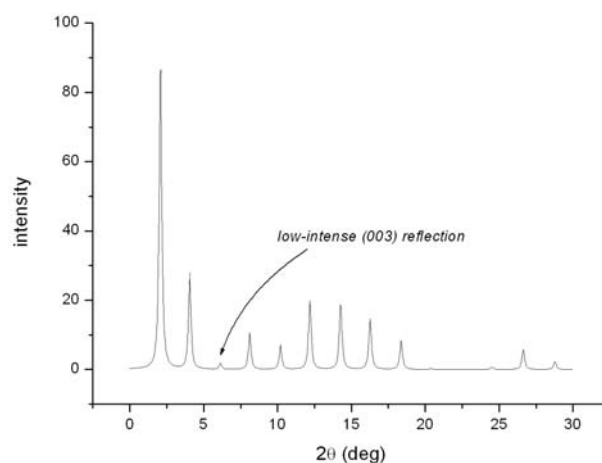

Fig. 9.16: Simulated intensity of (*0 0 l*) reflections of an AFE synclinic model with the molecules tilted by an angle 40 deg

experimentally observed X-ray patterns. Introduction of the thermal fluctuations as well

as the decrease of the inter-layer correlations will smear out the reflections in the wide-angle region, as it was observed experimentally.

Obviously, the difference between theses structures influences the intensity of (h k l) reflections with $l = 2n+1$ and does not affect (0 0 l) reflections. Since (h k l) reflections are absent in structures without interlayer correlation what, actually, takes place in case of smectic liquid crystals, it is not possible to differentiate such structural nuances as AFE-FE, synclinic-anticlinic or helical ordering of the smectic layers on the base of "conventional" X-ray studies. Therefore, there can be many B$_5$-like subphases which differ in the direction of the molecular tilt.

On the other hand, the low intensities of the 003 reflection is an essential feature in the experimental diagram. Inclining the molecule with respect to the layer normal, the intensity of the meridian (0 0 l) reflections changes, and at the tilt angle $\psi \approx 38 - 42$ deg the intensity of the (0 0 3) reflection becomes very low in agreement with our experimental data (Fig. 9.16). Assuming that such model describes a crystalline state, an additional modification by the high Debye-Waller factor will increase the effect of extinction.

Another way to estimate the tilt angle comes from the ratio of the layer spacing d to the length of the molecule. Taking L as the length of the stretched molecule, than the effective length is determined by $L_{eff} = L\sqrt{2(1-\cos\alpha)}$, which describes the length of a bent molecule with the angle α at the apex. From NMR experiment the angle α have been estimated to be ~ 114 deg. With $L = 6.3$ nm, $L_{eff} = 5.3$ nm and the layer thickness $d = 4.3$ nm the result is $\psi = 36$ deg, which is in a good agreement with the tilt angle obtained from outer-diffuse scattering and molecular modeling.

Electro-optical measurements have shown that the high temperature B$_{5A}$ phase of IX/**12** is antiferroelectric and has a synclinic ground state. On the other hand the low-temperature B$_{5F}$ phase is ferroelectric and synclinic. As it has been mentioned above, the difference between the two phases cannot be detected in "conventional" X-ray experiments. The case of the compound IX/**8** is similar, although the ferroelectric property of the low-temperature B$_5$ phase has not been evidently proved. The occurrence of the AFE and FE phases in calamitic chiral compounds is quite well investigated [31, 89, 90] and there is a number of theoretical works on ferro-, antiferro- and ferri- electricity in liquid crystals. However, reviewing the experimental data on calamitic and bent-core compounds one can notice that ferroelectric phases are more usual for calamitics [31], and antiferroelectric phases are common for "banana-phases" [16]. A naïve illustration of such phenomena can be given similar to a discussion in S. Lagerwall's book [31]. Let us consider fluctuations in the smectic layers involving partial permeation of molecules from layer to layer. In calamitic compounds such fluctuations are permitted by the synclinic order (Fig. 9.17a) and they themselves stabilize this order. Out-of-layer fluctuations give a thermodynamic (entropic) driving force for synclinic order, which is ferroelectric. In contrast, anticlinic stacking suppresses the out-of-layer fluctuations and thus carries an entropic penalty. Thus, the ferroelectric phase is the high-temperature one and the antiferroelectric phase occurs at lower temperatures in compounds with rod-like molecules. In the case of bent molecules the same argument is valid if we consider each smectic layer as a connected pair of anticlinicly arranged rods (Fig. 9.17b). Then the penetration of the layers is favorable in AFE arrangement of the molecules – not in FE, which means that AFE phases are preferable. Regarding the tilt of molecules synclinic order has higher
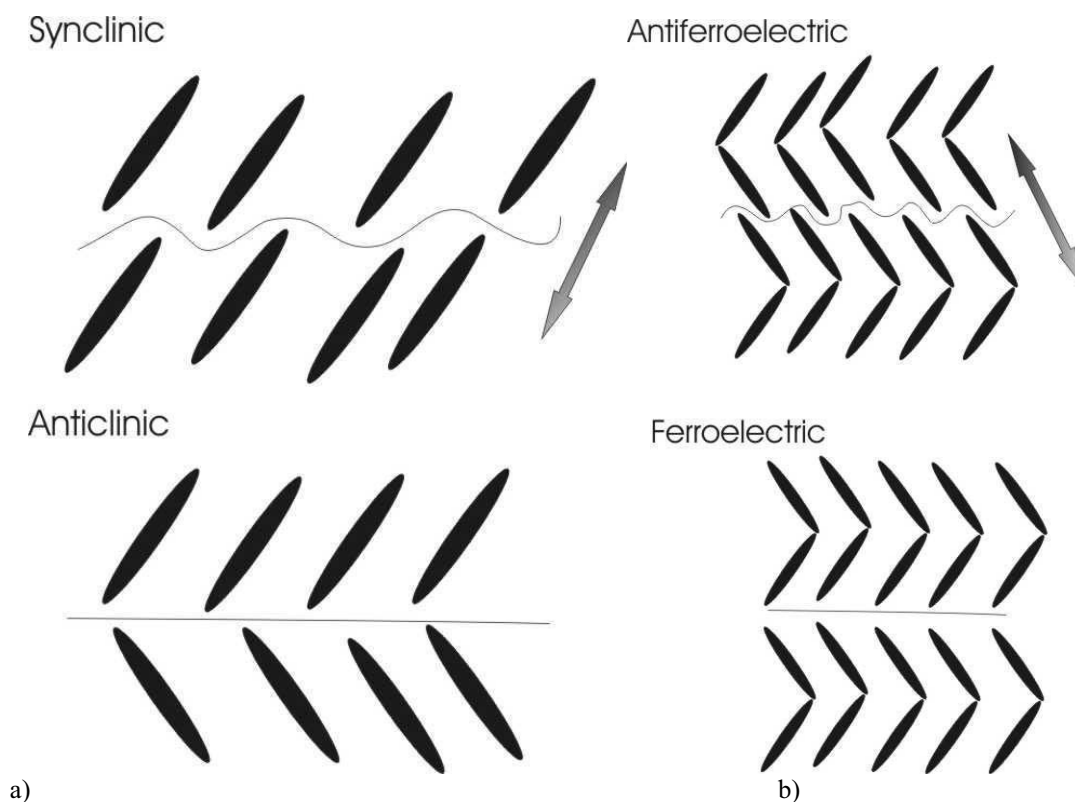
Fig. 9.17: Fluctuations in a) synclinic and anticlinic structures of calamitics and b) AFE and FE structures with bent-core mesogens

entropy. This is consistent with our observations that the most frequently observed B_2 (SmCP) and B_5 phases are antiferroelectric and synclinic (racemic), rarely anticlinic antiferroelectric; the ferroelectric B_{5F} phase observed in compound IX/**12** is still synclinic and occurs at the temperature lower than the AFE B_{5A} phase.

The appearance of the B_5 phase was up to now a more or less side issue in the field of "banana-shaped" liquid crystals. The results under discussion gave not only a new prove for its existence but also clear evidence of the appearance of some sub-phases of it. Two of them could be characterized as antiferro- (B_{5A}) and ferroelectric (B_{5F}). A closer look at the DSC curve made on heating of compound IX/**12** (as well as IX/**8**) reveals some more sub-phases between B_{5A} and B_{5F}. A small temperature range of these sub-phases complicates a thorough investigation. Yet the following features have been found:

- the sub-phases occur between antiferroelectric and ferroelectric phases
- they exist in quite narrow temperature intervals
- they are hardly noticeable by polarizing microscope
- they can be seen on the DSC curve, however indistinguishable in X-ray.

This behavior is reminiscent of the behavior of ferrielectric phases SmC^*_γ, etc., which differs in the sequence of the anticlinic and synclinic layers, and appear as a result of a competition between two different interactions: one favoring ferroelectric order and the other favoring antiferroelectric order. Although, there might be some other explanations, to explore these sub-phases and ascertain their structure further investigations like resonant X-ray technique are required. It is important to notice that

so far there has not been observed any straight transition from an antiferroelectric phase into ferroelectric as well as from an antiferromagnetic into a ferromagnetic one without occurrence of any sub-phases between them.

Chapter 10

Ferroelectric SmCP_F phase

10.1 Introduction

In the previous chapter we discussed a ferroelectric version of the B_5 phase and the role of the interlayer interface in stabilizing ferro- or antiferroelectric structure. There have been some attempts to change the character of the interface by suitable molecular designing: for example, affecting the shape of the terminal chains [91]. Among others, another way to create a ferroelectric phase is to make use of a microphase separation designing molecules consisting of different incompatible units [92].

In this chapter we present an asymmetrical bent-shaped compound (X/**1**) with an oligosyloxane terminal chain presented by G. Dantlgraber *et al* [93] (Fig. 10.1). This compound, having quite low transition temperatures, proved itself as a very convenient and interesting liquid crystalline substance for electro-optical investigation.
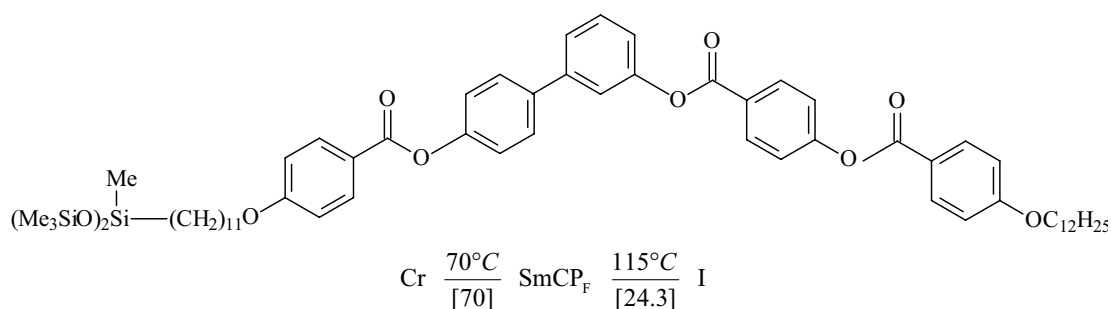

$$\text{Cr} \quad \frac{70°C}{[70]} \quad \text{SmCP}_\text{F} \quad \frac{115°C}{[24.3]} \quad \text{I}$$

Fig. 10.1: Structural formula of the compound X/**1**

10.2 Texture observation and electro-optical measurements

10.2.1 Texture formation

On cooling the isotropic liquid the mesophase forms fractal nuclei which coalesce into an unspecific grainy texture. This texture is nearly dark between crossed polarizers. The most remarkable feature is that domains of opposite handedness can be distinguished. Rotating the analyzer by a small angle (5-10 deg) dark and light domains become visible. If the analyzer is rotated in the opposite direction the reversed effect is observed. Such chiral domains have already been reported for the B_2-like smectic phases of the bent-shaped compounds in ref. [94 – 97]. Applying an electric field (threshold: 0.2-0.5V/µm) the dark texture is changed into an unspecific bright birefringent texture which is transformed into a fan-like texture at higher fields (10-15 V/µm) (Fig. 10.2). The field-induced texture change is not pronounced, the textures of the switched states are independent of the polarity of the field. It is remarkable that there is nearly no relaxation if the applied field is switched off.
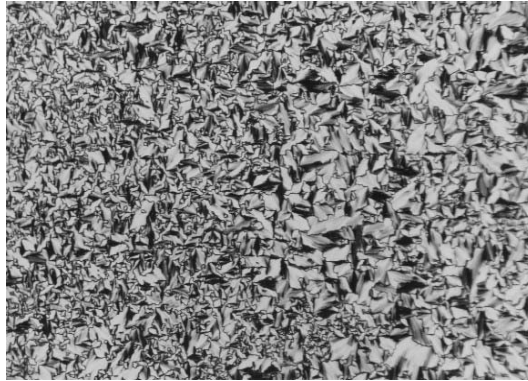
Fig. 10.2: Field-induced fan-like texture (E = 10 V/µm)

10.2.2 Current response measurements

The electro-optical measurements were carried out using commercial ITO cells (EHC) with the thickness 5 µm with rubbed polyimide layers and 10 µm without them. The cells were filled with a liquid crystal in the isotropic state and slowly cooled down in the presence of a d.c. electric field ~2V/µm. The measurements were made employing triangular-wave technique as well as a modified triangular-wave technique with a duty between two impulses.

The repolarization current in response to a triangular-wave field contains only one peak (Fig. 10.3). Since most of compounds with bent-shaped molecules exhibit AFE switching, we had to make a deeper investigation about the character of the switching. It is known that the viscosity in AFE liquid crystals can affect on the current response and at relatively high frequency it can suppress transitions from the FE state into the AFE one [83]. It means that at high frequency the AFE switching turns into switching between two FE states and, therefore, only one repolarization current peak per half a period can be recorded. Therefore it becomes a challenge for us to find whether the compound is anti- or ferroelectric in its ground state.

Lowering the external field frequency and introducing a lag between two triangular pulses, we observed only one sharp current response peak down to 20 mHz. This supports our observations made in d.c. field and gives evidence for the ferroelectric character of the switching. The frequency dependence of the threshold field E_{tr} reaches its minimum at f = 0.3 Hz and does not change at lower frequencies (Fig. 10.4).

The temperature behavior of the spontaneous polarization is similar to the one of the AFE B$_2$ phase. It is quite high and reaches its saturation value very fast (Fig. 10.5).
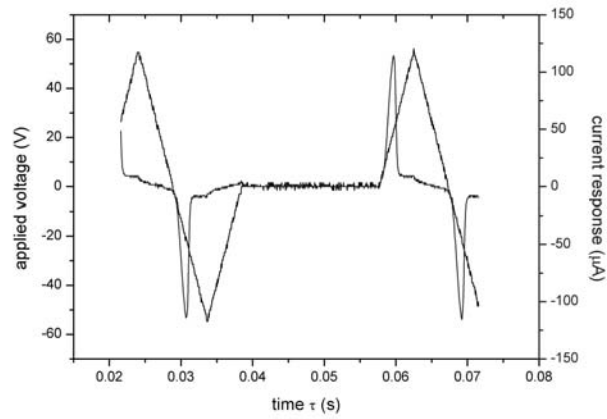
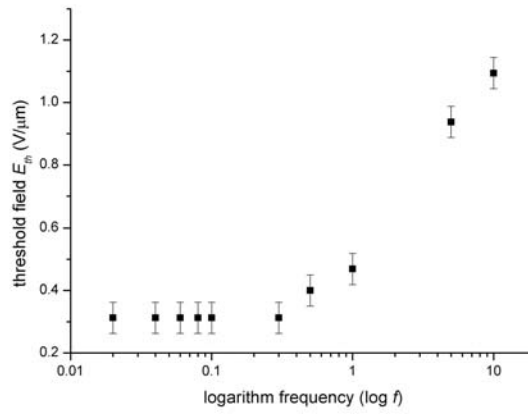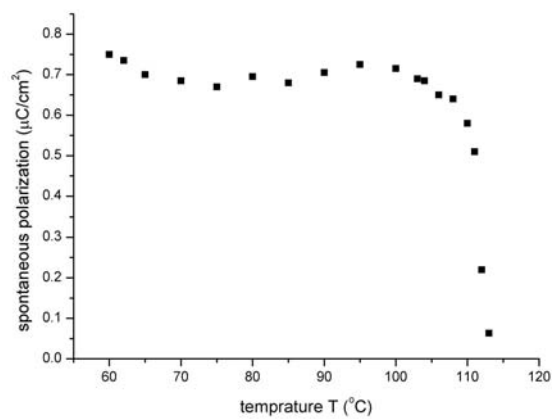Fig. 10.3: Current response curve

Fig. 10.4: Switching time τ

Fig. 10.5: Spontaneous polarization

10.2.3 Behavior of circular domains

If the isotropic liquid is slowly cooled down under an applied 10V/μm d.c. electric field a texture with many circular domains appears. In these domains the smectic layers are circularly arranged around the center of the domains. The direction of the extinction brushes corresponds to the direction of the optical axes of the smectic layers. In these bright birefringent field-induced circular domains the extinction cross is shifted by 30 – 40 deg with respect to the polarizer-analyzer directions indicating a tilt of the molecules within the smectic layers of 30 – 40 deg. Under the influence of a sufficiently high electric field the extinction cross rotates clock-wise or anticlock-wise depending on the sign of the applied field (Fig. 10.6a and b). It should be emphasized that the extinction cross remains unchanged if the field is switched off, that means, there is no relaxation of the switched state as observed in the antiferroelectric SmCP phase. The switching angle of ~ 70 – 80 deg corresponds to the double tilt angle (see Fig. 10.6). This bistable switching clearly points to a ferroelectric ground state which confirms the results of the current response measurements. In the ferroelectric ground state the smectic layers are synclinic and the handedness is uniform in subsequent layers. In the nomenclature of D.R. Link *et al* [15] this state can be designated as SmC$_S$P$_F$.

a)

b)
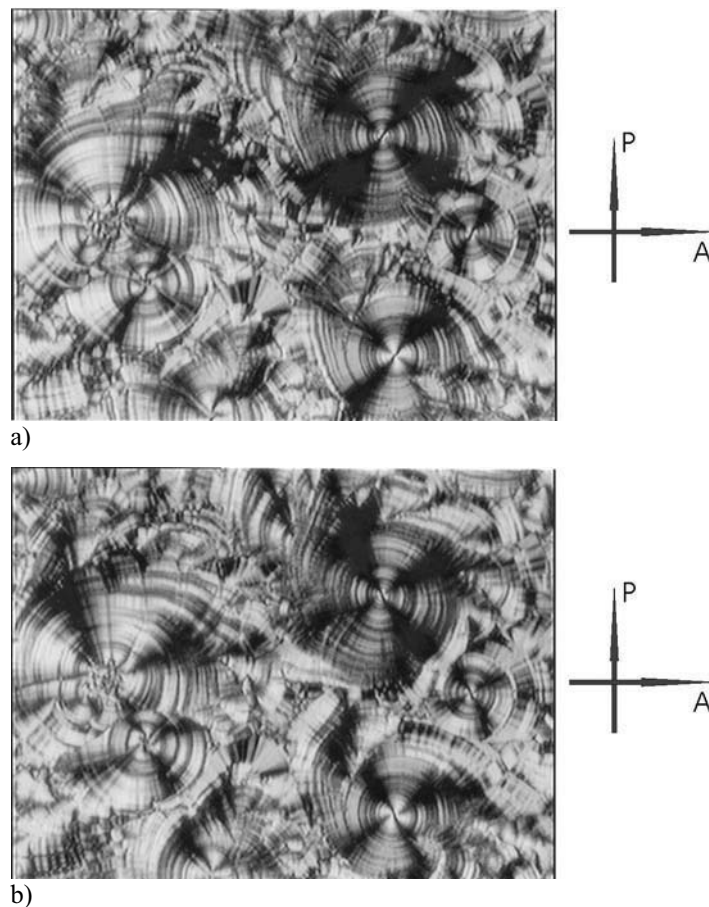
Fig. 10.6: Electro-optical switching of the circular domains

If an alternating field (10V/µm, 200 Hz) is applied on cooling the isotropic liquid, besides a weakly birefringent fan-like texture circular domains are also formed. In these domains the extinction cross coincides with the direction of polarizer and analyzer (Fig. 10.7). On applying an electric field the extinction cross does not move although a switching process is clearly visible. But this switching is not pronounced and the switched states are independent of the polarity of the field. The ferroelectric ground state can be assumed to be anticlinic where not only the tilt but also the handedness alternates from layer to layer which corresponds to a racemic state. This state can be designated by the symbol SmC$_A$P$_F$. In this case the average optical axis is perpendicular to the layer plane, which explains the coincidence between extinction cross and the crossed polarizers. It is also plausible that here the switched states are optically identical.

10.3 X-ray measurements

X-ray investigations made on non-oriented samples confirm the presence of a well-defined layer structure by the appearance of a sharp layer reflection and its higher orders (up to four) with $d = 44$ Å (Fig. 10.8). Preliminary simulations of the conformation of

Fig. 10.7: Switching of the dark domains

Fig. 10.8: Goniomiter curve for compound X/**1**

Fig. 10.9: Structure model of the SmCP$_F$ phase [93]

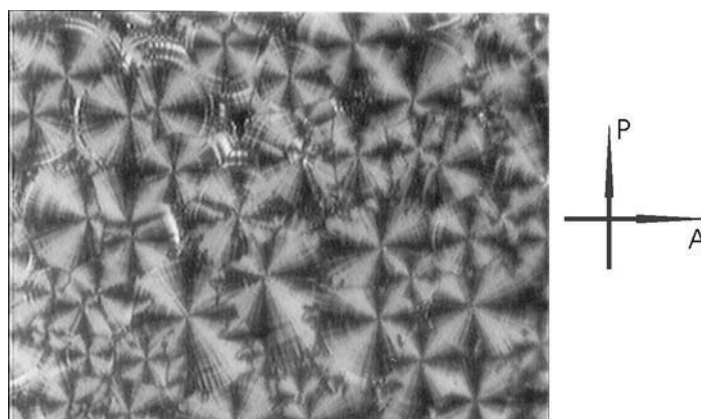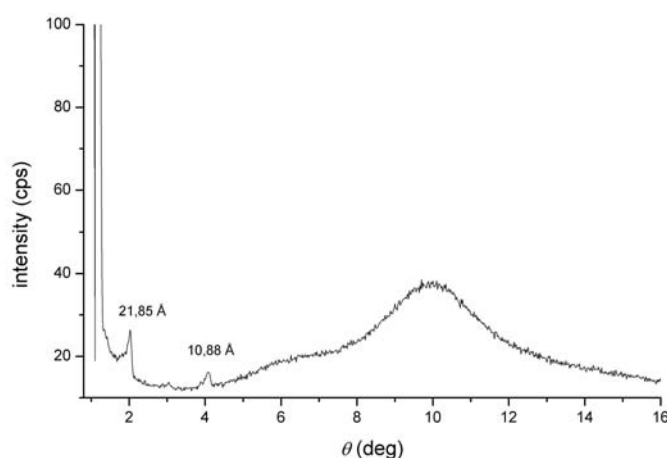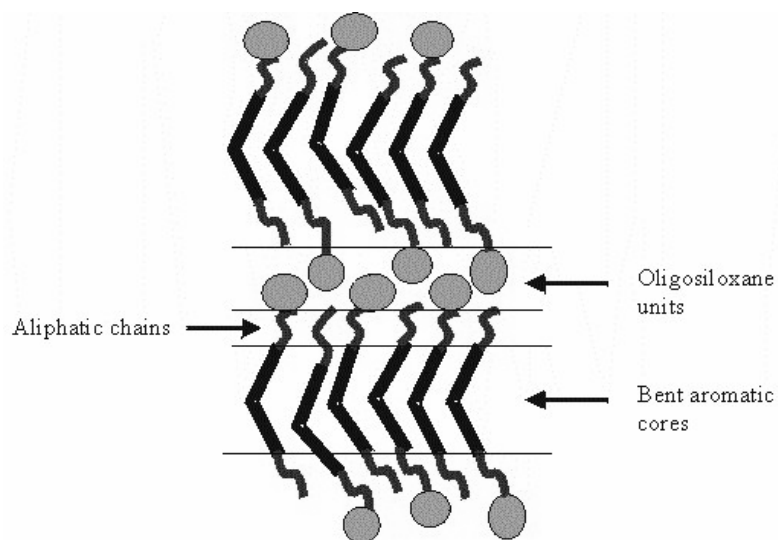the central core evidence a bent form of the molecule and the effective molecular length of about 55 Å. Comparing this value with the thickness of the smectic layers we conclude that the molecules are tilted by ~ 36 deg. Unfortunately, the attempts to obtain an oriented sample have been failed so far. The wide-angle scattering is broad indicating a liquid-like order within smectic layers. Another feature of the wide-angle scattering is asymmetry, which is more pronounced at the homologues with longer siloxane chains.

10.4 Discussion

At the present stage of research nearly all "banana phases" possess an AFE ground state. An exception is the ferroelectric B$_5$ phase. A ferroelectric B$_2$ phase was reported for achiral bent mesogens [98, 99]. Here we present the first example of non-chiral molecules forming a ferroelectric switchable fluid smectic phase SmCP$_F$. It is a novel type of polyphilic liquid crystal composed of three incompatible units: a bent rigid aromatic core, two flexible alkyl chains and a bulky oligosiloxane unit at one end. Such compounds can form nano-segregated structures where different units fill different sublayers. A proposed triple-layer organization of the molecules is shown in Fig. 10.9. The oligosyloxane units are very bulky and in case of side chain polymers [100, 101] they do not follow the order of the mesogenic units, which results in microphase separation. The mesogenic cores are arranged in the smectic layers and concurrently the oligosyloxane chains are in isotropic state in the neighboring sublayer. Such structures give a characteristic X-ray pattern which is a superposition of a pattern of the smectic phase with a pattern of the isotropic phase. Similar behavior can explain asymmetry of the wide-angle X-ray pattern in the compound X/**1**. When the oligosiloxane chain is very short it follows the order of the mesogenic core. The longer chains are disordered resulting in isotropic scattering in wide-angle region.

Similarly, the occurrence of the ferroelectric B$_{2F}$ phase as the ground state in the absence of the external field can be explained in the same frame of the interlayer penetrations highlighted in Chapter 9. The character of an interlayer interface in this compound is much affected by the siloxane terminal unit which causes the microphase separation (detected by X-ray). Decoupling the layer interfaces by the siloxane sublayers reduces or inhibits these interlayer penetrations and therefore their importance

for molecular organization is reduced, which allows ferroelectric order having lower free energy.

Chapter 11

SmC$_G$ → SmCP transition

11.1 Introduction

Almost 25 years ago a simple smectic phase with triclinic symmetry was proposed by P.G. de Gennes [2] and was called SmC$_G$ phase (where G stands for general). However, experimental attempts to find such mesophase among calamitic compounds did not succeed until recently. The discovery of the liquid crystalline mesophases formed by bent-shaped molecules promoted further research on the way to the SmC$_G$ phase. Theoretical evidence for triclinic symmetry of a smectic phase with bent-shaped molecules can be found in the work by H.R. Brand *et al* [12]. The tilt (clinic) ψ of the molecular plane defined by the shape of the molecule results in the SmCP phase with C_2 symmetry (Fig. 11.1). Additionally, leaning of the molecules in the molecular plane leads to C_1 symmetry of the SmC$_G$ phase. H. Pleiner *et al* [102] suggested that the experimentally observed B$_7$ phase is identical to the SmC$_G$ phase. Regarding experimental realization, an attempt to find triclinic symmetry in asymmetric bent-shaped molecules did not give any conclusive results [103]. At the same time recent evidence of C_1 symmetry in free-standing films were reported by N. Chattham *et al* [104].

Among the "banana phases" candidates for C_1 symmetry the B$_7$ phase has attracted particular interest because of the formation of exotic optical textures as well as the growth of serpentine-like germs and beaded filaments. Such behavior of optical textures clearly indicates a helical superstructure [18, 91, 105, 106, 107] of the B$_7$ phase. It can be assumed that the chirality of the phase [15] is responsible for the formation of the macroscopic helical domains. The structure of this mesophase has not been understood up to now. X-ray investigations exclude a simple layer structure and point to a two- or three-dimensional superstructure. Although it should be emphasized that the lateral arrangement of the molecules is liquid-like in the B$_7$ phase.

There are also "banana phases" with the structural characteristics of the SmCP phase (simple layer structure, tilt of the molecules, polar order) which form screw-like

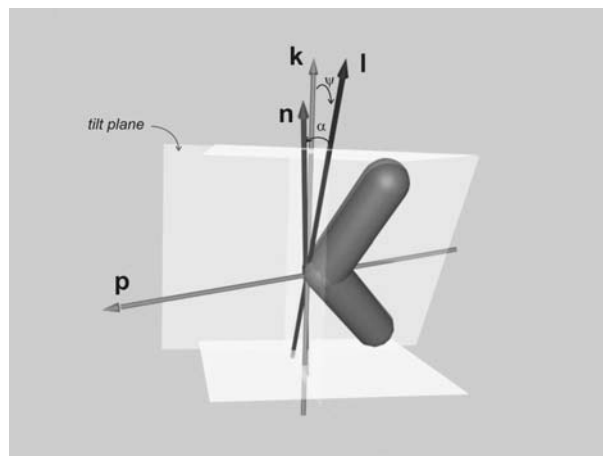Fig. 11.1: Orientation of a bent-shaped molecule in the SmC$_G$ phase. The molecular plane is tilted by tilt angle ψ ("clinic"). The molecular long axis is inclined in the tilt plane by the "leaning" angle α
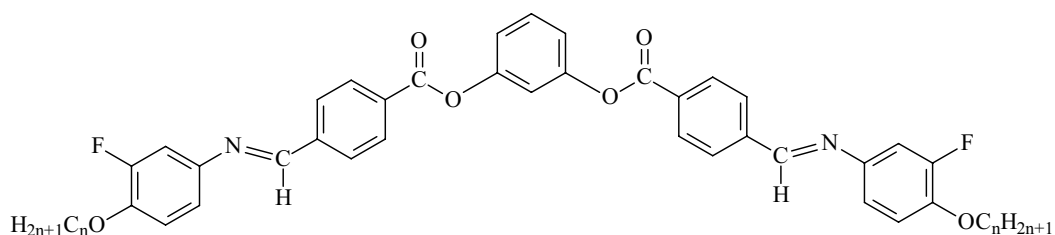
Fig. 11.2: Molecular structure of compounds XI/**8** – **12.**

nuclei on cooling of the isotropic liquid quite similar to the B$_7$ phase [108 – 110]. Nevertheless, because of a different structure this phase should not be designated as B$_7$ phase; it is another mesophase. A completely different type of chiral domains was observed by J. Thisayuktu *et al* [94, 95] in the high-temperature phase of a bent-shaped mesogen with naphthalene as central core. These domains of opposite handedness grew as fractal nuclei and showed distinct circular dichroism. For instance, such domains were also generated by an exposure to a triangular-wave field in a sulfur-containing bent-core mesogens [111].

Of particular interest was a bent-shaped compound with lateral fluorine substituents which was first described by G.Heppke *et al* [110]. The mesophase of this compound which possesses a SmCP like structure and exhibits a B$_7$-like texture was the subject of detailed investigation done by A.Jákli *et al* [112]. On the base of electro-optical measurements a smectic phase with triclinic symmetry (SmC$_G$) was suggested.

In order to get a deeper insight in the nature of this phase we investigated shorter and longer homologues of this compound. Employing X-ray and electro-optical techniques we found a phase sequence I – SmX – SmCP – B$_4$ for all members of the series. From the experimental findings some plausible arguments can be derived that the high-temperature phase SmX is a smectic phase with C_1 symmetry. Furthermore, this high-temperature phase is able to form screw-like and telephone-wire like nuclei as well as large chiral domains depending on the experimental conditions. It is remarkable that the large chiral domains remain unchanged at the transition into the B$_4$ phase.

The compounds under investigation are 1, 3-phenylene bis[4-(4-*n*-alkyloxy-3-fluoro-phenylimino-methyl)benzoates] *n* = 8…12 (Fig. 11.2). The phase transition temperatures (Table 11.1) were determined with a Perkin-Elmer differential scanning calorimeter (DSC Pyris 1) at a rate of 5 K/min.

Table 11.1

compound	n	Cr		B$_4$		SmCP		SmX		I
XI/**8** [112]	8	●	129	(●	98)*	●	164	●	166	●
XI/**9**	9	●	123	(●	101)*	●	153	●	163	●
XI/**10** [110,112]	10	●	123.5	(●	99)*	●	147	●	163	●
XI/**11**	11	●	120.5	-		●	141	●	162	●
XI/**12**	12	●	120	(●	98)*	●	132	●	159.5	●

* The B$_4$ phase can be supercooled up to room temperature, the inverse transition B$_4$ → SmCP takes place about 10˚ -12˚C above this temperature.

11.2 X-ray diffraction measurements

11.2.1 Powder samples

X-ray diffraction measurements have been performed using film Guinier technique. The patterns of the SmX possess two commensurable small angle reflections and one diffuse scattering maximum in the wide angle region (~ 10 deg), which points to a layered structure with liquid-like order within the layers. No incommensurable reflections have been observed indicating that the structure of the SmX phase is different from the structure of the B$_7$ phase described in ref. [18]. The layer spacing is temperature independent, neither does it change during the SmCP → SmX transition nor at the transition into the B$_4$ phase.

In Table 11.2 the layer spacing *d* and the effective molecular lengths *L* are given. A bending angle of 120 deg based on our previous experimental observations [16, 68] is assumed in the estimation of the effective molecular length.

Table 11.2

compound	molecular length *L* (Å)	spacing, $d \pm 0.5$ (Å)	tilt angle (deg)
XI/**8**	45.3	38.5	31.3
XI/**9**	47.5	40.5	31.4
XI/**10**	49.5	41.8	32.5
XI/**11**	51.6	43.5	32.6
XI/**12**	54.4	45.5	33.2

The dependence of the layer spacing on the length of the terminal chain exhibits a linear trend. The layer spacing is clearly smaller than the effective molecular length which can be caused by a tilted arrangement of the molecules within the smectic layers. From the ratio *d/L* the tilt angle of ~ 32 deg has been estimated.

Measurements of the correlation lengths from the full-width-at-half-maximum give us some more information on the difference between the SmX, SmCP and B$_4$ phases (Fig. 11.3). In the high temperature SmX phase of the compound XI_**12** the correlation length (ξ = 900 Å) is nearly temperature independent. The transition into the SmCP phase is accompanied with a continuous increase of the correlation length. The
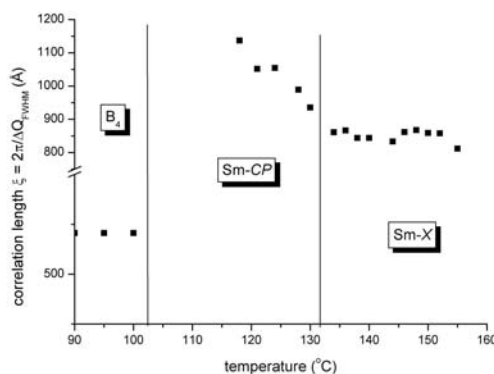
Fig. 11.3: Temperature dependence of the longitudinal correlation length ξ compound XI/**12**

small angle reflection becomes considerably broaden in the B$_4$ phase resulting in an abrupt decrease of the correlation length till 600 Å (Fig. 11.3). It is in agreement with the earlier described results [16] where a line broadening was observed for the wide- and small-angle reflections on cooling the sample from the crystalline B$_3$ into the B$_4$ phase.

11.2.2 Oriented samples

A characteristic feature of the patterns obtained from surface-oriented samples on the SmX phase, is the occurrence of four reflections in the small angle region (Fig. 11.4a, b). The pairs of reflections – along the equator and the meridian) have quite different mosaicity and, therefore, cannot correspond to one common lattice. Additionally, they reflect the same periodicity which has also been proved by the Guinier method on powder-like samples. Thus, it is obvious that these reflections originate from differently oriented domains where the smectic layers are parallel and perpendicular to the substrate surface. When the terminal chains are short (compound XI/**8**) the smectic layers prefer laying parallel to the substrate. The longer chained
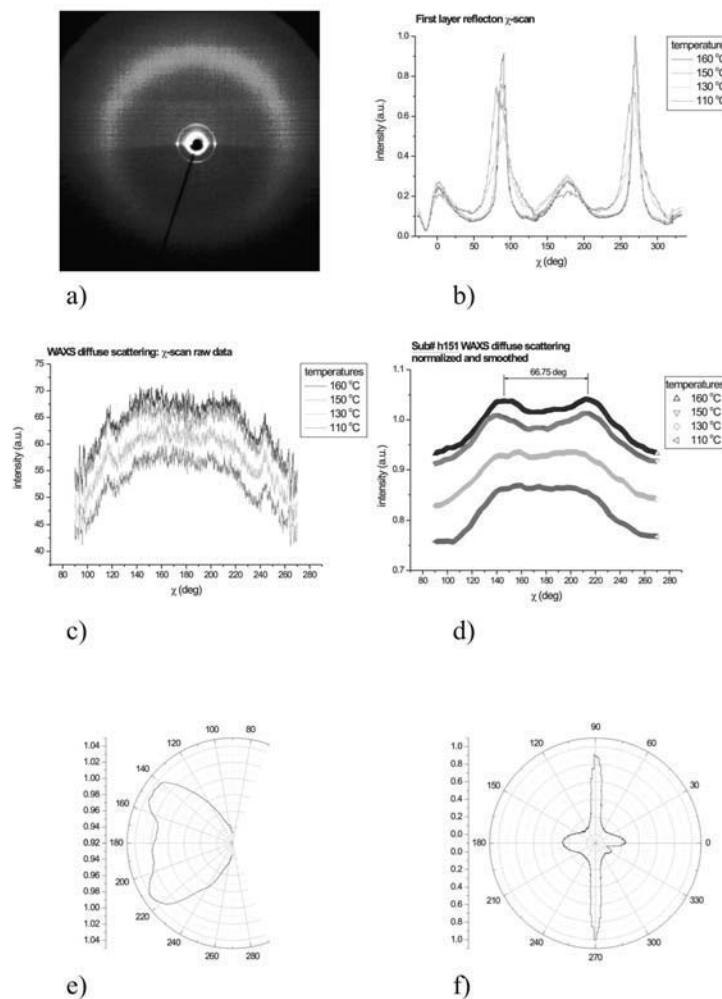

Fig. 11.4: (a) X-ray pattern of the surface oriented sample; (b) extracted intensity distribution of the wide-angle diffuse scattering; (c) χ-scan of the layer reflections showing four maxima: along and perpendicular to the equator of the pattern (compound IX/**12**)

homologues prefer orienting perpendicular to the substrate surface (compound XI/**12**). For compound XI/**9** the probability is equal for growing in both directions.

In the wide-angle region there is a broad diffuse halo showing the absence of positional order within the smectic layers. At a first sight the diffuse halo is uniformly distributed over a circle. Normalization technique described in chapter 2 enables us to extract the structure of the diffuse scattering distribution. The maxima in a wide-angle region have been found to be out of the equator (Fig. 11.4c), which stands for the tilt of the molecules with respect to the layer normal. The tilt angle of ~ 33 deg estimated from the diffuse scattering measurement is in good agreement with the value obtained from the analysis of the layer spacing. The orientation completely disappears after the transition into the B$_4$ phase. Finally the results of the X-ray experiments suggest that the SmX phase is a smectic phase without in-plane order formed by tilted molecules. To differentiate between the properties of the SmX and the SmCP phases we performed electro-optical measurements.

11.3 Electro-optical investigations and texture observations

The electro-optical measurements have been made using 10 μm ITO cells (EHC Corp.) and triangular wave technique. On rapid cooling the sample from the isotropic phase a grainy non-specific texture appears. When the cooling rate is slow (0.1K/min) different kinds of growing domains are observed: colored and grey ribbon-like domains as well as screw-like and telephone-wire filaments (Fig. 11.5). When the texture is not completely formed and the growing domains are surrounded by the isotropic liquid, application of an electric field can affect the microscopic texture. Depending on the polarity of the field, the grey ribbons grow or shrink. Exposure of the ribbons to an electric field results in coiling of the grey ribbons into spirals. Depending on the polarity of the external field the spirals are formed clock- or anticlockwise (shrinking of a ribbon leads to growing and coiling of another end of the ribbon). This effect is thresholdless, even weak fields can promote growing or shrinking of the domains. This finding shows that the ribbons are polar and the polarization vector has a component parallel to the substrate surface. Application of an electric field produces a torque $\vec{M} = \vec{p} \times \vec{E}$ of the grey ribbon-like domains. The direction of the momentum depends on the orientation of
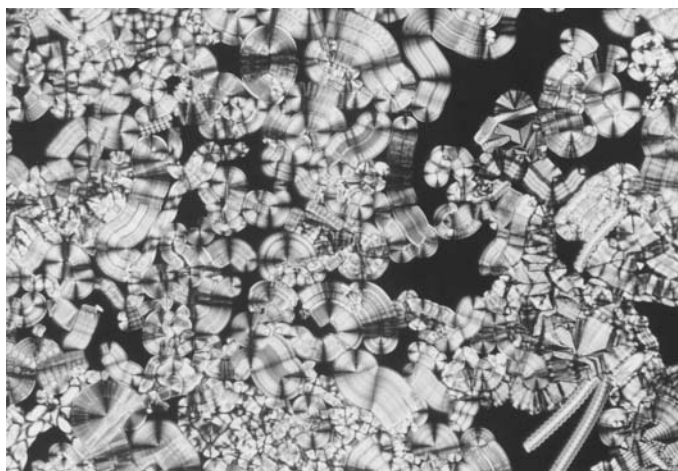

Fig. 11.5: Formation of the Sm*X* phase on slow cooling of the isotropic liquid (compound IX/**9**)

a)   b)
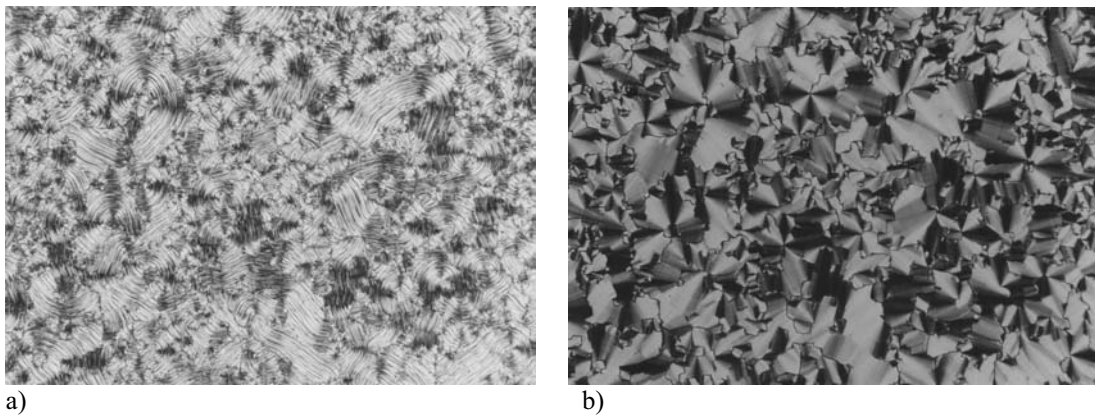
Fig. 11.6: Microscopic texture of the SmCP phase of the compound XI/**10** at T = 133 ˚C: a) *E = 0,* b) *E = ±20 V/µm*
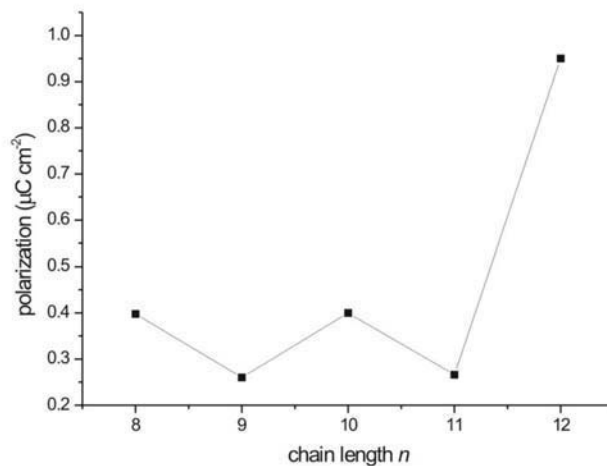
Fig. 11.7: Odd-even effect of the dependence of the spontaneous polarization on the length of the terminal chains

the electric field $\vec{E}$ and makes the ribbons twist into spirals: right- or left-handed depending on the direction of the field. These observations are consistent with those given by A. Jákli *et al* [112] in favor of the SmC$_G$ phase.

In contrast, the screw-like domains have quite different behavior. Coiling of filaments is another way to compensate their polarization to satisfy $\nabla \cdot \vec{p} = 0$. Fields above a threshold lead to an abrupt change of the sign of the gradient angle of the helix. Long exposure to an electric field eventually destroys screw-like domains and promotes growing of the flat nuclei.

As soon as the texture covers the whole view-field of the microscope the application of the electric field does not markedly affect the texture. The microscopic texture exhibits four kinds of flat domains with different birefringence (similar to ref. [105, 112]): grey, green, red and yellow. In high fields (~ 20 V/µm) small stripes appear and the extinction crosses of the green domains experience very small turns, but no current response could be detected. Other domains just slightly change birefringence. A

a)   b)

c)

Fig. 11.8: Field-induced SmX → SmCP transition: external field and current response in (a) the SmCP phase and (b) in the SmX (appearance of the repolarization current is marked by an arrow), (c) temperature dependence of the thresholds E_{th} (SmX→SmCP), E_{th1} (AFE→FE), E_{th2} (FE→AFE)
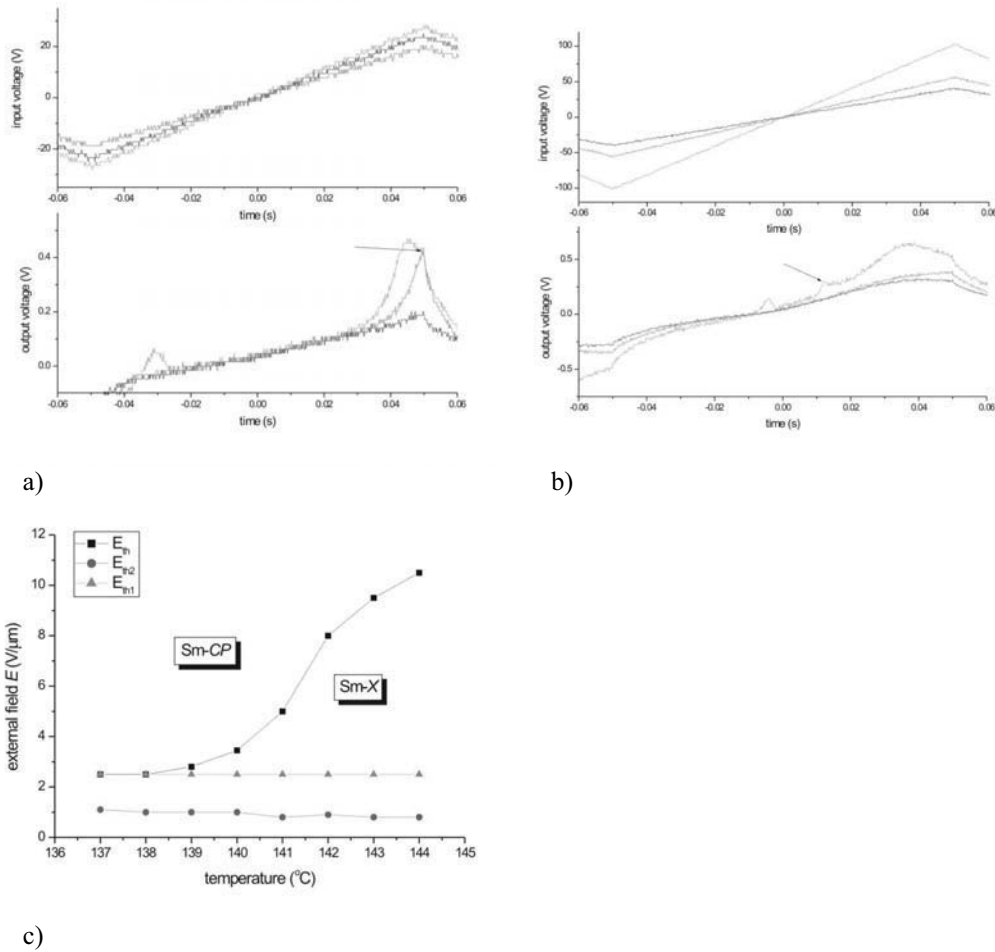
longer exposure to the strong electric field results in transformation of different domains into the red fan-like domains which are insensitive to the external field. On further cooling a phase transition takes place which can be easily seen by a change of the optical texture from fan-like into a grainy texture (Fig. 11.6a). In addition, the electro-optical response is completely different. In this low-temperature phase the switching occurs at a moderately low threshold (~ 2.5 V/µm), the field-induced texture change is independent of the polarity of the field (Fig. 11.6b). The repolarization current response exhibits two peaks per half period of the applied triangular voltage indicating an antiferroelectric (AFE) ground state. After the phase transition, the switching polarization fast reaches its saturated value and remains nearly independent of the temperature. This behavior is typical for the SmCP phase. Surprisingly, the values of the spontaneous polarization show pronounced odd-even effect even despite that the terminal chains are quite long (Fig. 11.7). The transition between the high-temperature phase, preliminary designated as SmX, and the SmCP (SmC$_S$P$_A$) phase was found for all homologues studied, but as seen from Table 11.1 the temperature of this transition increases with decrease of the terminal chain length. It should be noted that this transition could not be detected by calorimetry and X-ray measurements.
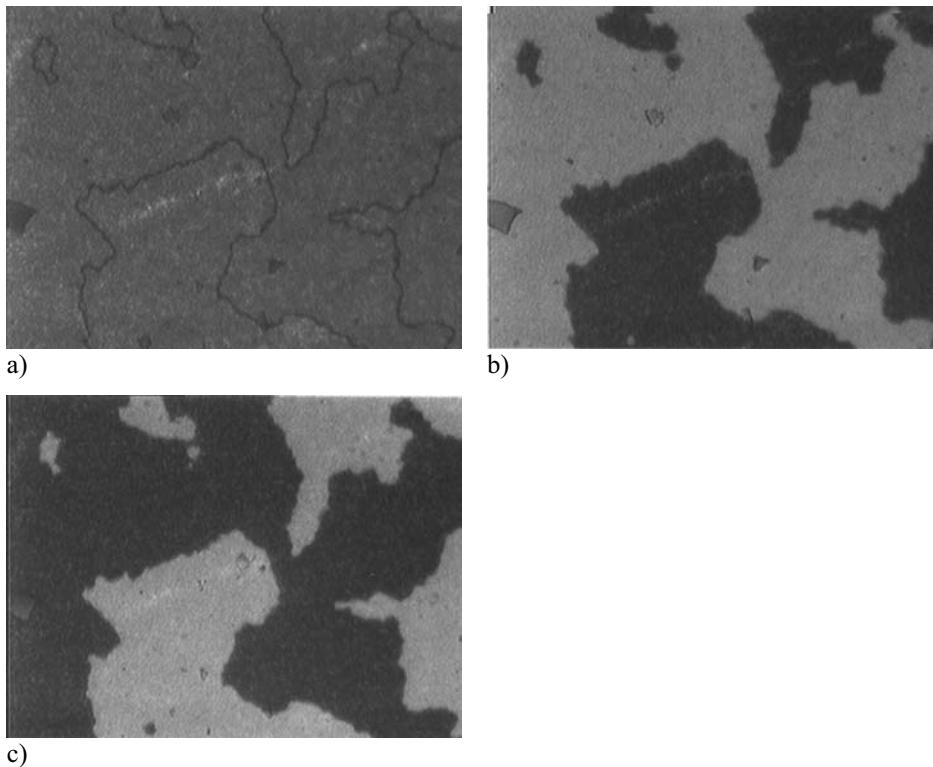
Fig. 11.9: Microscopic texture of the B$_4$ phase at (a) crossed polarizers; (b) and (c) with angles +2 deg and -2 deg between polarizer and analyzer respectively

It is remarkable that an application of a strong electric field may induce a transition from the SmX into the SmCP phase. Above a threshold which depends on the temperature a clear texture change is observed which is accompanied by current response characteristic for an antiferroelectric behavior. As an example in Fig. 11.8a a field dependence of the current response in the SmCP phase is shown. Below a threshold E_{th1} for AFE → FE transition there is no repolarization peak. As soon as the amplitude of the external field reaches the switching threshold a current peak centered in the maximum of the external field (top of the "triangular") arises. In contrast, above the SmCP → SmX transition there is no current response above the threshold and the optical texture looks intact. However, when the amplitude of the external voltage is higher than a threshold E_{th} ($E_{th1} < E_{th}$) the switching suddenly appears (Fig. 11.8b). Moreover, the maximum of the current response peak is not in the maximum of the external field anymore: the threshold for AFE → FE remains as in the SmCP phase (~ 2.5 V/µm). Such effect can be caused by a field-induced phase transition from the SmCP into the SmX phase governed by the temperature dependent threshold E_{th}. The diagram in Fig. 11.8c shows the temperature dependence of the threshold E_{th} for the SmCP → SmX transition as well as the thresholds for AFE ↔ FE transitions (E_{th1} and E_{th2}).

As it was shown before, on very slow cooling the isotropic liquid screw-like domains and beaded filaments of the SmX phase appear indicating a helical superstructure like in the B$_7$ phases. In the compounds under discussion another kind of chiral domains can occur at certain cooling rates. These domains grow as fractal nuclei and coalesce into large areas with opposite optical rotation. When one of the polarizers

is turned away from the crossed position clockwise by a small angle (2 – 10 deg), dark (blue) and light (yellow) domains become visible. Rotating the analyzer anticlockwise by the same angle the effect is reversed; that means, the previously dark domains now appear light and vice versa (Fig. 11.9). These chiral domains rotate the polarized light clockwise or anticlockwise, respectively. The domains can be also distinguished by illuminating the sample with left or right circular polarized light in the reflection mode of the microscope. Depending on the sign of the circular polarized light bright and dark domains could be observed. It should be noted that the chiral domains do not affect the color or the light transmission if the sample is rotated. This is a clear indication that the axis of the helical structure is perpendicular to the substrate planes. Such chiral domains were first described by J. Thisayukta *et al* [99, 100]. We found that the tendency to form such domains is different for the homologues compounds and if the glass substrates are treated with a surfactant solution the formation of these domains is promoted; sometimes nearly the whole preparation adopts such texture.

On cooling the SmX phase the chiral domains remain unchanged at the transition into the SmCP and B$_4$ phases. In the B$_4$ phase the texture shows nearly extinction between the crossed polarizers and the contrast between the domains of opposite handedness is less pronounced. These domains neither change upon a reversed transition on heating from the B$_4$ phase. Only the formation of the SmCP phase from the B$_4$ phase is delayed, taking place at about 10 deg higher temperature. Similar behavior has also been found in other compounds with a phase sequence B$_4$ – B$_2$ [113]. It should be noted that by adding of a chiral dopant the ratio of domains with a different handedness can be clearly changed.

Depending on the experimental conditions (cooling rate; surface treatment) we observed an interesting behavior. During the nucleation of the SmX phase one-dimensionally growing screw-like domains as well as large chiral domains grow simultaneously (Fig. 11.10). The screw-like domains further transform into a grainy texture, whereas the large chiral domains remain unchanged.

It seems that the screw-like domains and the chiral ones have the same origin – the chirality of the smectic layers. Obviously, the nucleation energy of both types of chiral domains is not much different so that they can coexist under certain conditions.

11.4 Discussion

Basing on our XRD measurements we can conclude that the high-temperature SmX phase is a tilted smectic phase without in-plane order like a Sm-*C* phase. It excludes two- or three dimensional structures as assumed for the original B$_7$ phase [18, 68, 91, 106, 107]. Really, the ribbon-like filaments are polar and the extinction crosses are oriented parallel to the analyzer and the polarizer. At the same time an assumption of a ferroelectric anticlinic structure (SmC$_A$P$_F$) is not satisfactory. The SmC$_A$P$_F$ phase has been found only in chiral bent-shaped molecules and it can be switched within milliseconds, while the SmX phase lacks of the electro-optical response.

On the other hand, the growth of the helical filaments indicates essentially chiral structure of the phase. As shown by A. Jákli *et al* [105] screw-like domains are built up by smectic filaments. The growth of the smectic filaments takes place via the absorption of the molecules from the surrounding isotropic phase by the outermost layers. The molecules in inner layers have to be pushed by the absorbed molecules. It results in an increasing compression force and leads to an undulation instability [105]. The difference between non-helical and helical filaments becomes apparent only when

modulation appears. Non-helical filaments take a serpentine-like form, whereas helical

Fig. 11.10: Coexistence of the screw-like and large chiral fractal domains

domains form coils. Two kinds of helical filaments (screw-like and telephone-wire like) have quite different behavior. Experimentally we observed that the bright, tight screw filaments grow under slow cooling. In contrast, the thin telephone-wire filaments appear at fast cooling and their growth is accompanied with bending. Slow cooling allows minimizing the surface free energy in the isotropic-liquid crystal interface by forming the coils. On fast cooling, there is no time to minimize the surface energy and thin bent filaments appear. The twist deformation caused by chirality of the phase is replaced by formation of the coils since a helical shape has less elastic energy than the corresponding twisted form [105].

The behavior of the ribbon filaments in the electric field suggests a non-zero polarization component perpendicular to the smectic layers. This finding excludes the SmCP structure with C_2 symmetry for the high-temperature SmX phase. At the same time if the molecules in addition to the anticlinic arrangement experience leaning in the tilt plane, the out-of-plane polarization is allowed. It corresponds to the lowest - C_1 symmetry [112] which is possessed by the general SmC$_G$ phase considered by P.G. de Gennes [2]. A. Jákli *et al* [112] concluded from the experimental findings that the leaning angle α decreases with decreasing temperature so that, in principle, a transition SmC$_G$ → SmCP seems to be possible.   Our experiments have shown that such transition does exist in the homologues. The high temperature SmX (SmC$_G$) phase is not switchable which can be due to the stronger sterical hindrance which does not let the leaning molecules turn in the smectic plane compared with non-leaning molecules in the SmCP phase. A continuous decreasing of the leaning angle α with decreasing temperature may result in the second or weakly first order transition into the switchable SmCP phase [112], which is in agreement with the theoretical predictions [114]. In our experiments no signal on the DSC curve was observed indicating the second order SmC$_G$ → SmCP transition. This interpretation is also in a good agreement with the observed field-induced transition into the SmC$_G$ phase. A few degrees above the transition temperature an electric field can decrease the leaning angle α resulting in the switchable structure with C_2 symmetry of the SmCP phase. One of the possibility for

decreasing in the molecular tilt has been proposed in the ref. [115] by a so-called electro-disclinic effect. An external electric field reduces the mean square fluctuations $<u^2(E)>$ of the smectic layer spacing leaving the d-values constant which results in the decrease of the tilt. In case of the SmC$_G$ phase the molecular tilt can be separated in two components "clinic" angle ψ and "leaning" α. Leaning of the bent molecules creates large difference in free volume within the smectic layer which makes leaning of the molecules sterically "un-favorable". Therefore, it seems plausible that the leaning angle α should decrease faster than ψ leading to the transition into the SmCP phase with $\alpha = 0$ and $\psi \neq 0$. Probably, sterical constraints and a need of a smoother bow-like shape can be a reason why the SmC$_G$ phase has not been found in bent-shaped asymmetric compounds [87].

The arrangement of the molecules in chiral domains of the B$_4$ phase [22, 116, 117] is not yet clear. Our optical studies show that the light transmission of these domains does not change on rotating the sample. On the other hand, these experimental findings point to a helical arrangement of the molecules like in a Sm-C^* phase where the helix axis is perpendicular to the substrate plane. This assumption is also confirmed by the observation that in thin samples of the B$_4$ phase these chiral domains show nearly extinction between crossed polarizers. In this case the smectic layers are parallel to the substrate planes. The results of our optical studies are also compatible with an arrangement of the smectic layers perpendicular to the substrates like in a TGB phase.

Chapter 12

Switching between the states of opposite chirality

In this Chapter we present a new banana-shaped compound is presented which exhibits besides a nematic phase also a smectic phase with unusual electro-optical properties. The phase transition temperatures are given in the transition scheme where the numbers in square brackets designate the corresponding transition enthalpies in kJ/mole (Fig. 12.1).

$$Cr \frac{99°C}{[34.8]} \left(SmX \frac{88°C}{[3.5]} \ N \ \frac{92°C}{[1.2]} \right) I$$
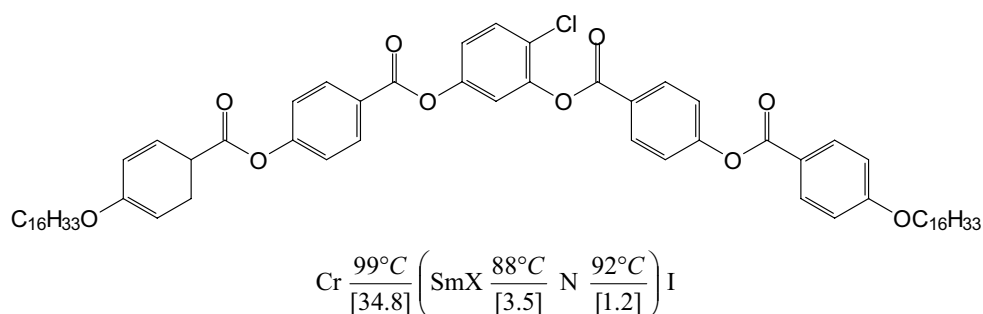
Fig. 12.1: Structural formula of the mesogen

As it is seen from the transition scheme both mesophases are monotropic. Preliminary X-ray diffraction measurements on non-oriented samples show a strong Bragg reflection in the small angle region which indicates a layer structure. The diffuse scattering maximum in the wide angle region ($\theta \sim 10$ deg) points to a liquid-like order within the smectic layers. From the small angle reflection a layer spacing d of 36 Å has been determined which is considerably smaller than the length L of the bent molecules (60 Å assuming a bending angle of 120 deg).

On cooling the nematic phase, the smectic phase appears as a fan-shaped texture (Fig. 12.2) in which the molecules are more or less parallel to the substrates. The electro-optical response is very weak. Only at relatively high electric fields (≥ 15 V/μm) a minor change of the interference color could be observed, but the textures of the switched state are independent of the polarity of the field. If the strength of the applied field is further increased (25V/μm at 186 ^{o}C) the fan-shaped texture is continuously being transformed into a quasi-homeotropic texture. It is remarkable that the threshold of this field-induced reorientation decreases with decreasing temperature (15 V/μm at 74 ^{o}C) The extinction of the texture does not change if the sample is rotated. At temperatures above 83 °C the dark texture relaxes into a birefringent "grainy" texture if the field is switched off. Below 83 °C the extinction of the texture remains unchanged if the field is removed. Optical investigations give evidence for the existence of chiral domains of opposite handedness. If one polarizer is rotated clockwise by a small angle (+8 deg) with respect to the crossed position two kinds of domains (dark and bright) become visible. Rotating the polarizer anticlockwise by the same angle the inverse situation is observed, that means, that the dark domains become bright and vice versa (Fig. 12.3). Since the sample between crossed polarizers shows a complete extinction on rotating the sample the symmetry axis must be perpendicular to the substrates and this axis obviously corresponds to the helix axis. If a sufficiently high electric field (< 10-15
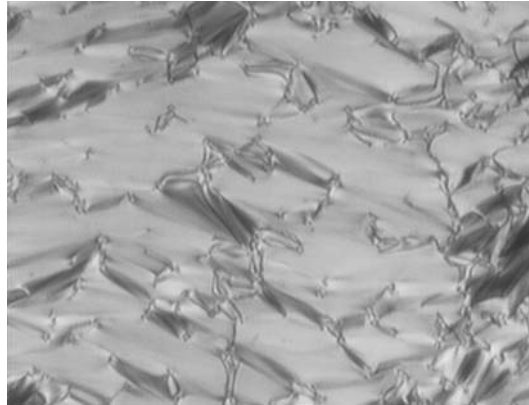
Fig. 12.2: Fan-shaped texture of the SmX phase formed on cooling the planar oriented nematic phase

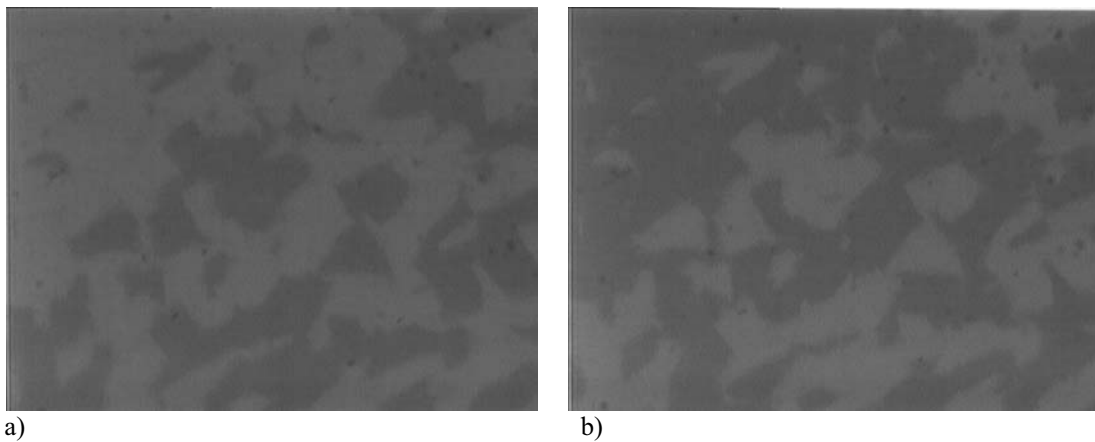a)   b)

Fig. 12.3: Chiral domains of opposite handedness in the SmX phase visualized by rotating of one
polarizer by 8 deg from the crossed polarizer position a) clockwise b) anticlockwise. The
same texture is observed when the angle between the crossed polarizers is fixed and the
field (15 V/μm) of a) positive or b) negative polarity is applied

V/μm) is applied to this texture the dark domains (observed by a small shift of one
polarizer) become bright and the bright domains become dark. By a field of opposite
polarity this effect is made inversed (Fig. 12.3). That means, the chiral domains can be
reversibly switched into a state of opposite handedness. The switching between opposite
chiral states could be observed up to about 70 °C, then the sample begins to crystallize.

In the fan-shaped and the quasi-homeotropic texture the current response to a
triangular voltage gave only one broad peak which also exists in the nematic phase and
does not completely disappear in the isotropic phase. This finding may result from the
dielectric switching as well as from the field-dependent conductivity.

A more fruitful approach seems to be the pulse method. In Fig. 12.4 the
temperature dependence of the current response to the pulse wave $V_{pp} = 20$ V/μm and a
frequency of 5 Hz is shown. The response curve of the SmX phase contains two peaks,
a broad and a narrow one indicated by the arrows. The narrow peak disappears upon the
transition into the nematic phase. The broad peak remains in the nematic and isotropic
phase and it disappears somewhere below 70 °C when the crystallization takes place.
The field dependence of the narrow peak is different from the broad one. The narrow
peak appears only when the field is higher than a threshold. It should be noted that the
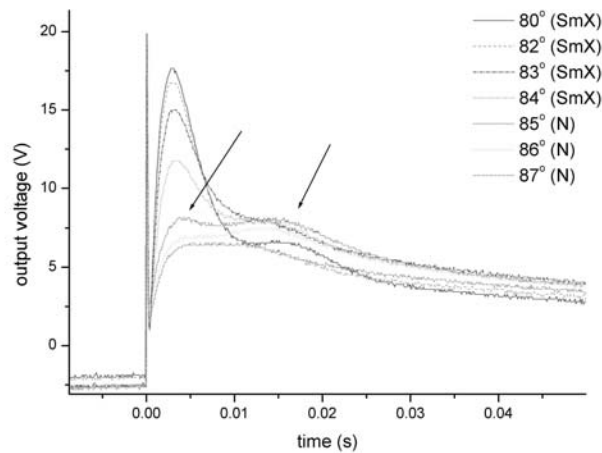
Fig. 12.4: Current response to a pulse wave voltage V_{pp} = 20V/ μm (frequency: 5 Hz) in dependence on the temperature

current response was found in case of the fan-shaped texture as well as the quasi-homeotropic texture.

It can be assumed that in the fan-shaped texture of the SmX phase the director is more or less parallel to the substrates. On the other hand, the field-induced transition into the quasi-homeotropic state where the layers are parallel to the substrates can be understood if the smectic layers had a considerable polarization component parallel to the layer normal since the dielectric anisotropy is negative. It follows from X-ray measurements that the molecules might be tilted within the smectic layers. But the uniaxial symmetry of the dark texture leads to the assumption that the tilted molecules form a helical superstructure alike in SmC* phases. Since in our case the molecules are achiral the helical structure is obviously the consequence of chirality of the smectic layers. It is a first observation of a field induced switching between the states of opposite chirality.

Although, the mechanism of this effect is not yet clear the experimental findings can be understood if there is a spontaneous polarization component perpendicular to the layers. This could be compatible with a smectic structure with triclinic symmetry.

Summary

Liquid crystals are extraordinary and challenging systems for both theoretical and experimental research as well as technological applications. A rich variety of mesophases exhibited by liquid crystalline materials shows symmetries intermediate between those of the highest symmetry homogeneous isotropic liquid and the lowest symmetry three-dimensional periodic crystals. In contrast to solid-state systems, whose ordering is driven by energy-entropy competition, liquid-crystal phase transitions are of predominantly entropic origin.

Recently a new class of liquid crystalline materials those formed by *bent-shaped* molecules, has become one of the topical field in current liquid crystalline research. In contrast to the *rod-like* mesogens (calamitics) the *bent-shaped* molecules possess a strong sterical moment. Thereby such compounds tend to exhibit various mesophases not typical for calamitics, for example, chiral ferro- and antiferroelectric phases formed by achiral molecules.

The aim of my thesis is structural determination and physical characterization of new mesophases formed by bent-shaped molecules. In the frame of this research the following experimental techniques have been used:

- thermal behavior and phase transitions were studied using differential scanning calorimetry (DSC)
- optical textures and electro-optical switching were investigated by means of polarizing microscopy
- information on the conformation (bending angles ε, α) and the ordering (orientational order parameter S) of the bent molecules was obtained from ^{19}F-, ^{1}H-, ^{2}H- and ^{13}C-NMR spectroscopy
- structural characterization of the mesophases was performed using X-ray diffraction methods
- ferroelectric and antiferroelectric properties were investigated by means of electro-optical measurements

Physical characterization of the new mesophases was not the only goal of this work. Much effort has been applied to investigate the influence of the molecular bending on the formation of the "banana" phases. In particular, the transitions from the conventional smectic mesophases into the mesophases characteristic for the bent-shaped compounds have been thoroughly studied.

Additionally some theoretical studies have been done on molecular modeling and simulation of X-ray scattering from smectic phases formed by rod-like and bent-shaped molecules. In these simulations we have analyzed the effect of both molecular tilt and bent on the appearance of the X-ray diffraction patterns. Besides, some accessory software has been developed to manage the data exchange between the commercial and custom-made computer programs.

The experimental results of this thesis can be summarized as the following:

➢ A *polar biaxial orthogonal* mesophase (SmAP) has been observed and characterized for the first time (Chapter 5). This phase was formed on cooling of the SmA phase. The bending angle between the two "wings" of the bent-shaped molecules was continuously decreasing from ~142 deg (less bent) in the SmA phase till ~ 132 deg (more bent) in the SmAP phase. It

suggests, that in the high-temperature SmA phase a smaller bending does not provide a strong enough *sterical moment* to break the cylindrical symmetry of the mesophase, which is characteristic for rod-like molecules. Whereas, a stronger bent (in the SmAP phase) results in hindering the free rotation of the molecules around their long axis and a *polar* ordering arises. Also the orientational order parameter S was increasing from a rather high value of 0.7 yet encountered in calamitics till ~0.83 in the SmAP phase.

➢ The formation of the SmCP phase from the isotropic phase is a quite usual phenomenon among bent-shaped liquid crystalline materials. Yet the new fluorinated compounds used in this work give much more valuable information on the *conformation* (bending angles ε, α) and the *ordering* (orientational order parameter S) from ^{19}F-NMR technique. The results given in Chapters 6 - 11 show that characteristic features of the SmCP phase formed by means of the first order transition on cooling from the isotropic phase are

- high values of the longitudinal order parameter ($S \approx 0.75 - 0.9$) which scarcely depend on the temperature
- negligibly small values of the transversal order parameter D
- temperature independence of the bending angle
- temperature independent tilt angle
- temperature independent smectic layer thickness
- high values of switching polarization and its weak temperature dependence

It is important to mention that the estimation of the *transversal* order parameter for bent-shaped mesogens in the SmCP phase has been made in this work for the first time.

➢ In the course of this work for the first time we found a bent-shaped mesogen with the SmCP – N dimorphism (compound VI/**4F** in Chapter 6). The switching polarization measured in this compound turned out to be considerably reduced in comparison with compounds that formed the SmCP phase from the isotropic phase.

➢ The importance of the bending angle for the formation of the "banana" phases has been studied in dichlorosubstituted materials (VII/**3**–VII/**12**) exhibiting conventional N, SmA, SmC as well as the "banana" SmCP phase (Chapter 7). In contrast to the other bent-shaped mesogens these compounds show quite unusual properties. More explicit investigations of the SmCP phase, formed on cooling of the apolar SmC phase by means of a *weakly* first order transition, showed that the molecular *bending is changing* with temperature. In particular, it was found that in the SmA and the SmC phases the molecules are nearly *stretched* whereas in the SmCP phase the bending angle clearly decreases with decreasing temperature (160 – 140 deg). The estimations of the tilt angle suggest a very small inclination of the molecules in the SmC and the SmCP phase (~ 5 deg). The spontaneous polarization in the SmCP phase shows a pronounced temperature dependence and the dielectric permittivity at the transition SmCP – SmC experiences a λ-like peak.

➢ Polymorphic SmCP phases have been observed in 2-methyl resorcinol derivatives (VIII/**1** and VIII/**2**). The results of the experimental study might be explained by the existence of the thermodynamically different mesophases corresponding to the different values of the tilt angles. The transition between such polymorphic SmCP phases is accompanied with a jump of the tilt. Besides, we report a higher ordered low-temperature crystalline phase exhibiting the elctro-optical switching.

➢ Some polymorphic B_5 phases have been found in 5-fluororesorcinol derivatives (IX/**8** and IX/**12**). All phase transitions have been detected by calorimetry, although the transition enthalpies are rather low. The experimental investigations give evidence that among these polymorphic phases there is an antiferroelectric B_{5A} as well as a ferroelectric B_{5F} phase.

Besides, the transition from the antiferroelectric B_{5A} into the ferroelectric B_{5F} phase is not straight: it is accompanied by occurrence of some sub-phases alike in other ferroelectric and ferromagnetic systems. It is important to notice that it is a first observation of the ferroelectric variant of the B_5 phase.

➢ The first characterization of the SmCP phase with a *ferroelectric ground state* has been done in the course of this thesis on asymmetrical bent-core mesogens with a bulky oligosiloxane unit at one end (compound X/1, Chapter 10). The appearance of siloxane sub-layers seems to have an essential influence on the formation of the ferroelectric ground state.

➢ In Chapter 11 we have presented the experimental evidence for a mesophase with *triclinic* symmetry (SmC_G). Two liquid crystalline phases have been observed in compounds XI/**8 –** XI/**12**. The X-ray examination of the high-temperature phase suggested a layer structure of tilted molecules. In addition, the behavior of the microscopical textures in the electric field indicated the presence of a polarization component perpendicular to the smectic layers; On the other hand, on cooling of the isotropic liquid *chiral domains* of the opposite handedness were detected. All these findings are compatible with C_1 symmetry of the SmC_G phase. The lower-temperature mesophase formed by means of the second order transition on cooling of the SmC_G phase was identified as the SmCP phase. In addition we found a field-induced $SmC_G \rightarrow SmCP$ transition.

➢ Spontaneously formed *chiral domains* have be detected for the first time in the nematic phase of a 4-chlororesorcinol derivative (compound IV/**1**). Application of an electric field induced the formation of the fan-shaped textures. On cooling the nematic phase, an optically isotropic mesophase of high viscosity arose which possessed no long-range positional order. This first isotropic "banana phase" formed spontaneously chiral regions of opposite handedness.

➢ The switching between the chiral states of opposite handedness has been observed for the first time in a hexadecyloxy homologue compound XII/**1**. At sufficiently high electric fields the planar oriented texture of the smectic phase can be continuously reoriented into a homeotropic texture which displays randomly distributed *chiral domains*. Application of an external electric field gives rise to the switching of these domains into the states of opposite handedness. A preliminary investigation has also shown the presence of a current response. Such electro-optical behavior could also been understood by a possible tricilinic symmetry of the structure. However, further research is going to be done to elucidate this unusual and fascinating phenomenon.

Zusammenfassung

Flüssigkristalle sind außergewöhnliche Systeme sowohl für die experimentelle und theoretische Forschung als auch für die technische Anwendung. Flüssig-kristalline Materialien bilden eine reiche Vielfalt von Mesophasen aus, deren Symmetry zwischen den Systemen .niedrigster. Symmetrie, den Flüssigkeiten, und den Systemen höchster Symmetrie, den dreidimensional periodischen Kristallen liegt. Im Gegensatz zumKristall, dessen Ordnung durch den Wettstreit zwischen Energie und Entropie entsteht, werden Umwandlungen zwischen flüssig-kristallinen Phasen von der Entropie bestimmt.

Kürzlich hat sich eine neue Klasse flüssig-kristalliner Materialien, die von gebogenen Molekülen gebildet werden, zu einem wichtigen Gebiet der aktuellen Flüssigkristallforschung entwickelt. Im Gegensatz zu den stäbchenförmigen Mesogenen (den kalamitischen Verbindungen) besitzen die gebogenen Moleküle ein starkes sterisches Moment. Daher können solche Verbindungen verschiedene Mesophasen ausbilden, die bei kalamitischen Verbindungen nicht beobachtet werden, z. B. chirale ferro- und antiferrroelektrische Phasen, obwohl die Moleküle selbst achiral sind.

Das Ziel meiner Dissertation ist die Strukturaufklärung und physikalische Charakterisierung von neuen Mesophasen, die sich von gebogenen Molekülen ableiten. Im Rahmen der vorliegenden Arbeit wurden folgende experimentelle Methoden angewendet:

- Das thermische Verhalten und die Phasenumwandlungen wurden mit Hilfe der Differential-Scanning-Kalorimetrie (DSC) untersucht

- Die optischen Texturen und das elektrooptische Schalten wurden in einem Polarisationsmikroskop beobachtet.

- Informationen über die Konformation (den Biegungswinkel ε, α) und die Ordnung (den Orientierungsordnungsgrad S) der gebogenen Moleküle wurden mit Hilfe der 19F, 1H-, 2H- und 13C-NMR-Spektroskopie erhalten

- Die strukturelle Charakterisierung der neuen Mesophasen erfolgte mit verschiedenen röntgenographischen Methoden

- Die ferroelektrischen und antiferroelektrischen Eigenschaften wurden mit Hilfe elektrooptischer Messungen untersucht.

Die physikalische Charakterisierung der neuen Mesophasen war nicht das einzige Ziel dieser Arbeit. Es sollte auch geklärt werden, welchen Einfluß die Biegung der Moleküle auf die Bildung von „Bananenphasen"hat. Insbesondere wurden Umwandlungen von üblichen smektischen Phasen in „Bananenphasen" eingehend studiert. Außerdem wurden theoretische Untersuchungen zur Simulation der Röntgendiagramme durchgeführt, die von smektischen Phasen stäbchenförmiger und gebogener Moleküle erhalten werden. Bei diesen Simulationen wurde der Einfluß des Neigungswinkels und des Biegungswinkels auf die Topologie der Röntgendiagramme untersucht. Dabei wurde eine neue Software entwickelt, um die kommerziellen und eigenen Computerprogramme zu verknüpfen.

Die experimentellen Resultate sollen im folgenden zusammengefaßt werden:

➢ Es wurde erstmals eine polare biaxiale Mesophase mit orthogonaler Anordnung der Moleküle (SmAP) beobachtet und charakterisiert (Kap. 5). Diese Phase wird beim Abkühlen der SmA-Phase erhalten. Der Biegungswinkel zwischen den beiden Flügeln der gebogenen Moleküle nimmt kontinuierlich von 142 deg in der SmA-Phase auf 132 deg in der SmAP-Phase ab. Dies legt nahe, daß in der Hochtemperaturphase SmA das sterische Moment wegen der geringeren Biegung nicht stark genug ist, die zylindrische Symmetrie der Mesophase zu brechen. Dagegen bedingt die stärkere Biegung in der SmAP-Phase eine Rotationslinderung um die Längsachse und es entsteht eine polare Ordnung. Der Orientierungsgrad S nahm von 0.7 in der SmA-Phase bis 0.83 in der SmAP-Phase zu.

➢ Die SmCP-Phase entsteht meist beim Abkühlen der isotropen Phase. Die neuen fluorierten Verbindungen, die in dieser Arbeit untersucht worden, liefern wertvolle Informationen über die Konformation (Biegungswinkel ε, α) und Ordnung (Orientierungsordnungs-Parameter S) mit Hilfe der 19F -NMR-Spektroskopie. Die Ergebnisse, die in den Kapiteln 6-11 vorgestellt werden, zeigen die Besonderheiten der SmCP-Phase, die durch eine Phasenumwandlung 1. Ordnung aus der isotropen Flüssigkeit gebildet wird:

  • hohe Werte des longitudinalen Ordnungsparameters ($S = 0.75 – 0.9$), welcher nahezu temperaturunabhängig ist.
  • vernachlässigbar kleine Werte des transversalen Ordnungsparameters
  • einen temperaturunabhängigen Biegungswinkel
  • einen temperaturunabhängigen Tiltwinkel
  • eine temperaturunabhängige Schichtdicke
  • hohe Werte der Polarisation
  • Es sollte erwähnt werden, daß erstmals der transversale Ordnungsparameter für die SmCP-Phase bestimmt werden konnte.

➢ Im Rahmen der Arbeit fanden wir erstmals eine gebogene mesogen Verbindung mit der Dimorphie SmCP-N (Verbindung VI/**4F** in Kap. 6): Die Polarisation ist deutlich geringer als die von solchen SmCP-Phasen, die direkt aus der isotropen Flüssigkeit gebildet werden.

➢ Die Bedeutung des Biegungswinkels für die Bildung von „Bananenphasen" wurde an homologen dichlor-substituierten Verbindungen (VII/**3** – VII/**7**) studiert, welche sowohl N-, SmA- und SmC-Phasen als auch die „Bananenphase" SmCP ausbilden (Kap. 7). Im Gegensatz zu anderen gebogenen Mesogenen zeigen diese Verbindungen sehr ungewöhnliche Eigenschaften. In der SmCP-Phase, die beim Abkühlen der SmC-Phase entsteht, ändert sich der Biegungswinkel in starkem Maße mit der Temperatur. Es wurde gefunden, daß in der SmA- und SmC-Phase die Moleküle nahezu gestreckt sind, während in der SmCP-Phase der Biegungswinkel deutlich mit fallender Temperatur abnimmt (160 – 140 deg). Andererseits ist der Tiltwinkel in der SmC- und der SmCP-Phase sehr gering (~ 5 deg). Die Polarisation zeigt eine ausgeprägte Temperaturabhängigkeit und die Dielektrizitätskonstante zeigt einen λ–ähnlichen Peak bei der Umwandlung SmCP-SmC.

➢ In 2-Methyl-Resorcinderivaten (VIII/**1** and VIII/**2**) wurden neben einer B5-Phase polymorphe SmCP-Phasen beobachtet. Aus den experimentellen Untersuchungen folgt, dass es sich bei den SmCP-Phasen um thermodynamisch verschiedene Mesophasen handelt,deren Neigungswinkel sich unterscheidet. Außerdem berichten wir über eine dreidimensional geordnete Tieftemperaturphase, die elektrooptisch geschaltet werden kann.

➢ Mehrere polymorphe B5-Phasen wurden in 5-Fluorresorcinderivaten (IX/**8** und IX/**10**) gefunden. Alle Phasenumwandlungen konnten kalorimetrisch nachgewiesen werden,

obwohl die Umwandlungsenthalpien ziemlich gering sind. Die experimentellen Untersuchungen erbrachten den Nachweis, daß sowohl eine antiferroelektrische B_{5A} als auch eine ferroelektrische B_{5F}-Phase auftritt. Allerdings erfolgt der Übergang von der antiferroelektrischen B_{5A}- in die ferroelektrische B_{5F}-Phase nicht direkt; zwischen ihnen existieren mehrere Subphasen, wie man sie auch bei anderen ferroelektrischen oder ferromagnetischen Systemen findet. Es sollte erwähnt werden, daß die ferroelektrische Variante der B_5-Phase erstmals in dieser Arbeit beschrieben wird.

➢ An einem asymmetrischen gebogenen Mesogen mit einer voluminösen Oligosioxaneinheit an einem Ende des Moleküls wurde erstmals eine SmCP-Phase mit ferroelektrischem Grundzustand nachgewiesen (Verbindung X/**1**). Die Ausbildung von Siloxan-Subschichten scheint eine wesentliche Voraussetzung für das Auftreten des ferroelektrischen Grundzustandes zu sein.

➢ In Kap. 11 wird der experimentelle Nachweis für eine Mesophase mit trikliner Symmetrie (SmC6) vorgestellt. An den Verbindungen XI/**8** – XI/**12** wurden zwei flüssig-kristalline Phasen beobachtet. Die Röntgenuntersuchungen an der Hochtemperaturphase zeigen eine Schichtstruktur mit geneigter Molekülanordnung an. Das Verhalten der mikroskopischen Texturen im elektrischen Feld weist auf eine Polarisationskomponente senkrecht zu den smektischen Schichten hin; außerdem wurden beim Abkülen der isotropen Flüssigkeit chirale Domänen von entgegengesetzter Händigkeit beobachtet. Diese Befunde sind verträglich mit der C1-Symmetrie einer SmCG-Phase. Die Tieftemperaturphase, die aus der SmCG-Phase nach einer Phasenumwandlung 1. Ordnung gebildet wird, wurde als SmCP-Phase identifiziert. Außerdem wurde eine feldinduzierte SmCG → SmCP-Umwandlung gefunden.

➢ In der nematischen Phase eines 4-Chlorresorcinderivates (Verbindung IV/**1**) werden spontan chirale Domänen ausgebildet. Beim Anlegen eines elektrischen Feldes konnte die Ausbildung einer Fächertextur induziert werden. Beim Abkühlen der nematischen Phase erscheint eine optisch isotrope Mesophase von relativ hoher Viskosität, welche keine Positionsfernordnung besitzt. Diese erstmalig beobachtete isotrope „Bananenphase" bildet ebenfalls spontan chirale Bereiche entgegengesetzter Händigkeit aus.

➢ An dem Hexadexyloxy-Homologen XII/**1** wurde erstmals das Schalten zwischen chiralen Zuständen entgegengesetzter Händigkeit beobachtet. Bei hinreichend hohen elektrischen Feldern kann die planar orientierte smektische Phase kontinuierlich in eine homöotrope Textur umorientiert werden, welche statistisch verteilte chirale Domänen zeigt. Beim Anlegen eines elektrischen Feldes können diese Domänen in einen Zustand von entgegengesetzter Händigkeit geschaltet werden. Vorläufige Untersuchungen ergaben den Nachweis einer Stromantwort. Das gefundene elektrooptisches Verhalten weist auf die Existenz einer triklinen Symmetrie dieser Struktur hin. Weitere Untersuchungen sind erforderlich, die Ursache für dieses bemerkenswerte Phänomen zu ergründen.

Bibliography

[1] P.M. Chaikin, T.C. Lubensky, *Principles of Condensed Matter Physics,* University Press, Cambridge, 1995

[2] P.G. de Gennes, *The Physics of Liquid Crystals,* Clarendon Press, Oxford, 1974

[3] T. Niori, T. Sekine, J. Watanabe, T. Furukawa, H. Takezoe, *J. Mater. Chem.,* **6,** 1231 (1996)

[4] T.C. Lubensky, *Science*, **228**, 2146 (2000)

[5] T.C. Lubensky, *Molec. Cryst. Liq. Cryst.,* **13**, 1 (2001)

[6] T. Lubensky, L. Radzihovsky, *Phys. Rev. E*, submitted

[7] L. Radzihovsky, T. Lubensky, *Eur. Phys. Lett.* **54**, 206 (2001)

[8] T.C. Lubensky, A.B. Harris, R.D. Kamien, G. Yan, *Ferroelectrics*, **212**, 1 (1998)

[9] A.B. Harris, R.D. Kamien, T.C. Lubensky, *Rev. Mod. Phys.*, **71**, 1745 (1999)

[10] R. Memmer, *Liq. Cryst,* **29,** 483 (2002)

[11] I. Dozov, *Europhys. Lett.,* **56** (2), 247 (2001)

[12] P.E. Cladis, H.R. Brand, H. Pleiner, *Eur. Phys. J. B,* **6**, 347 (1998)

[13] D. R. Link, N. A. Clark, B. I. Ostrovskii, E. A. Soto Bustamante, *Phys. Rev. E*, **61**, R37 (2000)

[14] A. Eremin, S. Diele, G. Pelzl, H. Nádasi, W. Weissflog, J. Salfetnikova, H. Kresse *Phys. Rev. E*, **64**, 51707 (2001)

[15] R.Link, G.Natale, R.Shao, J.E.Maclennan, N.A.Clark, E.Körblova, D.M. Walba, *Science*, **278**, 1924 (1997)

[16] G. Pelzl, S. Diele, W. Weissflog, *Adv. Mater.,* **11**, 707 (1999)

[17] S. Diele, S. Grande, H. Kruth, Ch. Lischka, G. Pelzl, W. Weissflog, I. Wirth, *Ferroelectrics,* **212**, 169 (1998)

[18] G. Pelzl, S. Diele, C. Lischka, I. Wirth, W. Weissflog, *Liq. Cryst.*, **26**, 135 (1999)

[19] H.R. Brand, P.E. Cladis, H. Pleiner, *Europhys. Lett.*, **57**, 368 (2002)

[20] N.A. Clark, D.R. Link, D. Coleman, W.G. Jang, J. Fernsler, C. Boyer, J. Zasadzinski, D.M. Walba, E. Körblova, W. Weissflog, Abstracts of the 19th International Liquid Crystal Conference 2002 in Edinburgh, UK

[21] T. Sekine, T.Niori, M. Sone, J. Watanabe, S. Choi, Y. Takanishi, Takezoe, *Jpn J. Appl., Phys.,* **36,** 6455 (1997)

[22] J. Thisayukta, H. Takezoe, J. Watanabe, *Jpn. J. Appl. Phys.*, **40**, 3277 (2001)

[23] I. Wirth, S. Diele, A. Eremin, G. Pelzl, S. Grande, L. Kovalenko, N. Panchenko, W. Weissflog, *J. Mater. Chem.*, **11**, 1642 (2001)

[24] M.W. Schröder, S. Diele, G. Pelzl, N. Panchenko, W. Weissflog, *Liq. Cryst.*, **29**, 1039 (2002)

[25] J. Valsek, Phys. Rev. **15**, 537 (1920)

[26] H.R. Jaffe, *PhysRev.*, **51**, 43 (1937)

[27] H. Mueller, *Phys. Rev.*, **57**, 829 (1940)

[28] В.Л. Гинзбург, *ЖЭТФ*, **15**, 739 (1945); V.J. Ginzburg, *J. Phys. USSR*, **10**, 107 (1946)

[28a] В.Л. Гинзбург, *УФН*, **171**, 1123 (2001)

[29] Л.Д. Ландау, *Статистическая физика,* Наука, Москва 1991; L.D. Landau, *Statistical Physics,* Pergamon Press, Oxford 1993

[30] M.P. Marder, *Condensed Matter Physics*, Wiley, New York 2001

[31] S.T. Lagerwall, *Ferroelectric and Antiferroelectric Liquid Crystals*, Wiley-VCH, Weinheim 1999

[32] H.S. Kitzerow, *Chirality in Liquid Crystals*, Springer, New York 2001

[33] R.B. Meyer in 5th Int. Liquid Crystal Conference, Stockholm, June 1974

[34] R.B. Meyer, L. Liebert, L. Strzelecki, P. Keller, *J. Phys. (Paris) Lett.*, **36**, L69 (1993)

[35] W. Kuczynski, H. Stegemeyer, *Chem. Phys. Lett.*, **70**, 123, (1980)

[36] M.A. Osipov, S.A. Pikin, *Mol. Cryst. Liq. Cryst.,* **103**, 57 (1983)

[37] D. Walba, E. Körblova, R. Shao, J.E. Maclennan, D.R. Link, N.A. Clark, *Mat. Res. Soc. Symp. Proc.*, **559**, 3 (1999)

[38] S. V. Shilov; S. Rauch; H. Skupin; G. Heppke; F. Kremer, *Liq. Cryst.*, **26**, 1409 (1999)

[39] A. Eremin, S. Diele, G. Pelzl, W. Weissflog, *Phys. Rev.* E, submitted

[40] G. Heppke, A. Jákli, Rauch, H. Sawade, *Phys. Rev. E*, **60**, 5575 (1999)

[41] M. I. Barnik; L. M. Blinov; N. M. Shtykov; S. P. Palto; G. Pelzl; W. Weissflog, *Liq. Cryst.*, **29**, 597 (2002)

[42] L. M. Blinov, M.I. Barnik, E. Soto Bustamante, G. Pelzl, W. Weissflog, *Phys. Rev. E.*, submitted

[43] J.F. Li, X.Y. Wang, E. Kangas, P.L. Taylor, C. Rosenblatt, Y. Susuki, P.E. Cladis, *Phys. Rev. B*, **52**, 13075 (1995)

[44] A. Abragam, *The Principles of Nuclear Magnetism*, Oxford University Press, London 1961

[45] K. Schmidt-Rohr, H.W. Spiess, *Multidimensional solid-state NMR and polymers,* Academic Press, London 1994

[46] H. Lippmann, *Ann Phys,* **2**, 287 (1958)

[47] R. Blinc, *Liq. Cryst*, **26**, 1295 (1999)

[48] E. Ciampi, M.I.C. Furby, L. Brennan, J.W. Emsley, A. Lesage, L. Emsley, *Liq. Cryst.*, **26**, 109 (1999)

[49] F. Roussel, J-P. Bayle, M.A. Khan, B.M. Fung, O. Yokokohji, T. Shimizu, H. Koh, S. Kumai, *Liq. Cryst.*, **26**, 251 (1999)

[50] D.W. Allender, G.P. Crawford, J.W. Doane, *Phys. Rev. Lett.*, **67**, 1442 (1991)

[51] H.D. Koswig, *Seleted Topics in Liquid Crystal Research*, Akademie Verlag, Berlin 1990

[52] H. Schmiedel, B. Hiller, S. Grande, A. Lösche, St. Limmer, *J. Magn. Reson.*, **40**, 369 (1980)

[53] R.Y. Dong, *Nuclear Magnetic Resonance of Liquid Crystals*, Springer Verlag, New York (1994)

[54] T. M. Duncan, *A Compilation of Chemical Shift Anisotropies*, The Farragut Press, Chicago, 1990

[55] J. Als-Nielsen, D. McMorrow, *Elements of Modern X-ray Physics,* Wiley, New York 2001

[56] Б.К. Вайнштейн, *Дифракция ренгеновских лучей на цепных молекулах,* Изд. Акад. Наук, Москва 1963

[57] И.А. Квасников, *Термодинамика и статистическая физика,* Изд. Московского Университета, Москва 1995

[58] J.M. Thijssen, *Computational Physics*, Cambridge University Press, Cambridge 2000

[59] R. Hosemann, S.N. Bagchi, *Acta Cryst*, **5**, 612 (1952)

[60] С.М. Никольский, *Курс математического анализа*, Наука, Москва 1991

[61] M. J. Freiser, *Phys. Rev. Lett.*, **24**, 1041 (1970)

[62] L.J.Yu, A.Saupe, *Phys. Rev.Lett.*, **45**, 1000 (1980)

[63] H.Leube, H. Finkelmann, *Makromolek. Chem.*, **191**, 2707 (1990)

[64] H.R. Brand, P.E.Cladis, H. Pleiner, *International Journal of Engineering Science*, **38**, 1099 (2000)

[65] H. Matsuzaki, Y. Matsunaga, *Liq. Cryst.*, **14**, 105 (1993)

[66] J. Szydlowska, J. Matraszek, J. Mieczkowski, E. Gorecka, D. Pociecka, *Mol. Cryst. Liq. Cryst.*, **365**, 107 (2001)

[67] W.Weissflog, Ch.Lischka, S. Diele, G. Pelzl, I. Wirth, S. Grande, H. Kresse, H. Schmalfuss, H. Hartung, A. Stettler, *Mol. Cryst. Liq. Cryst.*, **333**, 203 (1999)

[68] W.Weissflog, H. Nádasi, U. Dunemann, G.Pelzl, S.Diele, A. Eremin, and H. Kresse, *J.Mater. Chem.*, **11**, 2748 (2001)

[69] R. Amaranetha Reddy, B.K. Sadashiva, and Surajit Dhara, *Chem. Commun.*, 1972 (2002)

[70] V.L. McMillan, *Phys. Rev. A*, **4**, 1238 (1971)

[71] V.L. McMillan, *Phys. Rev. A*, **8**, 1921 (1973)

[72] H.R. Brand, P. Cladis, H. Pleiner, *Macromolecules*, **25**, 7223 (1988)

[73] H. F. Leube, H. Finkelmann, *Makromol. Chem.*, **192**, 1317 (1991)

[74] R. Pratibha, N. V. Madhusudana, B. K. Sadashiva, *Science*, **288**, 2184 (2000)

[75] T. Niori, T. Sekine, J. Watanabe, H.Takezoe, *J. Mater. Chem.*, **6**, 1231 (1996)

[76] T, Hegmann, J. Kain, S. Diele, G. Pelzl, and C. Tschierske, *Angew.Chem.*, **113**, 911 (2001)

[77] B.K. Sadashiva, R. Amaranatha Reddy, R. Pratibha, N.V. Madhusudana, *J. Mater. Chem.*, **12**, 943 (2002)

[78] W. F. Harris, *Philos. Mag.*, **22**, 949 (1970)

[79] Y. Takanishi, H. Takezoe, A. Fukuda, J. Watanabe, *Phys. Rev. B*, **45**, 7684 (1992)

[80] W. Weissflog, S. Richter, E. Dietzmann, J. Risse, S. Diele, P. Schiller, G. Pelzl, *Cryst. Res. Technol.,* **32**, 271 (1997)

[81] E. A. Soto Bustamente, S. V. Yablonskii, B. I. Ostrovskii, L. A. Beresnev, L. M. Blinov, W. Haase, *Chem.Phys. Lett.*, **260**, 447 (1996)

[82] G. Pelzl, S. Diele, S. Grande, A. Jákli, Ch. Lischka, H. Kresse, H. Schmalfuss, I. Wirth, W. Weissflog, *Liq. Cryst.*, **26**, 401 (1999);

[83] J. Lee, A.D.L. Chandani, K. Itoh, Y. Ouchi, H. Takezoe, A. Fukuda, *Jpn. J. Appl. Phys.,* **29**, 1122 (1990)

[84] J.P. Bedel, J.C. Rouillon, J.P. Marcerou, M. Laguerre, H.T. Nguyen, M.F. Achard, *Liq. Cryst.,* **28**, 1285 (2000)

[85] Schmalfuss, H., Hauser, A., Kresse, H., *Mol. Cryst. Liq. Cryst.,* **351**, 221 (2000)

[86] A. Hauser, H. Schmalfuss, H. Kresse, *Liq. Cryst.*, **27**, 629 (2000)

[87] H.T. Nguyen, J.C. Rouillon, J.P. Marcerou, J.R. Bedel, P. Barois, S. Sarmento, *Mol. Cryst. Liq. Cryst.,* **328**, 177 (1999)

[88] H. Nádasi, W. Weissflog, A. Eremin, G. Pelzl, S. Diele, B. Das, S. Grande, *J. Mater. Chem.*, **12**, 1316 (2002)

[89] A.P.L. Chandani, Y. Ouchi, H. Takezoe, A. Fukuda, H. Tereshima, K. Furukawa, A. Kishi, *Jpn. J. Appl. Phys.*, **28**, L1261 (1989)

[90] A. Fukuda, Y. Takanishi, T. Isozaki, K. Ishikawa, H. Takezoe, *J. Mater. Chem.,* **4**, 997 (1994)

[91] D.M. Walba, E. Körblova, R. Shao, J.E. Maclennan, D.R. Link, M.A. Glaser, N.A. Clark, *Science*, **288**, 2181 (2000)

[92] F. Tournilhac, L.M. Blinov, J. Simon, S.V. Yablonski, *Nature,* **359**, 621 (1992)

[93] G. Dantlgraber, A. Eremin, S. Diele, A. Hauser, H. Kresse, G. Pelzl, C. Tschierske, *Angew. Chemie,* **41**, 2408 (2002)

[94] J. Thisayuhta, H. Kamee, S. Kawauchi, J. Watanabe, *Mol.. Cryst. Liq. Cryst.*, **346**, 63 (2000)

[95] J. Thisayuhta, Y. Nakayama, S. Kawauchi, H. Takezoe, J. Watanabe, *J. Am. Chem. Soc.*, **122**, 7441 (2000)

[96] G. Heppke, D.D. Parghi, H. Sawade, *Liq. Cryst.*, **27**, 313 (2000)

[97] J. Thisayukta, H. Niwano, H. Takezoe, J. Watanabe, *J. Mater. Chem.*, **11**, 2717 (2001)

[98] E. Gorecka, D. Pociecha, F. Araoka, D.R. Link, M. Nakata, J. Thisayukta, Y. Takanishi, K. Ishikawa, J. Watanabe, H. Takezoe, *Phys. Rev. E,* **62**, R4524 (2000)

[99] M. Nakata, D.R. Link, J. Thisayukta, Y. Takanishi, K. Ishikawa, J. Watanabe, H.Takezoe, *J.Mater. Chem.*, **11**, 2694 (2001)

[100] S. Diele, B. Hisgen, B. Reck, H. Ringsdorf, *Makromolec. Chem.*, *Rapid Commun.,* **7**, 267 (1986)

[101] S. Diele, B. Oelsner, F. Kuschel, B. Hisgen, H. Ringsdorf, R. Zentel, *Makromolec. Chem.*, **188**, 1993 (1987)

[102] H. Pleiner, H.R. Brand, and P.E. Cladis, *Ferroelectrics*, **243**, 291 (2000)

[103] A. Jákli, Ch. Lischka, W. Weissflog, G. Pelzl, *Liq. Cryst.*, **27**, 715 (2000)

[104] N. Chattham, E. Körblova, R. Shao, D.M. Walba, J.E. Macmillan, and N.A. Clark, Abstracts of the 8th International Conference of Ferroelectric Liquid Crystals, Washington 2001

[105] A. Jákli, Ch. Lischka, W. Weissflog, G. Pelzl, A. Saupe, *Liq. Cryst.*, **27**, 1405 (2000)

[106] D.S Shankar Rao, Geetha G. Nair, S. Krishna Prasad, S. Anita Nagamani, and C.V. Yelamaggad, *Liq. Cryst.*, **28**, 1236 (2001)

[107] J.P.Bedel, J.C.Rouillon, J.P.Marcerou, M.Laguerre, H.T.Nguyen, and M.F.Achard, *Liq. Cryst.*, **27**, 1411 (2000)

[108] C.K. Lee, L.C. Chien, *Liq. Cryst.*, **26**, 604 (1999)

[109] C.K. Lee, and L.C. Chien, *Ferroelectrics*, **243**, 231 (2000)

[110] G. Heppke, D.D. Parghi, H. Sawade, *Ferroelectrics*, **243**, 269 (2000)

[111] G. Heppke, D.M. Parghi, H. Sawade, *Liq. Cryst.*, **27**, 313 (2000)

[112] A. Jákli, D. Krüerke, H. Sawade, and G. Heppke, *Phys. Rev. Lett.*, **86**, 5715 (2001)

[113] H. Nádasi, Ch. Lischka, W. Weissflog, I. Wirth, S. Diele, G. Pelzl, and H. Kresse, *Mol. Cryst. Liq. Cryst.*, submitted

[114] H. Pleiner, H.R. Brand, P.E. Cladis, *Ferroelectrics*, **248**, 291 (2000)

[115] A. Jákli, G.G. Nair, C.K. Lee, L.C. Chien, *Liq. Cryst.*, **28**, 489 – 494 (2000)

[116] T. Sekine, T. Niori, M. Sone, J. Watanabe, S.W.Choi, Y.Takanishi, H. Takezoe, *J. Jpn. Appl. Phys.*, **36**, 6455 (1997)

[117] G. Heppke, D.Krüerke, C.Löning, D. Lötzsch, S.Rauch, Sharma, *Proceeding Freiburger Arbeitstagung Flüssigkristalle* 1997 (Poster P 70)

Theodor-Lieser Str. 2,
06120 Halle (Saale),
Germany

Phone: +49 (345) 292-8553
E-Mail: aeryomin@gmx.de

Alexey B. Eremin

Personal details	Date of birth	14 February 1976
	Place of birth:	Moscow. Russian Federation

Education

1999 - 2003
Martin-Luther University Halle-Wittenberg; Institute for Physical Chemistry, Halle (Saale), Germany
PH.D. / Major: Physics of Liquid Crystals
- Summa cum laude

1993 - 1999
"Lomonossov" Moscow State University, Moscow, Russia Physical Chemistry, Halle (Saale), Germany
Master of Science I Major: Physics; Minor: Biophysics
- Diploma of Honors (summa cum laude)

1989 - 1993
High School # 978 (Classes of Moscow Institute for Physics and Technology), Moscow, Russia
- Silver medal

Work experience

May 1, 2003 - present
Post-doctoral researcher
- Two-dimensional solid-state NMR of polymers
Martin-Luther University Halle-Wittenberg
Institute for Experimental Physics VI, Halle (Saale), Germany

1999 - 2003
PhD student
- Liquid crystals research
Martin-Luther University Halle-Wittenberg; Institute for Physical Chemistry, Halle (Saale), Germany

1996 - 1999
- diploma research on auto-wave kinetics of platelet activation in human blood

Laboratory for Physical Biochemistry, Hematological National Research Cater, Moscow, Russia

Skills

NMR spectroscopy
electro-optical measurements in liquid crystals
polarizing microscopy in characterization of liquid crystals
measurements of intercellular ionic concentrations using fluorescent dyes
intracellular ADP/ATP measurements
aggregometry

Computer skills	Programming:

Computer skills

Programming:

- Borland Delphi
- Compaq Visual Fortran (high-performance programming using IMSL, CXML; development of Windows applications)

General skills:

- MsOffice, Core1 Draw, Adobe Photoshop, Adobe Illustrator, Adobe PageMaker (designing of publications)

Mathematics and modeling:

- MathCad (MathSoft), Mathematica (Wolfram Research)
- Accelrys Cerius2 molecular simulations

Teaching experience

English as a Foreign Language (free-lance)

Training courses in mathematics and physics for undergraduates (free-lance)

Seminars on Physics of Materials at Martin-Luther University

Languages

Native Russian speaker; fluent English and intermediate German

Awards recieved

Diploma of Honors at "Lomonosov" Moscow State University

2nd place at the Kurchatov Competition in Physics (International Nuclear Society)

Diploma of Honors and a silver medal for the accomplishment of the secondary education (School # 978, Moscow)

Interests

Badminton, cooking, literature, languages

References

Prof. G. Pelzl, Institute für Physikalische Chemie, Martin-Luther Universität, Miihlpforte I, D-06108 Halle (Saale), Deutschland

Prof. S. Grande, Universität Leipzig, Fakultät für Physik und Geowissenschaften, Linnéstraße 5, D-04103 Leipzig, Deutschland

Prof. H.R. Brand, Theoretische Physik III, Universität Bayreuth, 95440 Bayreuth, Deutschland

Acknowledgments

Liquid crystal research is a large interdisciplinary field of natural science and requires much collaboration between physicists, specialists in material science and chemists. Therefore, I would like to express my most sincere thanks to everybody who took part or supervised this project. Especially I would like to thank my colleags who introduced me into the experimental techniques as well as the people I had the most interesting discussions with on the field of condensed matter physics:

U. Baumeister
L. Blinov
H. Brand
G. Dantlgraber
S. Diele
D. Gottschlich
S. Grande
V. Kaganer
J. Kain
L. Kovalenko
H. Kresse
H. Nádasi
B.I. Ostrovskii
G. Pelzl
M.W. Schröder
C. Tschierske
W. Weissflog
I. Wirth

Appendix

List of the investigated liquid crystalline materials used in this thesis
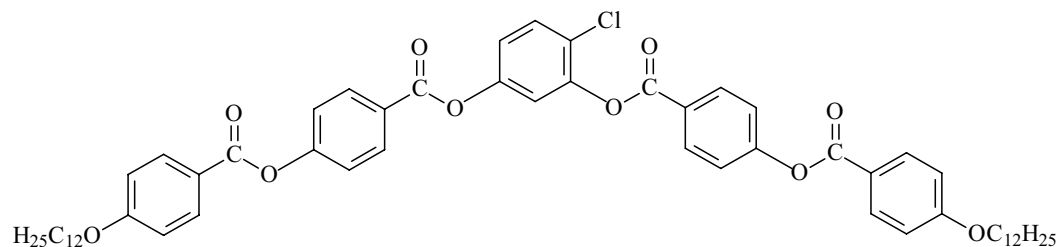
IV/**1**
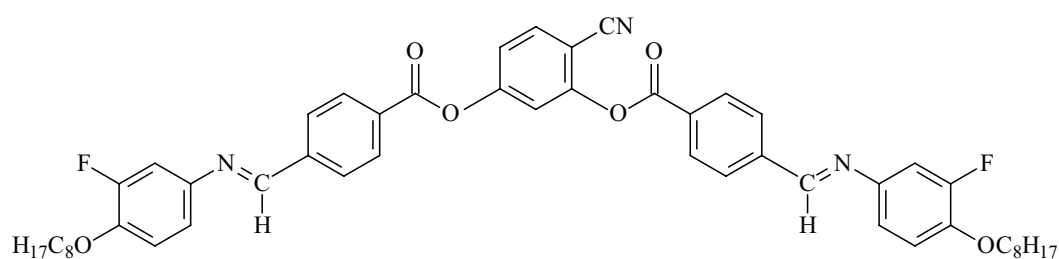
V/**1**
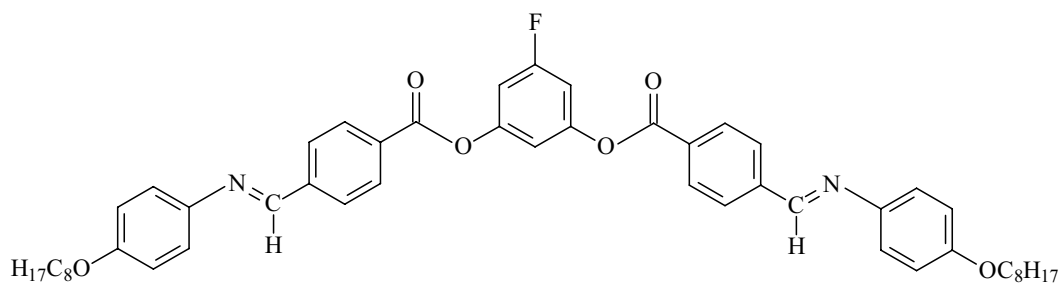
VI/**5F**
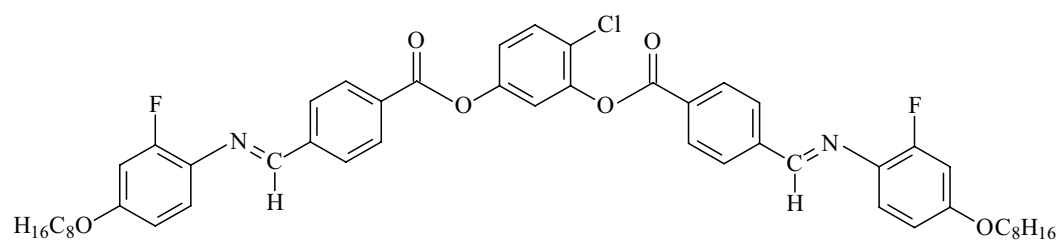
VI/**4Cl**
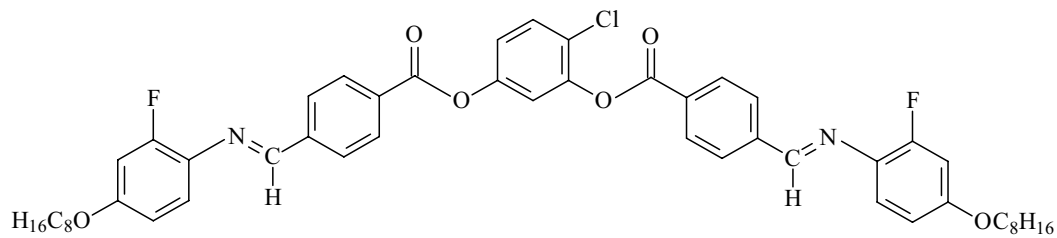
VII/*n* (*n* = 3, 8…12)
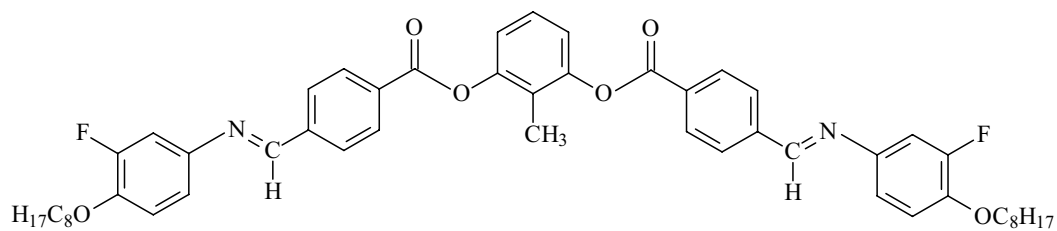
VIII/*n* (*n* = 1, 2)
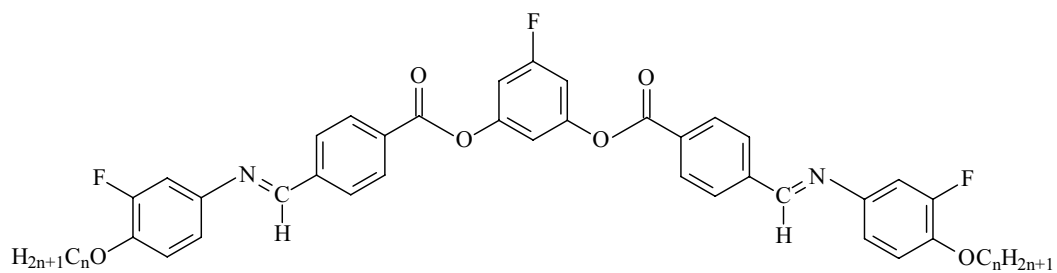
IX/*n* (*n* = 8, 12)
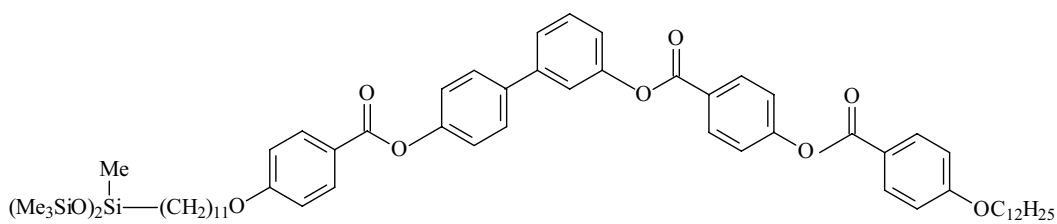
X/**1**
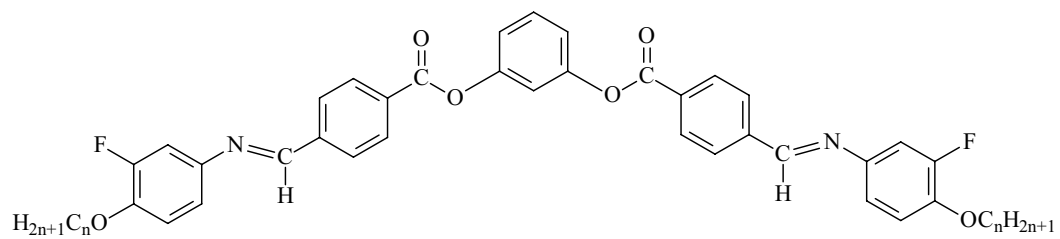
XI/*n* (*n* = 8…12)
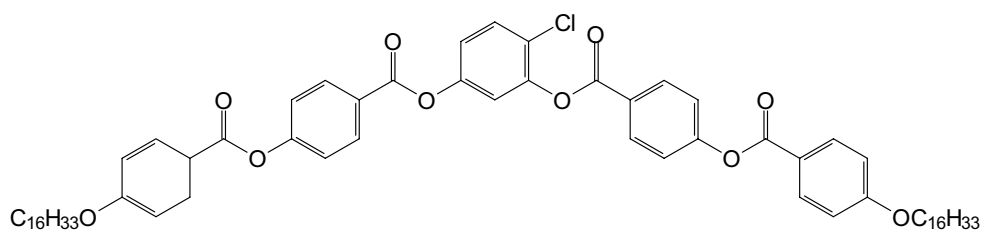
XII/**1**

Erklärung

Hermit versichere ich, daß ich die vorliegende Arbeit selbständig verfaßt habe und keine anderen als die von mir angegebenen Quellen und Hilfsmittel verwendet habe.

Diese Dissertation wurde bisher an keiner anderen Hochschule oder Universität vorgelegt. Sie wurde nicht anderweitig zwecks Erlangung eines Preises eingereicht oder schon mit Preis ausgezeichnet.

A.B. Eremin

Halle, den 10.02.03